

**PHARMACOLOGICAL AND GENETIC APPROACHES PROBING THE ROLE OF THE SLACK
POTASSIUM CHANNEL IN CHILDHOOD EPILEPSIES**

By

Brittany Duerk Spitznagel, Pharm.D.

Dissertation

Submitted to the Faculty of the
Graduate School of Vanderbilt University
in partial fulfillment of the requirements

for the degree of

DOCTOR OF PHILOSOPHY

in

Pharmacology

December 12th, 2020

Nashville, Tennessee

Approved:

C. David Weaver, Ph.D. (mentor)

Jerod S. Denton, Ph.D. (Committee Chair)

Kyle A. Emmitte, Ph.D.

Eric J. Delpire, Ph.D.

Andre H. Lagrange, Ph.D.

Joey V. Barnett, Ph.D.

W. Scott Akers, Pharm.D., Ph.D.

This work is dedicated to my loving husband, Frank, who has been a constant source of support and encouragement through the challenges of pharmacy school, graduate school, and life.

This work is also dedicated to my parents, David and Janet Duerk, who have always loved me unconditionally and whose good examples' have taught me to work hard for the things that I aspire to achieve.

ACKNOWLEDGEMENTS

First, I would like to thank Dr. Dave Weaver, his mentorship, encouragement and friendship have helped shape me into the scientist and person I am today. From the first moment I walked into Dave's office I knew I needed to be a part of his lab. His enthusiasm for science and life is unmatched. I would also like to acknowledge the rest of my thesis committee, who have pushed me to think critically about my work in order to become an independent scientist. I'd like to thank Eric Delpire and Andre Lagrange for their insight and collaboration in regards to the *in vivo* work done throughout this project. Scott Akers and Joey Barnett saw potential in me, even when I didn't, and pushed me to pursue the Pharm.D./Ph.D. pathway and for that I will be forever grateful. Kyle Emmitte has not only been an essential part of this work by providing copious amounts of compounds to test but he has also become a mentor throughout the process. And last, Jerod Denton, who deserves this placement for always being the last committee member to fill out scheduling surveys, has been a pillar of support and ideas throughout my graduate school career.

My time at Vanderbilt would not have been the same without the network of friends and colleagues I developed along the way. I would particularly like to thank Karen Gieg, who began as a mother figure and developed into a lifelong friend. I would like to acknowledge the Pharmacology Department leadership who supported me through a training grant and travel awards which allowed me to conduct my research and travel to share that work with others. Also, funding from the PhRMA Foundation through their Predoctoral Fellowship supported this work.

I would like to extend a huge thank you to all of the staff of the High-Throughput Screening Core facility and the Mouse Neurobehavioral Lab. Without their support I would not have been able to complete the work that follows. I would especially like to thank Paige Vinson for her work as the director of the Vanderbilt HTS Core Facility and always being willing to lend a helping hand. Thank you to Corbin Whitwell for providing an immense number of compounds throughout my screening process. Thank you to Fiona Harrison as the scientific director

of the Mouse Neurobehavioral Lab for helping our lab design our mouse studies and write animal protocols. And to John Allison who taught me how to run and analyze all of the neurobehavioral assays.

I would be remised if I did not acknowledge all of the collaborating labs that have allowed us to complete the studies herein. The Denton lab for developing and sharing many ion channel-expressing cell lines and for treating me as one of their own labmates. The Emmitte lab, in particular Nigam Mishra and Alshaima'a Qunies, who synthesized hundreds of compounds for this project. The Delpire lab for their generation of the KCNT1 mutant mouse model described below. Finally, the Harrison lab, who taught me to perform survival surgeries and mouse dissections. In particular Jordyn Wilcox who trained me in many new techniques and who was always willing to lend a hand. Fiona Harrison who became a guide for all of our animal work and a role model for women in science. I am grateful that she has given me the opportunity to complete a post-doctoral fellowship under her mentorship following completion of my Ph.D.

I would also like to thanks the members of the Weaver lab, past and present. Our time in the lab together provided a great environment to grow as a scientist. But our time outside of the lab provided some of my best graduate school memories. I would particularly like to thank Francis J. Prael II for our scientific discussions, for bringing new techniques into the lab, and for introducing me to new music, documentaries and podcasts. To Krystian Kozek, who has grown from labmate to a dear friend. Thank you to Yu (Sunny) Du for teaching me all aspects of molecular biology and for constantly bringing a smile, hard working and optimistic attitude to the lab every day.

Finally, I would like to thank all of my friends and family for their love and support. Pursuing dual doctoral degrees seemed crazy but you all never doubted me. I would specifically like to thank my parents and my husband for their never-ending support and unconditional love.

TABLE OF CONTENTS

DEDICATION	ii
ACKNOWLEDGEMENTS	iii
LIST OF TABLES	ix
LIST OF FIGURES	x
CHAPTER 1: INTRODUCTION	1
Epilepsy	1
Genetic-Related Epilepsies	2
MMPSI	3
Ion Channels	4
Slack	5
Slack Regulation	7
Slack Localization	7
Slack Mutations	9
Mouse Models	10
Mouse Models of Slack	11
Slack Pharmacology	13
CHAPTER 2: DISCOVERY OF NOVEL SLACK CHANNEL MODULATORS USING HIGH- THROUGHPUT THALLIUM FLUX ASSAYS	15
Introduction	15
Methods	22
Stable Cell Line Generation	22
Whole-Cell Voltage-Clamp Electrophysiology	23
Western Blots	23
Cell Preparation for Tl^+ Flux Experiments	24
Compound Plate Preparation for High-Throughput Experiments	25
Conducting a Tl^+ Flux Experiment	25
Data Analysis for HTS Experiments	26
Compound Libraries Screened	26
Results	27
Validating the Expression of Slack in HEK293 Cells	27
High-Throughput Tl^+ Flux Assay Development for Slack Channels	27
Four Cell Line Pilot High-Throughput Screen	29
Selection and Preliminary Counter Screening of Hits from the Slack Channel High-throughput Screen	29
Discussion	31
CHAPTER 3: CHARACTERIZATION OF VU0606170 ACTIVITY ON SLACK CHANNELS	36
Introduction	36
Methods	42

Stable Cell Line Generation	42
Synthesis and Purification	43
Characterization	44
Preparation of N-(5-chloro-2-methoxyphenyl)-2-(4-((4-methylpiperidin-1-yl)sulfonyl)piperazin-1-yl)acetamide	45
tert-Butyl 4-((4-methylpiperidin-1-yl)sulfonyl)piperazine-1-carboxylate	45
4-((4-Methylpiperidin-1-yl)sulfonyl)piperazin-1-ium 2,2,2-trifluoroacetate	46
Ethyl 2-(4-((4-methylpiperidin-1-yl)sulfonyl)piperazin-1-yl)acetate	46
2-(4-((4-Methylpiperidin-1-yl)sulfonyl)piperazin-1-yl)acetic acid	47
N-(5-chloro-2-methoxyphenyl)-2-(4-((4-methylpiperidin-1-yl)sulfonyl)piperazin-1-yl)acetamide	47
Preparation of 2-((5-chloro-2-methoxyphenyl)amino)-1-(4-((4-methylpiperidin-1-yl)sulfonyl)piperazin-1-yl)ethan-1-one	48
2-Chloro-1-(4-((4-methylpiperidin-1-yl)sulfonyl)piperazin-1-yl)ethan-1-one	48
2-((5-chloro-2-methoxyphenyl)amino)-1-(4-((4-methylpiperidin-1-yl)sulfonyl)piperazin-1-yl)ethan-1-one	49
Cell Culture Conditions and Preparation for Tl^+ and Ca^{2+} Flux Experiments	49
Modifications to Tl^+ Flux Experiments for Counter-Screens	49
T-type Calcium Channel Cell-based Ca^{2+} Flux Assay	50
Compound Plate Preparation for Concentration-Response Tl^+ Flux Experiments	51
Data Analysis for Concentration-Response Tl^+ Flux Experiments	51
Cell Preparation for Automated Electrophysiology	52
Automated Patch-clamp Electrophysiology	52
Rat Husbandry	53
Primary Neurons	53
Calcium Imaging of Primary Neurons	54
Immunofluorescence Staining of Primary Neurons	55
Results	56
Dependence of VU0606170 Activity on Slack Expression	56
Influence of VU0606170 on Slack Channels Current-Voltage Relationship Using Automated Whole-cell Voltage-clamp Electrophysiology	56
Characterization of VU0606170 Selectivity Among Slo Channels	58
Characterization of VU0606170 Selectivity Among a Broad Variety of Channels	60
Investigation of Slack Channel Expression in Rat Cortical Neurons	60
Discussion	62
CHAPTER 4: CHARACTERIZATION OF VU0606170 ANALOGS	69
Introduction	69
Methods	72
Cell Culture, Thallium-flux and Calcium-flux Assays	72
Drug Metabolism and Pharmacokinetic Assays	72
Results	74
Characterization of VU0606170 Drug Metabolism and Pharmacokinetic Properties	74

Overview of VU0606170 Structurally Related Analogs	76
Characterization of Amide Analogs	76
Characterization of 2,5-Substituted Phenyl Analogs	77
Characterization of Sulfonamide Analogs	77
Characterization of XCOR Analogs	78
Characterization of Linker Analogs	78
Characterization of Core Analogs	78
Characterization of the SAR of VU0606170 Analogs on Ca ²⁺ Oscillations	79
Discussion	79

CHAPTER 5: CHARACTERIZATION OF NEUROLOGICAL EFFECTS OF AN MMPSI-ASSOCIATED SLACK MUTATION IN A MURINE MODEL 89

Introduction	89
Methods	93
Generation of Mouse Line	93
Animal Care and Housing	94
Irwin Assay	94
Inverted Screen Assay	95
Rotarod Assay	95
Open Field Assay	95
Light/Dark Assay	96
Elevated Zero Maze	96
Three-Chamber Assay	96
Prepulse Inhibition Assay	97
Intracranial Electrode Placement	97
Electroencephalogram Recordings	98
Results	101
Characterization of Gross Physical and Behavioral State of Mutant Slack Mice	101
Characterization of Mutant Slack Mice Motor Function	102
Characterization of Anxiety-like Behaviors in Mutant Slack Mice	104
Investigation of Social Interaction in Mutant Slack Mice	106
Characterization of Mutant Slack Mice Sensorimotor Function	108
Investigation of Spontaneous Seizure Activity in Mutant Slack Mice	111
Discussion	111

CHAPTER 6: CONCLUSIONS AND FUTURE DIRECTIONS 118

Conclusions	118
Future Directions	120
Understanding the Mechanism of Action of VU0606170	120
Investigating Other Slack Inhibitor Scaffolds	120
Further Characterization of A913 Mutant Slack Mice	121
Interpretation and Impact	122

References126

LIST OF TABLES

Table	Page
1. Results of pilot high-throughput screen	34
2. Nine compounds that resulted from the Slack high-throughput screen	35
3. VU0606170 activity on a variety of engineered HEK293 cell lines	61
4. Amide analogs of VU0606170	82
5. 2, 5-substituted phenyl analogs of VU0606170	83
6. Sulfonamide Analogs of VU0606170	84
7. XCOR Analogs of VU0606170	85
8. Linker analogs of VU0606170	86
9. Core analogs of VU0606170	87
10. Effect of VU0606170 analogs on cortical neuron calcium oscillations	88
11. Scoring for modified Irwin assay	99-100

LIST OF FIGURES

Figure	Page
1. Model of an action potential	6
2. Models of Slack channels, three-state model of voltage-gated ion channels, and Slack channel structure	8
3. Models of the thallium flux assay	16
4. Slack channel structure with epilepsy mutations highlighted	18
5. Raw thallium flux traces of quinidine and loxapine	20
6. The compound screening and counter screening pathway	21
7. Slack protein expression in engineered HEK293 cells	28
8. Current-voltage relationship of Slack and mutant Slack channels.	30
9. Reproducibility of thallium flux assay	32
10. Representative data of high-throughput screen plate	33
11. Structure of VU0606170 and activity of VU0606170 in Slack and mutant Slack-expressing HEK293 cells	37
12. The concentration-dependent effects of VU0606170 on the Slack and mutant Slack channel current-voltage relationship	39
13. Structure of VU0849686 and the effect of VU0849686 on the Slack and mutant Slack channel current-voltage relationship	40
14. Raw thallium flux traces of VU0606170 activity.....	57
15. Representative electrophysiology data and the effects of VU0606170 on the Slack and mutant Slack channel current-voltage relationship	59
16. The activity of VU0606170 on hERG channels.....	63
17. Representative traces and the concentration-dependent effect of VU0606170 on calcium oscillations	65
18. Representative traces and the concentration-dependent effect of VU0849686 on calcium oscillations	67
19. Representative immunofluorescent staining of Slack protein in excitatory and inhibitory neurons	68
20. Structure of VU0606170 with amenable regions for medicinal chemistry marked	73
21. Model of three-chamber assay	92
22. Motor function activity of mutant Slack mouse model in rotarod assay	103
23. Anxiety-like behaviors of mutant Slack mouse model in open field assay	105
24. Anxiety-like behaviors of mutant Slack mouse model in elevated zero maze assay	107
25. Social interaction of mutant Slack mouse model in three-chamber assay	109
26. Sensorimotor function of mutant Slack mouse model in three-chamber assay	110

27. Spontaneous seizure activity of mutant Slack mouse model in three-chamber assay	112
28. Structure of VU0531245 and activity of VU0531245 in Slack and mutant Slack-expressing HEK293 cells	124
29. Structure of VU0915290 and activity of VU0915290 in Slack and mutant Slack-expressing HEK293 cells	125

CHAPTER 1

INTRODUCTION

Epilepsy

Epilepsy is the most common chronic neurologic disorder in the world, affecting 65 million people worldwide¹. This neurological condition is characterized by recurrent seizures², or electrical disturbances in the brain. Seizures can be the result of a host of underlying causes including: head injuries, stroke, brain tumor, prenatal brain damage, neurological infections, genetic basis. However, approximately 60% of all epilepsies are idiopathic, meaning there is no known cause or association^{1,2}. Epilepsy can develop in any person at any age; however, the disorder is bimodal, affecting young children and older people at a higher rate³. The health burden of epilepsy is greater than that of Alzheimer's, all other dementias and Parkinson's combined.

Seizure symptoms can vary widely and have been reclassified into three groups based on their onset by the International League Against Epilepsy (2017)⁴. Seizures are classified as being of generalized onset, focal onset or of unknown onset. Generalized onset seizures affect both sides of the brain, these result in patients having an impaired awareness to their surroundings. This class may be further broken down into two groups, those who have motor involvement, such as tonic-clonic seizures or non-motor, such as absence seizures. Focal onset seizures differ in that they arise from one area or group of cells in only one side of the brain. This class is further separated by the level of consciousness of the patient. Patients may be aware their seizure is occurring, known as a focal aware seizure or they may be confused or their awareness is affected in some way during the seizure, called a focal impaired awareness seizure (previously known as a complex focal seizure). As the name implies, unknown onset seizures are when the beginning of a seizure is not known due to a lack of witnesses. As more information is learned, an unknown seizure may later be diagnosed as a focal or generalized seizure. Diagnosis is often based on descriptions of what an observer has seen. Additional tests such as magnetic resonance imaging (MRI) scan or an electroencephalogram (EEG) to record the changes in electrical activity can aid in diagnosis.⁵

Generally, epilepsy, no matter the classification, is treated with one or more antiepileptic drugs (AED). To date there are 28 drugs indicated as antiepileptics, while many other are used off label, or unapproved AEDs. While the majority of patients' seizures can be controlled with the use of one or more AED, 30% of patients, meaning over 1 million people in the U.S., remain pharmaco-resistant, or resistant to all medications currently available². There is increasing interest in the concept of precision medicine for therapy. Particularly treatments aimed at the level of an ion channel or single pathway has provided benefits for a small number^{6,7} of individuals with genetically mediated cases.

Genetic-Related Epilepsies

While epilepsies as a whole affect 1 in 26 people in the United States at some point in their lifetime, monogenetic epilepsies are much rarer¹. These include examples of the different mechanisms underlying progressive myoclonus epilepsies, a group of neurogenetic disorders that can be due to either developmental abnormality, defects in energy metabolism or metabolic disturbances, as well as neuronal migration disorders, with the majority being dysfunctions of mutated voltage- or ligand-gated ion channels⁸. Ion-channel mutations are a known cause of rare monogenic idiopathic epilepsies, but are also suspected to play a major role in more common epilepsies⁹. Ion channels implicated in genetic epilepsies include sodium (Na⁺), potassium (K⁺), hyperpolarization-activated cyclic nucleotide-gated (HCN), calcium (Ca²⁺), and chloride (Cl⁻) channels, as well as gamma-Aminobutyric acid (GABA), N-Methyl-d-aspartic acid (NMDA), and acetylcholine receptors. Potassium channels make up the largest proportion of these mutations, accounting for 228 mutations in 22 different genes reported at this time¹⁰.

Over the past decade, the scientific community has coordinated to apply the genome wide association studies (GWAS) approach to common genetic variations in complex diseases including focal epilepsies. These studies resulted in a complex architecture of the genetic contributions in many focal epilepsies^{8,11}. Familial aggregation and twin studies revealed several familial epilepsies exhibiting Mendelian inheritance. While molecular diagnoses of these disorders can influence clinical management in many of these cases the most

perplexing cases remain those of *de novo* mutations resulting in severe epilepsies. One such disorder is malignant migrating partial seizures of infancy.

MMPSI

Malignant migrating partial seizures of infancy (MMPSI), also known as epilepsy of infancy with migrating focal seizures (EIMFS), is a rare, severe form of early-onset epileptic encephalopathy¹²⁻¹⁶. First described by Coppola et al.¹⁷ in 1995, MMPSI is characterized by malignant focal seizures that arise from various regions of either brain hemisphere and migrate between brain regions^{12,14,18}. The majority of these patients experience recurrent seizures before six months of age, typically ranging from 5 to 30 seizures per day¹⁵, although a portion of patients have reported suffering from hundreds of seizures per day. Due to the severity and number of seizures, affected individuals suffer profound developmental delays and intellectual impairment^{14,19}. While these severe seizures are the most discussed and studied symptom associated with MMPSI patients have a plethora of other diagnoses and issues.

Notably MMPSI patients have arrest or regression of motor skills obtained prior to the onset of seizure activity^{12,14,15,20}. Most patients have very little or no self-directed control of their body, do not speak and have limited ability to process sensory information from their environment. While individual developmental milestones vary, most children are not able to walk, talk, or feed themselves. Many patients lose the ability to eat orally and require placement of a feeding tube for nutrition. Patients also suffer from secondary complications due to poor muscle tone as infants. As their tone gradually develops over the first few years of life issues such as scoliosis, hip dysplasia, aspiration and gastrointestinal issues are common. Additionally, cortical visual impairment (CVI) appears to be a common symptom of the MMPSI phenotype²¹. CVI describes a dysfunction in the vision center of the brain that prevents the brain from properly interpreting visual information. While patients can technically see, their brains cannot process the images. The extent of the impairment, like more symptoms, varies, but many patients have difficulty seeing complex images and tracing objects. A variety of other neurogenic symptoms, such as neuroirritability, gastroesophageal reflux, constipation, and neurogenic bladder, are also typical in children

with MMPSI^{21,22}. MMPSI cases are considered pharmacoresistant, resulting in accelerated disease progression^{13-15,20,23}. Growing evidence suggests a genetic etiology for the development of MMPSI. Forty-four *de novo* mutations affecting a neuronal ion channel, have been reported in 50% of patients with MMPSI, making it the most frequent known genetic signature associated with MMPSI^{12,15,19,24-27}.

Ion Channels

Ion channels are pore-forming proteins that span the plasma membrane or the membranes of intracellular organelles, allowing for ions to pass through. Ion channels have a diverse physiologic role, including establishing resting membrane potential, shaping action potentials (APs), and regulating cell volume²⁸. A wide variety of ion channels with a broad spectrum of characteristics have been described²⁸. Ion channels are classified based on a variety of different properties, such as ion selectivity and gating mechanisms. Broadly, ion channels can be selective for individual ions, i.e. Na⁺, K⁺, Ca⁺ and Cl⁻, or for groups of ions, i.e. mixed cation and anion channels. In many ion channels, passage through the pore is governed by a gating mechanism, which may be opened or closed in response to chemical or electrical signals, temperature, or mechanical force.

Ion channels are essential in the generation of APs, which play a central role in cell-to-cell communication especially in neurons. APs are generated by special types of voltage-gated ion channels. These channels are shut when the membrane potential is near the resting potential of the cell, approximately -70 mV, but they rapidly begin to open if the membrane potential increases to a precisely defined threshold voltage, depolarizing the transmembrane potential. When the channels open, they allow an inward flow of Na⁺ (and occasional Ca²⁺) ions, which changes the electrochemical gradient, which in turn depolarizes the membrane. This then causes more channels to open, producing a greater electric current across the cell membrane and so on. The process proceeds until all of the available ion channels are open, resulting in a large upswing in the membrane potential to approximately +30 mV which causes the polarity of the plasma membrane to reverse, and the Na⁺ channels to rapidly inactivate. As the Na⁺ channels close, Na⁺ ions can no longer enter the neuron, and they are then actively transported back out of the plasma membrane. K⁺ channels are then activated, and there is an

outward current of K^+ ions, returning the electrochemical gradient to the resting state. After an AP has occurred, there is a transient negative shift, called the afterhyperpolarization. A diagram outlining this process can be found in **Figure 1**.

K^+ channels are the most diverse and widely distributed family of ion channel and are fundamental regulators of excitability^{28,29}. They control the frequency and the shape of an AP waveform (repolarization and hyperpolarization), the secretion of hormones and neurotransmitters and are responsible for setting the cell membrane potential. Their activity may be regulated by voltage, Ca^{2+} and neurotransmitters (and the signaling pathways they stimulate). They consist of a primary pore-forming α subunit often associated with auxiliary regulatory subunits. There are over 70 different genes encoding K channels α subunits in the human genome³⁰, one being *KCNT1*, which encodes for neuronal K^+ channel Slack.

Slack

The neuronal K^+ channel, Slack (Slo2.2), encoded for by *KCNT1*, is an outwardly rectifying channel that assembles to form tetramers (**Figure 2a**). Overall, the structure of Slack is similar to that of the voltage-dependent family of K^+ channels. This allows for the channel to open upon membrane depolarization, this channel opening is transient followed by inactivation, after recovery the channel moves to a closed state until the membrane is depolarized once again, this is known as the three-state model of voltage-gated ion channels (**Figure 2b**). As with most classes of K^+ channels, Slack channels have six hydrophobic membrane spanning domains S1-S6 with a pore domain between S5-S6. Slack is a member of the Slo family of K^+ channels along with Slo1 (Maxi-K, BK or $K_{Ca1.1}$), Slick (Slo2.1) and Slo3. The term Slack is derived from “sequence like a Ca^{2+} -activated K^+ channel,” because of its regions of similarity to Slo1, the large-conductance Ca^{2+} -activated K^+ channel^{31,32}. Like Slo1’s α subunit, Slack has a large C-terminal region containing two regulators of conductance of K^+ domains (RCK), which act as the binding sites for Na^+ and regulate channel gating^{31,32}. However, this is the only similarity the two share, as Slack and Slo1 share only 7% sequence identity, in contrast to Slick which shares 74% identity with Slack with the greatest divergence in the large C-terminal domain following the nicotinamide adenine

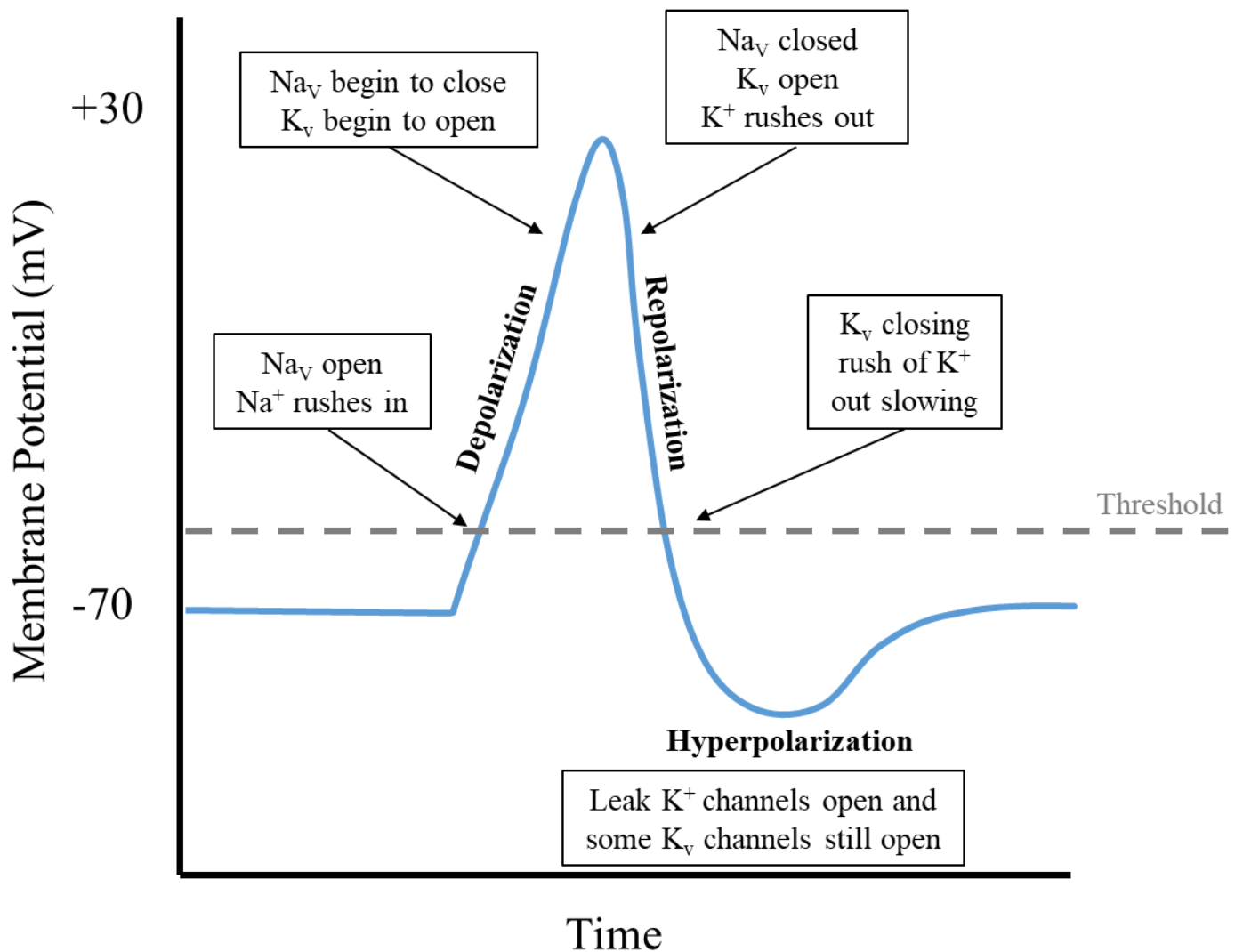


Figure 1: Approximate plot of a typical action potential shows its various phases as the action potential passes a point on a cell membrane. The membrane potential starts out at approximately -70 mV at time zero. A stimulus is applied which raises the membrane potential above the threshold potential. After the stimulus is applied, the membrane potential rapidly rises to a peak potential of $+30$ mV (depolarization). Just as quickly, the potential then drops (repolarization) and overshoots to -90 mV (hyperpolarization) and finally the resting potential of -70 mV is reestablished.

dinucleotide (NAD⁺) binding domain. At 138 kDa, Slack is the largest potassium channel subunit currently known³². A diagram of a Slack channel depicting the functional domains is shown in **Figure 2c**.

Slack Regulation

In contrast to other K⁺ channel families, Slack lacks positively charged residues in the fourth transmembrane domain which usually confers voltage sensitivity. However, elevations in intracellular Na⁺ concentrations, which occur during AP firing in the nervous system, promote Slack activation and provide an important feedback mechanism for controlling neuronal activity. Several groups have shown the EC₅₀ for activation of Slack channels by Na⁺ to be approximately 50 mM^{32,33}. However, this EC₅₀ is reduced to 17 mM in the presence of 1mM NAD⁺, leading to a 2-2.5-fold increase in the open probability (P₀) of the channel³³. In general, intracellular NAD⁺ levels are maintained between 0.2 and 0.5 mM, depending on the cell type or tissue. However, NAD⁺ levels can change, up to ~2-fold, in response to diverse physiological stimuli³⁴. For example, NAD⁺ levels increase in response to energy stresses, such as glucose deprivation, fasting, caloric restriction and exercise, and fluctuate in a circadian fashion, making this concept physiologically relevant³⁴. In addition to activation by elevated intracellular Na⁺ and NAD⁺, Slack channels are also activated upon phosphorylation by protein kinase C (PKC)^{32,35} and cell membrane depolarization following an AP. Slack is a neuronal K⁺ channel expressed in both excitatory and inhibitory neurons. In a neuron, upon membrane depolarization following the firing of an AP, Slack channels are rapidly activated (< 20 ms)³⁶. Taken together, the localized and transient large increase in intracellular Na⁺ and resulting membrane depolarization contribute to AP frequency adaptation and afterhyperpolarization potentials^{37,38}.

Slack Localization

Studies have confirmed that the highest levels of Slack channels are found throughout the central nervous system (CNS)^{39,40}, with detectable levels in the heart, testis and kidney^{31,39,41-43}. With the use of *in situ* hybridization and immunohistochemistry, these studies confirmed the presence of Slack transcripts in the adult

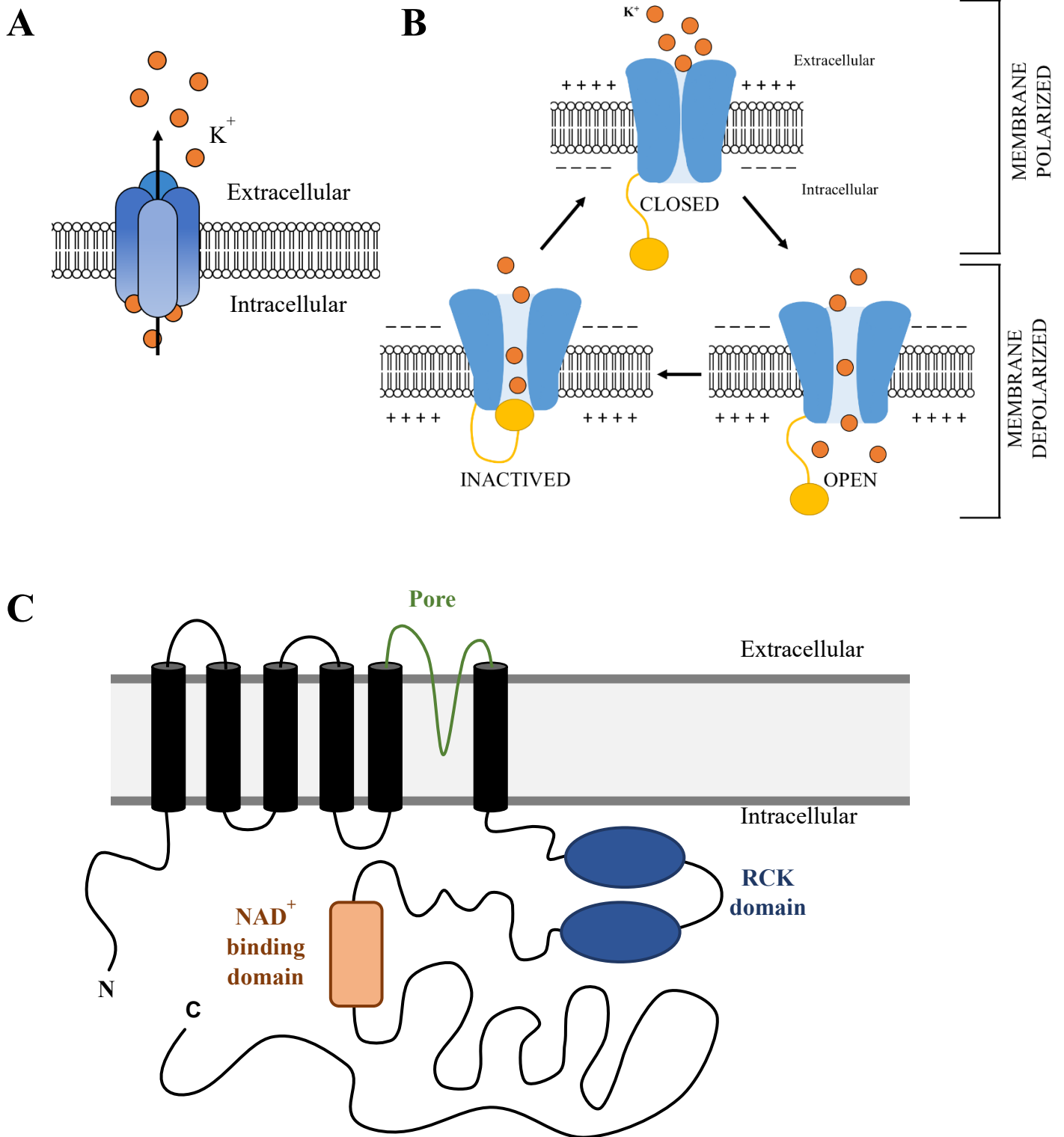


Figure 2: A) The Slack K⁺ channel passes K⁺ down the concentration gradient, extracellularly through the pore formed by four subunits assembling into a tetramer. B) Three-state model of voltage-gated ion channels. Closed, open and inactivated states with the corresponding transitions are shown. C) Slack structure depicting the three functional domains of the protein, pore domain in GREEN, RCK domain in BLUE and NAD⁺ binding domain in ORANGE.

rat which is likely an ortholog to human Slack (94% sequence identity). Within the CNS, Slack transcripts and protein were abundantly expressed in neurons throughout all regions of the brain, including the brainstem, cerebellum, frontal cortex and the hippocampus^{40,41,44,45}. Similar results have also been reported in the mouse brain⁴¹. It was long thought that Slack channels were present in both excitatory and inhibitory neurons and recently confirmed by Shore et al⁴⁶, however, Slack has yet to be described in glia⁴³. The presence of Slack channels in both neuronal populations sets the stage for how mutations in this channel lead to the development of epilepsy.

Slack Mutations

Slack channels are critical regulators of electrical activity in the nervous system and are highly expressed in both excitatory and inhibitory neurons^{31-33,44}. Pathological increases, in Slack activity leads to abnormal neuronal activity and ultimately intractable epilepsy. This increase in Slack activity has been attributed to gain-of-function mutations in the channel. Thirty-one epilepsy-associated mutations in Slack have been reported, these mutations are clustered around the three functional domains of the channel, the pore-forming region, RCK domain and NAD⁺-binding domain, both located in the large C-terminus of the channel (**Figure 2**). All of these mutations have been shown to induce a dominant gain-of-function by several mechanisms including 3-22-fold increases in current amplitudes^{12,24,37,47-50}, a left shift in the current-voltage relationship^{12,47}, or increasing the channel's sensitivity to Na⁺ ions³⁵.

Recent work has focused on elucidating the mechanisms by which this functional increase in Slack activity contributes to epilepsy. One proposed mechanism by which mutant Slack channels cause seizures is by enhancing K⁺ currents in GABAergic neurons⁴⁶, the primary inhibitory pathway. This increase in current, especially in non-fast spiking GABAergic neurons, leads to prolonged hyperpolarization resulting in a decrease in inhibitory activity^{46,49,51}. Secondly, this reduced excitability has been accompanied by an increase in excitatory-excitatory and inhibitory-inhibitory synaptic connectivity⁴⁶. It is thought that this increase in synaptic connectivity early in development predisposes the nervous system to develop circuits that generate epileptic discharges^{16,46}. The

resulting overall imbalance between neuronal excitation and inhibition leads to the development of seizures^{12,16,46,52}.

Mutations within the Slack channel have also been described in patients with autosomal dominant nocturnal frontal lobe epilepsy (ADNFLE),^{22,25,53} and other epilepsies including Ohtahara syndrome⁵⁴, multifocal epilepsy^{22,54}, and West syndromes^{22,24,48}. Several of the Slack mutations implicated in seizure disorders all share a common association with severe intellectual debility and other developmental delays, together give rise to an emerging role of Slack channels in intellectual disability^{14,16,19}. It has been shown that Slack channel activity is increased by direct complex formation with fragile X mental retardation protein (FMRP), the RNA-binding protein that is deleted in Fragile-X Syndrome, implicating Slack in this syndrome⁵⁵⁻⁵⁷. This evidence suggests that a key physiological role of Slack is its control over network excitability in regions of the brain involved in motor skill and intellectual development.

Mouse Models

The use of mice as model organisms has become the preferred mammalian model for genetic research over the past century. Mice are typically used to study human biology at a systems level due to their genetic and physiological similarities to humans⁵⁸. Genomic studies have highlighted the striking genetic homologies between the two species^{58,59}. These studies, together with the development of methods for the creation of transgenic, knockout (KO), and knockin mice, have provided added motivation and powerful tools for mouse research, and have led to a dramatic increase in the use of mice as model organisms. KO mice carry a gene that has been inactivated, which creates a loss of function; knockin mice are produced by inserting a transgene into an exact location where it is overexpressed. These methods are particularly useful if a single gene is shown to be the primary cause of a disease, as is the case with Slack and the development of MMPSI.

While animal disease models do not necessarily recapitulate all symptoms of a particular disease or disorder, the pathophysiology of disease in mice is often similar enough to that of humans allowing researchers to gain important physiological and mechanistic insights into the disease state. There are numerous behavioral

and neurological assays reported for mouse models including those that test for depression or anxiety-like behaviors, response to a noxious stimulus, locomotor activity, memory and sensory function. When investigating psychiatric disorders or symptoms quantitative assessments are used in place of qualitative assessments which could be used with human patients. Signs and symptoms of conditions such as anxiety often reflect motivations, emotions, and thought processes which we cannot translate in mice; therefore, we rely on quantitative assays modeling relevant behavioral paradigms⁶⁰. Classical models of anxiety-like behaviors in rodents focus on the similarity between anxiety and fear. Assays assessing approach versus avoidance behavior, baseline vigilance, or defensive behaviors⁶⁰.

Recordings such as electrocardiograms (ECG) and electroencephalograms (EEG) may also be performed on mouse models to investigate the cardiac or brain activity response to a variety of conditions: drugs, genetic mutations, aging, or changes in stimuli (environmental, social, physical). Mouse models of epilepsy include genetic mutations resulting in spontaneous seizures, or induction of seizures in normal animals. Seizure induction may be achieved by electrical, audiogenic caused by high-intensity acoustic stimulation, or chemical induction with kainate, pentylenetetrazol (PTZ), pilocarpine or flurothyl⁶¹. Seizures and epileptiform discharges in mice can be monitored via EEG following intracranial electrode placement, usually accompanied by continuous video monitoring or scored for behavioral phenotype based on experimenter observation, usually on a 0-5 scale, with 0 being no response and 5 being continual seizure activity known as status epilepticus⁶².

Mouse Models of Slack

In order to better understand the role Slack plays in normal neuronal development Slack KO mouse models were generated by three separate groups, Lu et al.⁶³, Bausch et al.⁴⁵ (followed by Bausch et al. (2018)⁶⁴ and Quraishi et al. (2020)⁵⁰) and Martinez-Espinosa et al.⁶⁵. Taken together, these groups showed the importance Slack plays in pain response, motor activity, anxiety-like behaviors, learning and memory, as well as the response to epileptogenic stimuli. Using a variety of pain models, including those representing nociceptive, inflammatory and neuropathic pain, mice lacking functional Slack channels showed an increase in neuropathic pain associated

with damage to the sciatic nerve or repeated injections to the hind paw. There was no observed difference between Slack KO mice and WT controls in models of inflammatory or nociceptive pain. Slack KO mice showed a decrease in exploratory behavior when in a novel environment⁴⁵. Additionally, mice deficit of Slack spent more time in the light, or open, side of a chamber with equal parts light and dark, or enclosed, space⁴⁵. The overall decrease in exploratory behavior and preference for open, or nonprotected, areas led to the conclusion that Slack KO animals have decreased anxiety-like behavior. Social preference was abnormal in the Slack KO animals, meaning that a higher percentage of these mice preferred to spend their time exploring an inanimate object rather than a novel mouse compared to WT controls⁶⁶. Usually, mice will choose to explore a new mouse since they are social animals that prefer to be together. Most relevant to the MMPSI patient population, seizure activity and response to epileptogenic stimuli was assessed in the KO Slack model. No spontaneous seizures were observed in the KO Slack mice. When challenged with increasing electroshock in order to induce a seizure the KO mouse population showed a significant decrease in the number of deaths due to electroshock (83% in WT, 22% KO Slack). Together these data suggest Slack KO provides a neural protective effect against seizure development.

Recently, two mouse models exhibiting MMPSI-associated Slack mutations have been described. Burbano et al. generated a P924L knockin mouse model⁶⁷. The P924L mutation is found within the NAD⁺ binding domain. While the group has not published their studies with the P924L mouse in a peer-reviewed journal, their poster presentation at the 2018 American Academy of Neurology Annual Meeting revealed the homozygous, *KNCTI*^{P924L/P924L}, mice suffer from spontaneous tonic-clonic seizures; however, heterozygous, *KNCTI*^{+/P924L}, mice showed no difference in susceptibility to thermal or chemical induction of seizure compared to WT, *KNCTI*^{+/+}, mice⁶⁷. The second knockin mouse model expresses the R455H mutation, found in the RCK domain of the Slack channel⁵⁰. Unlike the *KNCTI*^{P924L/P924L} mice, *KNCTI*^{R455H/R455H} mice were stillborn, making this genotype unable to be further studied. *KNCTI*^{+/R455H} mice had normal survival rate and normal procedural learning when tasked with an increasing acceleration on a rotating rod⁵⁰. These heterozygous mice did exhibit spontaneous seizures (0.8/day in 3/7 mice), while no seizures were seen in their WT littermates⁵⁰. Additionally, when challenged with 60 mg/kg of Pentylentetrazol (PTZ), a drug used to induce seizures in animal models, 5

of 6 heterozygous mice experienced seizures, opposed to WT which only had 1 of 6 mice exhibit seizures⁵⁰. The increase in seizure activity in these mutant Slack models are in contrast to the effects seen in the Slack KO animals, providing clear evidence that Slack is necessary for normal brain function. Taken together, these two mutant-Slack models, along with the models of Slack KO have been instrumental in our understanding the role Slack plays in pathophysiology. The two mutant-Slack mouse models provide assurance that we are able to model at least some symptoms of MMPSI, making these models crucial in future *in vivo* drug discovery studies. In **Chapter 5**, we describe our efforts to characterize a novel mouse model expressing the homolog to the A934T mutant Slack channel.

Slack Pharmacology

Because of the identification of Slack mutations in MMPSI and other epilepsies, investigation of the channel's normal physiology function, as well as its role in disease, has become a topic of intense interest in recent years. However, the development of pharmacological probes to study both WT and disease-associated mutant Slack channels remains an urgent need. Selective Slack inhibitors would allow us to test the hypothesis that selective small molecule modulators will safely and effectively correct the epileptiform behavior caused by Slack mutations. Several compounds have been shown to modulate Slack currents *in vitro*, most notably quinidine^{32,47,68-71}, bepridil^{15,37,71} and recently BC1-BC17⁷¹ have been shown to reduce current amplitudes. Unfortunately, each of these compounds are known to inhibit multiple other targets^{51,68,72,73} or their selectivity profile among a broad range of other ion channels has yet to be investigated.

In recent years, case studies have reported partially successful treatment of MMPSI with the addition of the non-specific blocker, quinidine, to conventional antiepileptic therapy^{22,48,73}. While treatment with quinidine shows some potential for therapeutic benefit, the narrow therapeutic index, limited brain penetration, sensitivity to drug interactions by numerous CYP-450s, and possible life-threatening cardiac side effects limit its use^{37,68,72}. Additionally, quinidine's severe lack of selectivity makes it unclear whether its partial efficacy as an MMPSI treatment can be attributed to the inhibition of Slack currents or one/more of the other channels it is known to

inhibit. More recently, additional studies aimed at investigating the clinical efficacy of quinidine in the treatment of MMPSI have been disappointing, primarily due to a lack of efficacy and QT prolongation associated with inhibition of hERG channels^{20,74,75}. There is currently an unmet need for effective drug therapy to treat MMPSI and numerous other Slack-related epilepsies.

Based on a preponderance of evidence for activating mutations in Slack playing a significant role in MMPSI and possibly other epilepsies, we undertook the task to discover selective small molecule Slack inhibitors which will provide the foundation for a novel therapeutic approach. In **Chapter 2**, we describe our high-throughput screening efforts in an attempt to discover Slack channel inhibitors. During this high-throughput screen (HTS) of 100,000 drug-like compounds we identified the Slack channel inhibitor, VU0606170. Extensive characterization of VU0606170 will be discussed in **Chapter 3**. In **Chapter 4**, we describe our efforts to improve the selectivity and efficacy profile of VU0606170 through structure-activity relationship studies. Finally, in **Chapter 6**, we conclude our discussions and provide insights into future experiments to be conducted following the discovery of VU0606170 and characterization of our A913T mouse model.

CHAPTER 2

DISCOVERY OF NOVEL SLACK CHANNEL MODULATORS USING HIGH-THROUGHPUT THALLIUM FLUX ASSAYS

Introduction

The identification of Slack mutations in MMPSI and other epilepsies, has led to increasing interest in the channel's normal function, as well as its role in disease, in recent years. However, the development of pharmacological probes to study both WT and disease-associated mutant Slack channels remains an urgent need in order to further elucidate the role Slack plays in the pathophysiology of epilepsy. Based on a preponderance of evidence for activating mutations in Slack playing a significant role in MMPSI and possibly other epilepsies, we undertook the task to discover selective small molecule Slack inhibitors. The development of inhibitor probes would allow us to investigate the hypothesis that selective small molecule modulators will safely and effectively correct the epileptiform behavior caused by Slack mutations. Previously described small-molecule inhibitors of Slack possess neither the selectivity nor potency required to probe the function of Slack channels^{16,32,68,69,72,73}. To discover selective inhibitors of Slack channels, we performed a high-throughput screen (HTS) using a fluorescence-based thallium (Tl⁺) flux assay in HEK293 cells engineered to express Slack channels.

High-throughput Tl⁺ flux assays have been used for over the last decade to discover and characterize compounds on targets such as G_{i/o} protein-coupled receptors (GPCR)⁷⁶⁻⁸¹, K⁺ channels⁸²⁻⁸⁴, Na⁺ channels⁸⁵ and K⁺-couple chloride co-transporters (KCC)^{86,38-40}. The Tl⁺ flux assay is an excellent HTS assay for K⁺ channels because Tl⁺ acts as a congener for K⁺. When K⁺ channels are open Tl⁺ passes through the channel into the cell where it can bind the Tl⁺-sensitive and fluorescent dye Thallos^{28,41} (**Figure 3**). Tl⁺ binding to Thallos increases the dye's fluorescence which is measured using a kinetic plate imager. The degree of change in Thallos

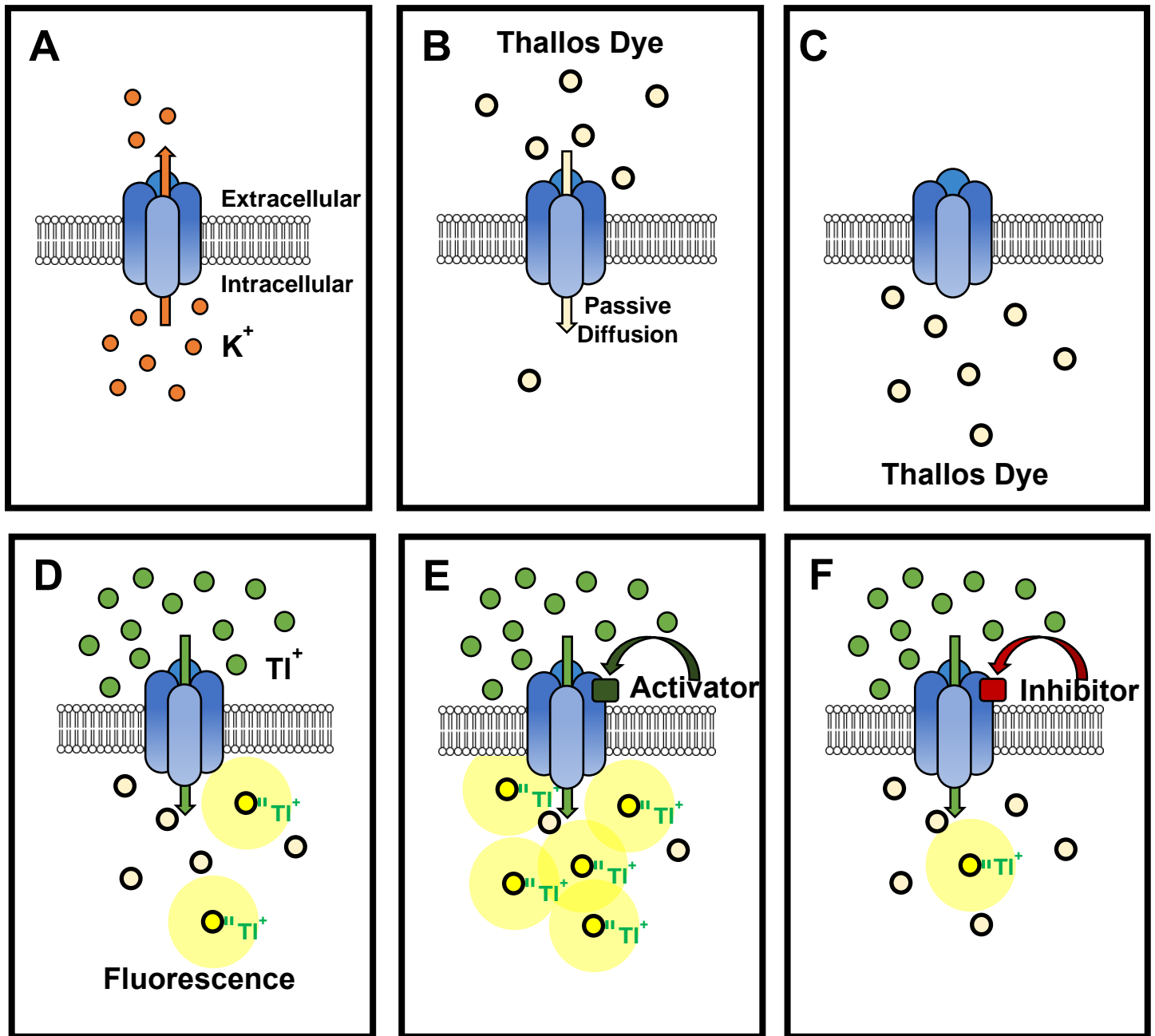


Figure 3: The Tl⁺ flux assay enabled identification of compounds that modulated Tl⁺ entry pathways on the cellular membrane. A) When Slack homotetrameric channels are expressed in a cell, they efflux K⁺ under physiologic conditions. During a Tl⁺ flux assay, B) Tl⁺-sensitive dye, Thallos travels down its concentration gradient intracellularly, C) Thallos is intracellularly-loaded which enables D) measurements of the influx of Tl⁺ via fluorescence. E) Channel activators increase Tl⁺ influx while F) channel inhibitors decrease Tl⁺ influx, both of which change the fluorescence signal and enable compound identification.

fluorescence is proportional to the degree of channel activity and thereby the Ti^+ flux assay can be used to detect compound-dependent changes in channel activity.

In order to use a high-throughput Ti^+ flux assay to discover Slack inhibitors, we first generated cell lines expressing WT and disease-associated mutant Slack channels. We chose to utilize human embryonic kidney #293 (HEK293) cell due to their fast growth, ease of genetic manipulation, neuron-like gene expression⁸⁷, and our laboratory's experience with this cell line. Because Slack mutations are clustered around the three functional domains of the channel, the pore domain, RCK domains and the NAD^+ -binding domain, we chose to generate disease-associated mutation Slack cell lines expressing the most prevalent MMPSI-associated mutation within each cluster: G288S is a mutation in the S5 transmembrane segment of the pore-forming region, R428Q is a mutation in the RCK domain, and A934T is a mutation in close proximity to the NAD^+ -binding domain (**Figure 4**). Channel expression and activity were confirmed using western blot, Ti^+ flux and EP. Details of cell line construction can be found in the **Methods** below.

Prior to beginning this HTS, we spent time developing the Ti^+ flux assay to generate a system sensitive enough to identify hits. We began by testing all known Slack modulators to establish that our system is responsive to changes in activity of our target, Slack. We determined that 30 μM loxapine, a reported Slack activator^{32,37,63,65}, and 1mM quinidine were able to activate or inhibit fluorescence in our assay to the greatest degree, and hence were used as positive (loxapine) and negative (quinidine) controls, respectively. We then determined how well different activity states of the target are resolved from one another, which is described as the Z-prime (Z') of the assay. It is calculated across entire plates to compare the activity of any well on a plate to wells with inactive compounds or vehicle controls to determine if they are statistically different from one another. Z' 's between 0.5 and 1 are considered excellent, showing large separations between controls and untreated (vehicle) treated cells. Our assay showed outstanding performance for detecting activators and inhibitors in WT and mutant-Slack cell lines with $Z' > 0.5$ for activation and inhibition over multiple days for all four cell lines. The assays described herein are the final iterations of our labors to optimize assay parameters and create a reliable assay suitable for high-throughput Ti^+ flux screening of WT and mutant Slack-expressing HEK293 cells.

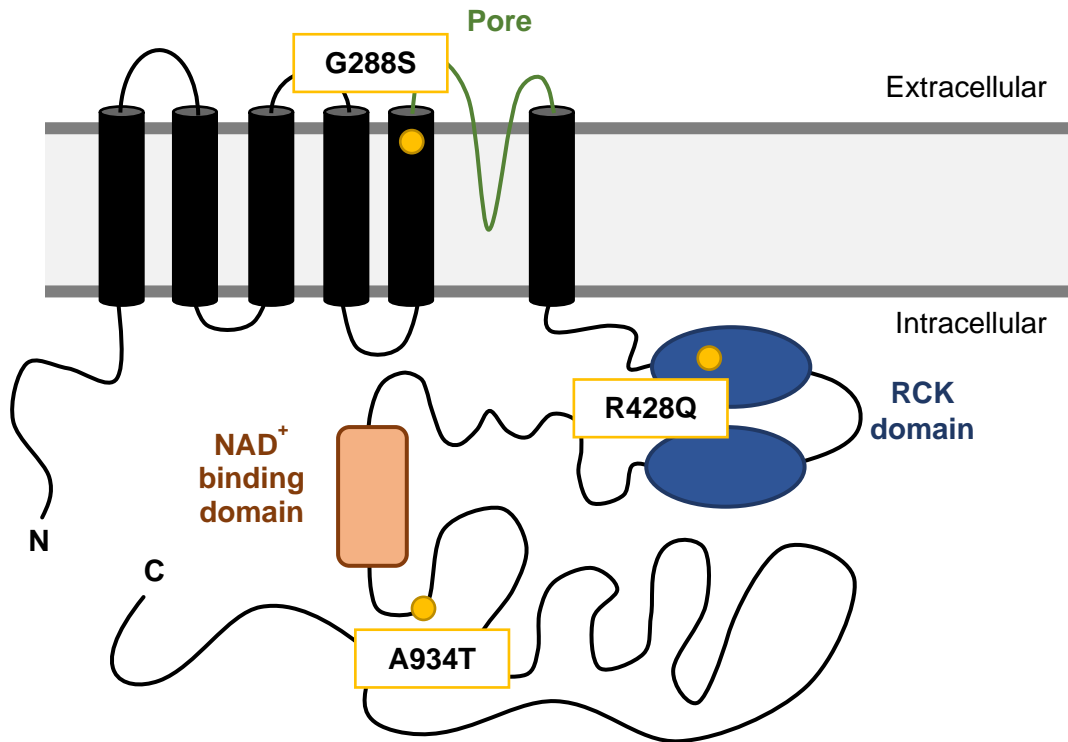


Figure 4: Slack structure with the MMPSI-associated mutation with the highest frequency in each mutation cluster shown in **GOLD**. The focus of this work, the A934T *KCNT1* mutation, alters an amino acid in the C-terminal domain. This represents the most prevalent *KCNT1* mutation associated with refractory epilepsy.

Throughout this HTS, we utilized a two-addition protocol (**Figure 5**) whereby the compound was added to Slack-expressing cells and incubated for 2 min to allow the compound time to engage the target. This was followed by TI^+ addition. Inhibitors were identified as compounds that caused a statistically significant decrease in TI^+ -evoked change in fluorescence compared to wells containing vehicle alone or inactive compounds. These compounds are henceforth referred to as “hits”. The best inhibitors were ranked according to their maximum effect, to determine which would be prioritized for further characterization. Within this chapter we will describe our process to confirm hits and investigate their ability to selectively modulate Slack channels through the use of additional assays and cheminformatic tools. A flowchart illustrating the experiments performed to characterize the hits is provided in **Figure 6**.

First, we established which hits replicated the activity that we observed during our HTS. Next, we identified whether Slack channel expression was necessary for hit activity. Naturally, HEK293 cells express a variety of TI^+ influx pathways, such as K^+ channels, Na^+ channels, transporters and non-selective cation channels. To eliminate hits that were active independent of Slack, we screened hits against untransfected (UT) HEK293 cells using the same TI^+ flux assay conditions as the initial screen.

Herein, we describe our work leading to the discovery of VU0606170, a synthetic small molecule inhibitor of WT and MMPSI-associated mutant Slack channels through HTS. We describe both the screen and initial counter screen results within this chapter. In **Chapter 3**, we describe the extensive characterization of VU0606170 yielding activity in whole-cell voltage-clamp electrophysiology (EP) and primary neuronal cultures. Followed by **Chapter 4** detailing our work with structurally similar small molecule modulators in an effort to develop a more efficacious, potent, and selective Slack channel inhibitor. Altogether, we provide a detailed account of our Slack channel HTS and experiments that followed.

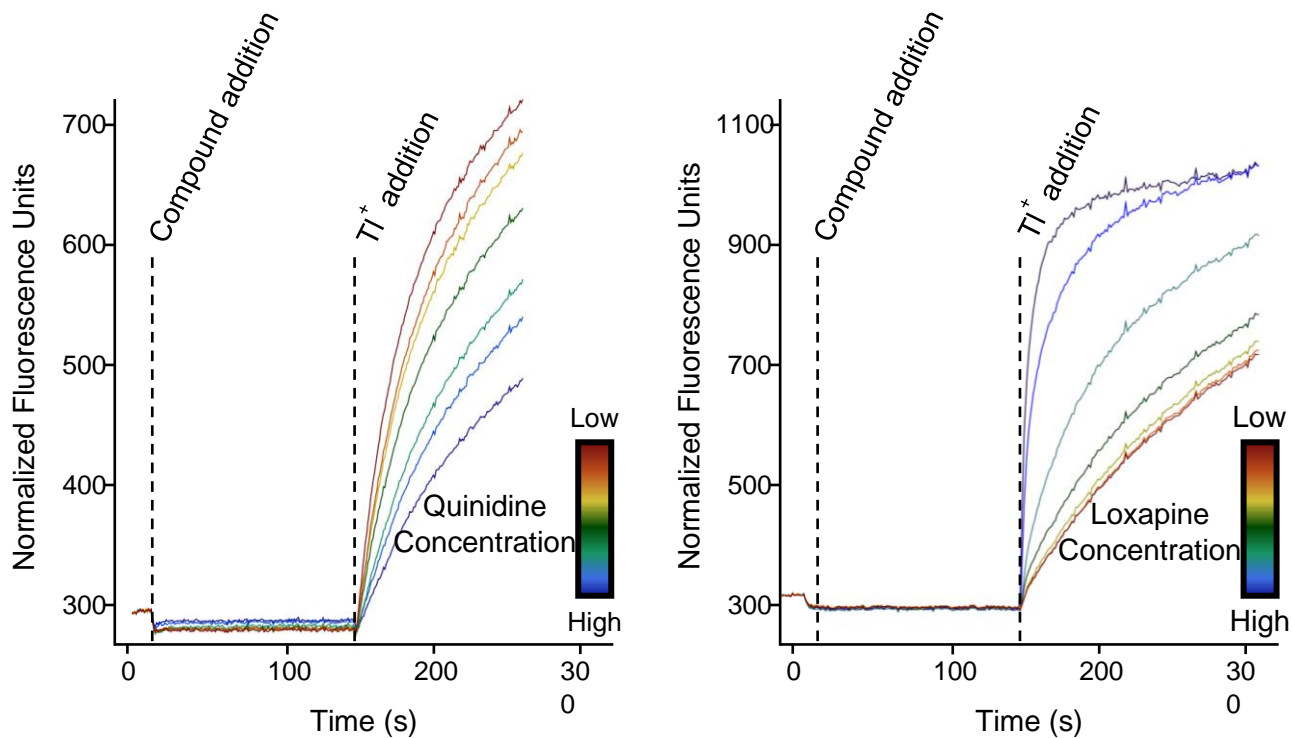


Figure 5: A) Concentration-dependent efficacy of quinidine (inhibitor) measured using Tl^+ flux. Quinidine concentrations begin at 1 mM and descend in 3-fold steps. B) Concentration-dependent efficacy of loxapine (activator) measured using Tl^+ flux. Loxapine concentrations begin at 100 μ M and descend in 3-fold steps. Time of compound and Tl^+ addition represented as dotted lines. Note y-axis differences between two graphs.

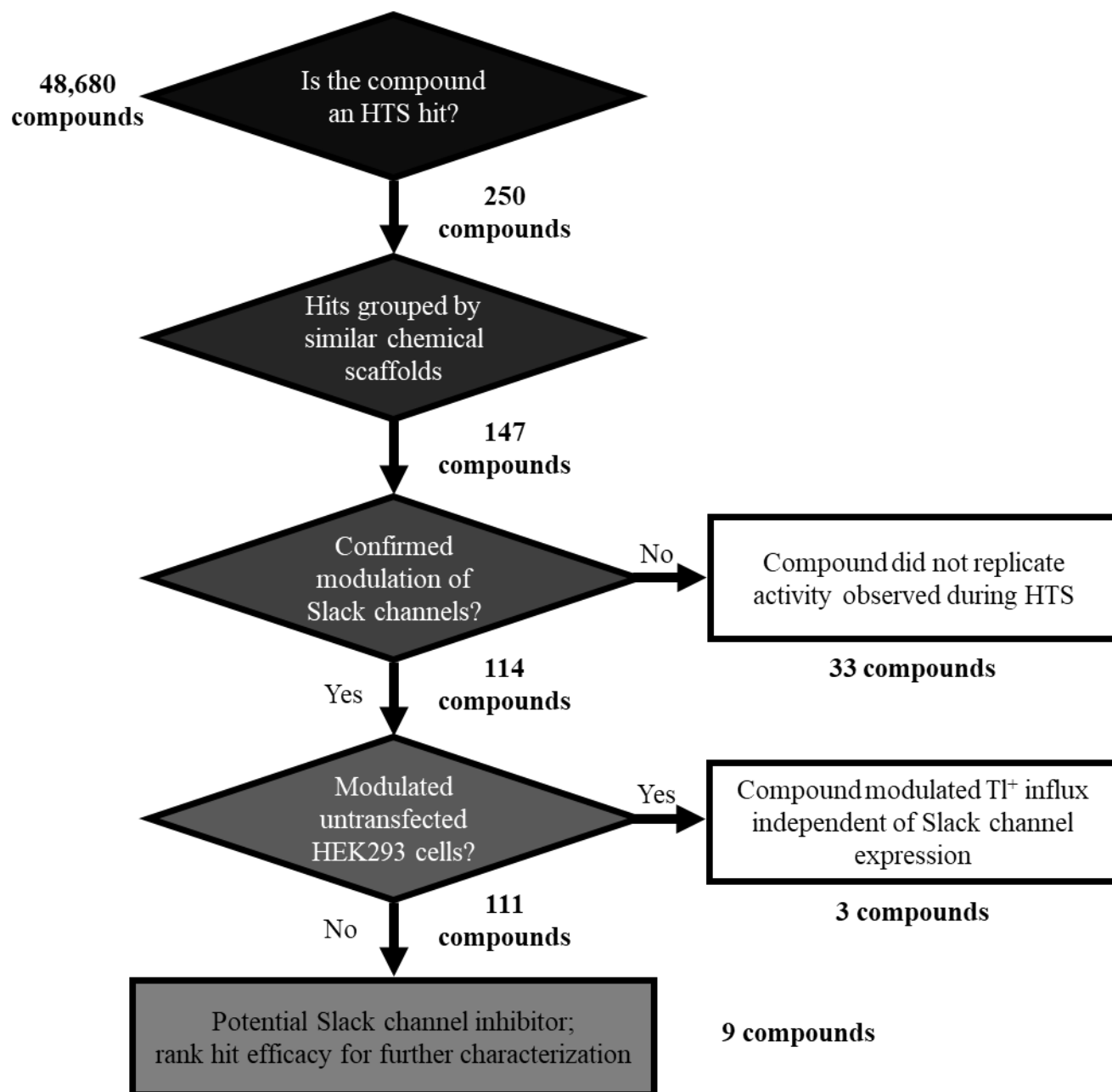


Figure 6: The initial counter-screening pipeline for Slack channel inhibitor discovery, with the different number of compounds filtered through each step during our Slack HTS.

Methods

Stable Cell Line Generation

HEK293 cells expressing human Slack cell line were generated by transfecting a pCMV6-Entry vector (Origene, Rockville, MD) containing KCNT1 and a pCMV6-A-puro vector (Origene, Rockville, MD) into low-passage HEK293 cells (CRL-1573, ATCC, Manassas, VA). The FuGENE 6 (Promega, Madison, WI) transfection reagent and protocol, together with Opti-MEM (Thermo Fisher Scientific, Waltham, MA), were utilized in all transfections herein. Similarly, three Slack mutant cell lines were generated. Mutations in KCNT1 were introduced using the GeneArt Site-Directed Mutagenesis System (Invitrogen, Carlsbad, CA) according to the manufacturer instructions. The complete cDNA was sequenced using Sanger sequencing (GenHunter Corporation, Nashville, TN) to verify the introduction of the intended codon changes.

Polyclonal cell lines were first tested in our Tl^+ flux assay (described below) for functional confirmation that our Slack channel of interest was expressed. Polyclonal cell lines consist of a heterogenous mixture of cells, with some expressing more functional channel than others, resulting in variability. This variability would make a HTS difficult to replicate day-to-day, therefore we generated monoclonal cell lines. Monoclonal cell lines provide a genetically homogenous population since they are derived from a single cell. These are generated by diluting the polyclonal cell line in order to plate 1 cell per well in a 96 well plate. These monoclonal cells are cultured until the colonies encompass approximately half of a well. These colonies were then assayed using our Tl^+ flux assay for their signal amplitude (maximum basal fluorescence) and their ability to be modulated by known Slack inhibitors, quinidine^{32,37,47,69-72} and bepridil^{15,37,71}, and activator, loxapine^{32,37,63,88}. Selected clones were expanded for use in experiments and for cryopreservation. Cell culture medium consisted of Minimal Essential Medium, Alpha Medium (Corning, Corning, NY) supplemented with 10% (v/v) heat-inactivated fetal bovine serum (Thermo Fisher Scientific, Waltham, MA) and GlutaGro (Corning, Corning, NY). Medium was supplemented with antibiotics, as appropriate, to maintain selection pressure.

Whole-Cell Voltage-Clamp Electrophysiology

Traditional, pipette-based, whole-cell voltage-clamp experiments on WT and A934T Slack cells were conducted in the Denton lab. The cells were dissociated on the day of experimentation and plated on Poly-L-Lysine-coated coverslips and allowed to recover for at least 1 hr in a 37°C 5% CO₂ incubator before starting experiments. Patch-clamp experiments were performed essentially as described previously^{89,90}. Briefly, patch electrodes (2–3 MΩ) were filled with an intracellular solution containing (in mmol/L) 135 KCl, 2 MgCl₂, 1 EGTA, 10 HEPES-free acid, and 2 Na₂ATP (Roche Diagnostics, Risch-Rotkreuz, Switzerland), pH 7.3, 275 mOsmol/kg water. The standard bath solution contained (in mmol/L) 135 NaCl, 5 KCl, 2 CaCl₂, 1 MgCl₂, 5 glucose, and 10 HEPES free acid, pH 7.4. Macroscopic currents were recorded under whole-cell voltage-clamp conditions using an Axopatch 200B Amplifier (Molecular Devices, Sunnyvale, CA). For I-V curves, whole-cell currents were measured from a holding potential of -80 mV and elicited with depolarizing steps (200 msec) from -80 to +50 mV (10 mV steps). Data were collected at 5 kHz and filtered at 1 kHz. Data acquisition and analysis were performed using the pClamp 9.2 software suite (Molecular Devices). Pharmacology experiments were terminated by applying 2 mM barium (Ba²⁺) chloride to measure leak current. Cells exhibiting <90% block by Ba²⁺ were excluded from analysis.

Western Blots

UT and engineered WT Slack and A934T Slack-expressing HEK293 cell lines were grown to 100% confluence in tissue culture treated 150 cm² dishes. The growth medium was aspirated and plates were twice washed with 5 mL phosphate-buffered saline (PBS) pH 7.4 (Thermo Fisher Scientific, Waltham, MA). Cells were scraped from the dish and triturated. Cell suspensions were then centrifuged at 500 g for 5 min at RT. Next, the supernatant solution was removed, and the pellet was resuspended in 1 mL of PBS and centrifuged once more. After removal of the supernatant solution, cells were resuspended in 1 mL of radioimmunoprecipitation assay (RIPA) buffer (Sigma-Aldrich, St. Louis, MO) containing Halt™ Protease Inhibitor Cocktail (Thermo Fisher Scientific, Waltham, MA) and stored on ice. Suspensions were then ultrasonicated in 4 brief 5 s pulses and

allowed to cool on ice for 15 min before centrifugation at 6,000 g for 10 min in a 4°C room. The supernatant solution was recovered, and the protein concentration was determined using the Pierce™ BCA Protein Assay Kit (Thermo Fisher Scientific, Waltham, MA) with a SpectraMax Plus 384 Microplate Reader (Molecular Devices, San Jose, CA). Samples were diluted to contain 10 µg of protein in 25 µL of Laemmli Sample Buffer (Bio-Rad, Hercules, CA) containing 355 mM β-mercaptoethanol (Sigma-Aldrich, St. Louis, MO). Samples were heated at 55 °C for 10 min before loading, and the gel was run according to the NuPage Bis-Tris/MOPS protocol using NuPage buffers and gel (Invitrogen, Carlsbad, CA). 25 µL/well of each sample was loaded onto a precast NuPAGE 4-12% Bis-Tris Gel and separated for 55 min at 200 V in NuPAGE MOPS SDS Running Buffer. The gel was transferred onto Odyssey Nitrocellulose Membrane (LI-COR Biosciences, Lincoln, NE) for 1.5 h at 30 V in NuPAGE Transfer Buffer. The membrane was rinsed using Tris-buffered Saline (TBS; Corning, Corning, NY) before blocking with 25 mL of TBS containing 5% (w/v) Blotting Grade Blocker Non-fat Dry Milk (Bio-Rad, Hercules, CA) at RT for 1 hour. Blocking is a very important step of western blotting, as it prevents antibodies from binding to the membrane nonspecifically. For the remainder of the membrane treatments, 0.05% Tween 20 was added to the milk-containing TBS buffer and will be referred to as TT20. Next, the membrane was incubated overnight at 4°C in TT20 containing a 1:100 dilution of a monoclonal IgG1 mouse anti-Slack antibody (cat# TA326566, Origene, Rockville, MD). On the next day, the membrane was washed 3 times with 5 mL of TT20 for 5 min each before incubating for 1 h at RT in TT20 containing a 1:20,000 dilution of fluorescent IRDye 680LT donkey anti-mouse antibody (LI-COR Biosciences, Lincoln, NE). Afterwards, the membrane was washed 3 times in 5 mL of TT20 for 5 minutes before a final rinse with TBS. Fluorescence from secondary antibodies was detected using the Odyssey CLx (LI-COR Biosciences, Lincoln, NE).

Cell Preparation for TI⁺ Flux Experiments

For use in TI⁺ flux experiments, monoclonal HEK293 cells engineered to express proteins of interest were grown in cell culture medium on tissue-culture-treated and vented T75, T150, or T300 flasks (TPP, Trasadingen, Switzerland) in a humidified incubator at 37°C and 5% CO₂. These cells were grown to reach approximately 90%

confluence on the day before experimentation. To prepare cells for transfer into 384-well plates, culture medium was removed from flasks, flasks were treated using TrypLE Express (Thermo Fisher Scientific, Waltham, MA) for 5 min to dislodge cells, and single-cell suspensions were created through trituration. Cells were resuspended in cell culture medium at 1,000 cells/ μ L. 20 μ L of cellular suspensions were plated in Corning® PureCoat™ Amine, 384-well microtiter plates (Corning, Corning, NY) to achieve a cell density of 20,000 cells/well. Cell plates were incubated overnight in a humidified incubator at 37°C and 5% CO₂.

Compound Plate Preparation for High-Throughput Experiments

Quinidine, at a maximally effective concentration (E_{max}) of 1mM, was used as a control to monitor the reproducibility of each plate. Quinidine was dissolved in assay buffer comprised of Hanks Balanced Salt Solution (HBSS) (Thermo Fisher Scientific, Waltham, MA) and 20 mM HEPES pH 7.3 (Corning, Corning, NY). All compounds received from the Vanderbilt HTS Core Facility were 10mM stocks in dimethyl sulfoxide (DMSO). Until the time of use, all compound plates were stored in desiccators at either room temperature (RT), 4°C, or -20°C as instructed by the originating source.

To generate compound plates for the HTS, compounds were dispensed as 120-200nL aliquots from the source plate. These samples were dissolved in 60-100 μ L/well with assay buffer. Each compound plate was designed to provide solution at concentrations twice the final concentration of compound. This is because solutions were diluted 2-fold during the assay, which resulted in the desired final concentration being applied to cell during imaging. Compound plates were used within 30 minutes (min) of preparation. Final concentrations of DMSO were 0.2% (v/v).

Conducting a TI⁺ Flux Experiment

The TI⁺ flux assays were conducted largely as previously described⁹¹. Cells were loaded with TI⁺-sensitive dye loading solution containing Thallo-AM (ION Biosciences, San Marcos, TX) in Assay Buffer. Dye loading solution was replaced with assay buffer after a 1-hour (h) dye incubation at RT. Cell plates were then loaded onto

the WaveFront Biosciences Panoptic (Franklin, TN). Data were acquired at 5 Hz (excitation 482 ± 35 nm, emission 536 ± 40 nm) for 10 sec (s), at which time 20 μ L/well of test compounds was added and allowed to incubated for 120 s. Next, 10 μ L/well of Ti^+ stimulus buffer (125 mM NaHCO_3 , 1.8 mM CaSO_4 , 1 mM MgSO_4 , 5 mM glucose, 12.5 mM Ti_2SO_4 , and 20 mM HEPES pH 7.3) was added. Imaging was concluded after an additional 120 s.

Data Analysis for HTS Experiments

Potential compounds of interest, or “hits”, from the HTS with WT and mutant Slack channels were identified by a means of the process described herein using the Vanderbilt screening analysis platform WaveGuide (Vanderbilt University, Nashville, TN). Compound activity was extracted from normalized and control-subtracted fluorescence waves generated over 300s of imaging. For data normalization, each data time point from each well (F) each well was normalized by dividing by the average fluorescence from the first 5 s of imaging (F_0). We perform this normalization process to account for dysuniformities in excitation and emission optics, as well as well-to-well cell plating variability. Next, the normalized waves from a minimum of 10 vehicle (VHL) control treated-wells were averaged and this average control wave was subtracted from normalized waves from each well on the plate to reveal the test compound-dependent changes in fluorescence. Finally, compound-dependent effects on fluorescence were measured as the change in wave amplitude (ΔA) due to stimulus buffer addition. These effects were measured as the minimum fluorescence value of the wave between time points 215 and 300s. Compounds were classified as hits if their maximum inhibition of VHL control Ti^+ flux was 3 standard deviations (SDs), below the mean of all compounds on a given plate, Z-score < -3 .

Compound Libraries Screened

The compound collection that we screened for this work was composed of the following libraries: Vanderbilt Discovery Collection, which were selected from the Life Chemicals (Ontario, Canada) collection for HTS. The compounds in this collection were chosen by Vanderbilt medicinal and computational chemists to

provide lead-like motifs, minimum pan-assay interference, and maximum diversity; NIH Clinical Collection I and II, which are small molecules that have history of use in human clinical trials; NCI Focused Natural Product Collection, which is comprised of pure compounds acquired by the NCI from Analytical and MerLion; Cayman Lipid Library, which is a broad variety of bioactive lipids; Ion Channel Library, which is a collection from Life Chemicals targeted to ion channels compiled using 2D fingerprint similarity methodology; Epigenetics Collection, which is a group of small molecule modulators with biological activity for use in epigenetic research; Marnett Collection, which contains NSAID derivatives that contain cyclooxygenase inhibitors, PPAR γ activators, and apoptosis inducers; and the Enzo Kinase Inhibitor Library, which is the Screen-Well Kinase Inhibitor Library containing 80 known kinase inhibitors of well-defined activity.

Results

Validating the Expression of Slack in HEK293 Cells

We confirmed the expression of the Slack protein in HEK293 cells by western blot (**Figure 7**). As expected, the Slack protein was identified as a band at approximately 138kDa. In collaboration with Dr. Jerod Denton's lab, we confirmed the activity of WT and A934T Slack channel expression by electrophysiology. I-V relationships of both WT Slack and A934T Slack resembled that of previously published Slack expressing cells. Using EP, we also confirmed the A934T mutation leads to a gain-of-function of the channel, as indicated by the significant increase in current density (**Figure 8**).

High-Throughput Tl⁺ Flux Assay Development for Slack Channels

With our validated WT and mutant Slack cell lines in hand we confirmed their ability to flux Tl⁺ resulting in an increase in fluorescence. Moreover, we confirmed the activity of known Slack modulators in our assay, with loxapine (activator) and quinidine (inhibitor) emerging as the most effective compounds. Representative raw Tl⁺ flux traces of loxapine and quinidine's concentration-dependent effect on Slack channels can be found in **Figure**

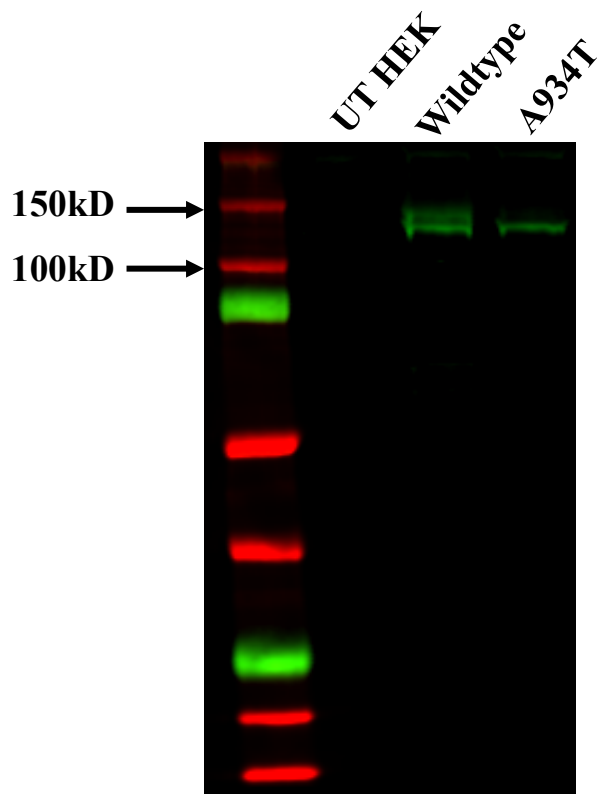


Figure 7: Stable expression of Slack in HEK293 cells. Shown is a Western blot of membrane fractions probed with a Slack-specific antibody: UT HEK293 cells, HEK293 cells stably expressing WT Slack, and HEK293 cells stably expressing A934T mutant Slack.

5. Finally, we established our ability to detect hits using this assay. Three 384-well plates per day were run on three consecutive days using all 4 Slack cell lines, each well's amplitude was plotted revealing a significant difference between vehicle, positive and negative control wells. All assays were determined to have a $Z' > 0.5$ (A934T data shown in **Figure 9**). Representative screening data for one library plate against A934T Slack cells is plotted in **Figure 10**, with the cutoff of 3 SDs below the mean indicated as the red dotted line. Wells whose minimum amplitude fell below this cutoff are classified as hits to be investigated as Slack inhibitors.

Four Cell Line Pilot High-Throughput Screen

We performed a pilot screen of approximately 5,000 compounds with our four cell lines, WT Slack and the three MMSPI-associated mutant Slack channels, G288S, R428Q, and A934T. This pilot screen clearly demonstrated that we were able to capture every hit compound using a two-cell line screen (WT and A934T), results shown in **Table 1**. We chose to focus on the A934T mutant, as it is the most prevalent disease-associated Slack mutation, representing approximately 14% of all *KCNT1*-related epilepsy cases reported in the literature at this time^{12,15,20,22,24,92-97}.

Selection and Preliminary Counter Screening of Hits from the Slack Channel High-throughput Screen

In total, we screened 97,359 compounds for activity on Slack channels. Of these, half were screened during the first phase of the HTS and half during the second phase. The second phase of this HTS was recently finished and is currently being analyzed. Herein, we will discuss the analysis and results from the first phase of the screen. Analysis of this HTS was performed using Vanderbilt WaveGuide, an inhouse data analysis program supported by the Vanderbilt High Throughput Screening Facility. A brief description of this analysis is outlined below, for a more detailed description see **Methods** above. In order to identify hits, the minimum amplitude was taken of each wave after being control-subtracted from the mean of all VHL treated wells. Hits were chosen if their amplitude fell 3-standard deviations below the mean amplitudes of all wells on a given plate. We identified approximately 250 inhibitors. In order to decrease the overall time and cost associated with retesting hits we

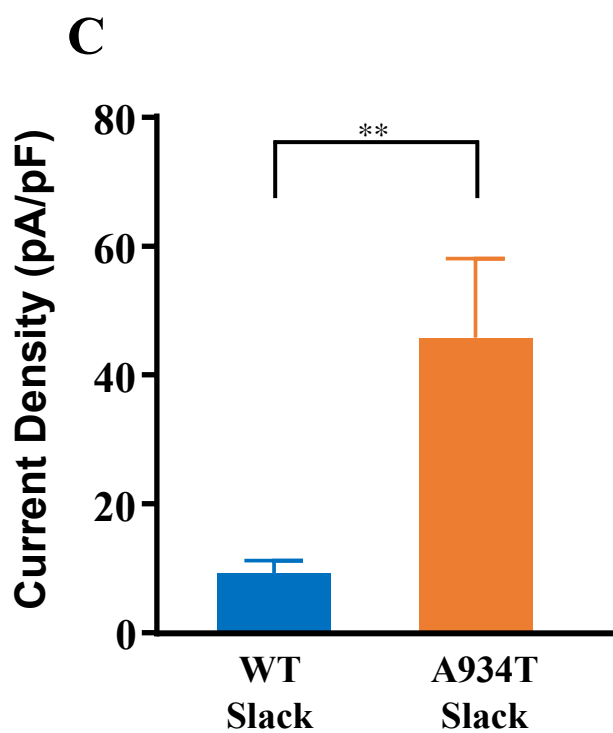
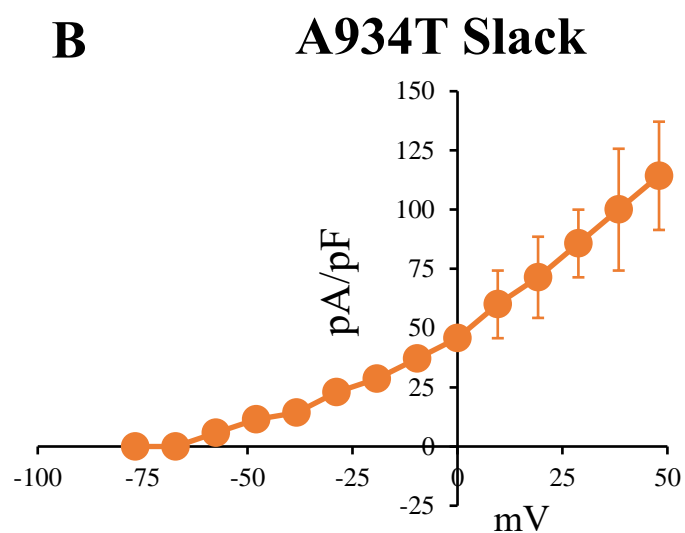
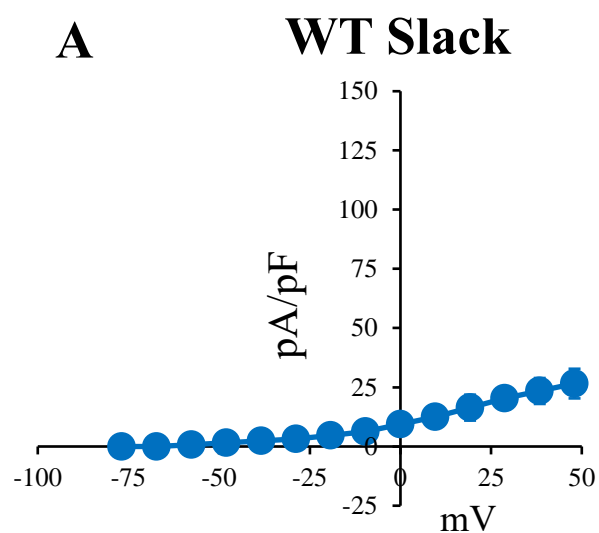


Figure 8: Voltage clamp electrophysiology of WT and A934T Slack channels. **A)** current density/voltage plot of WT Slack-expressing HEK293 cells, **B)** current density/voltage plot of A934T Slack-expressing HEK293 cells **C)** current densities comparing inhibition of WT and A934T Slack at 0 mV. Data expressed as mean \pm SEM, $n = 3$ or more cells. ** indicates $p < 0.0001$, student's t-test.

narrowed down our list based on similar structural characteristics. Additionally, we removed any compound was found to be a hit in another screen performed by our laboratory, since this would make it a nonselective, or having the ability to modulate multiple channels. This reduced our list to 147 hits to test for confirmation of activity in WT and A934T Slack cells. We observed that 114 of these compounds confirmed activity observed in the initial screen by decreasing fluorescence amplitude compared to VHL treated control wells in HEK293 cells expressing WT or A934T Slack channels. We then ranked hits based on their efficacy compared to that of 30 μ M quinidine. Nine compounds stood out as being the most interesting based on their efficacy compared to that of quinidine or their differential pharmacology, meaning they showed different activity against WT and mutant-Slack channels (**Table 2**).

Discussion

We developed and validated HTS compatible assays for WT and 3 representative MMPSI-associated mutant Slack channels. In a pilot screen we determined that WT and 1 of the disease-associate mutant channels offered sufficient coverage for large scale HTS. We screened WT and A934T resulting in identification of a plethora of potential Slack inhibitors. Our HTS identified a plethora of inhibitors, which we narrowed to 9 compounds. Of those, we identified 7 unique scaffolds, which refers to the core structure of a compound. Of these 7 scaffolds we chose to focus on the one exemplified by VU0606170 based on its top ranked inhibition of mutant-Slack channels. At this point we were fortunate to begin our collaboration with Dr. Kyle Emmitte, an expert medicinal chemist, who identified VU0606170 as a candidate for structure-activity relationship (SAR) studies, as it would be amenable to medicinal chemistry. These studies will be further discussed in **Chapter 4**. In **Chapter 3**, we describe our thorough characterization of VU0606170.

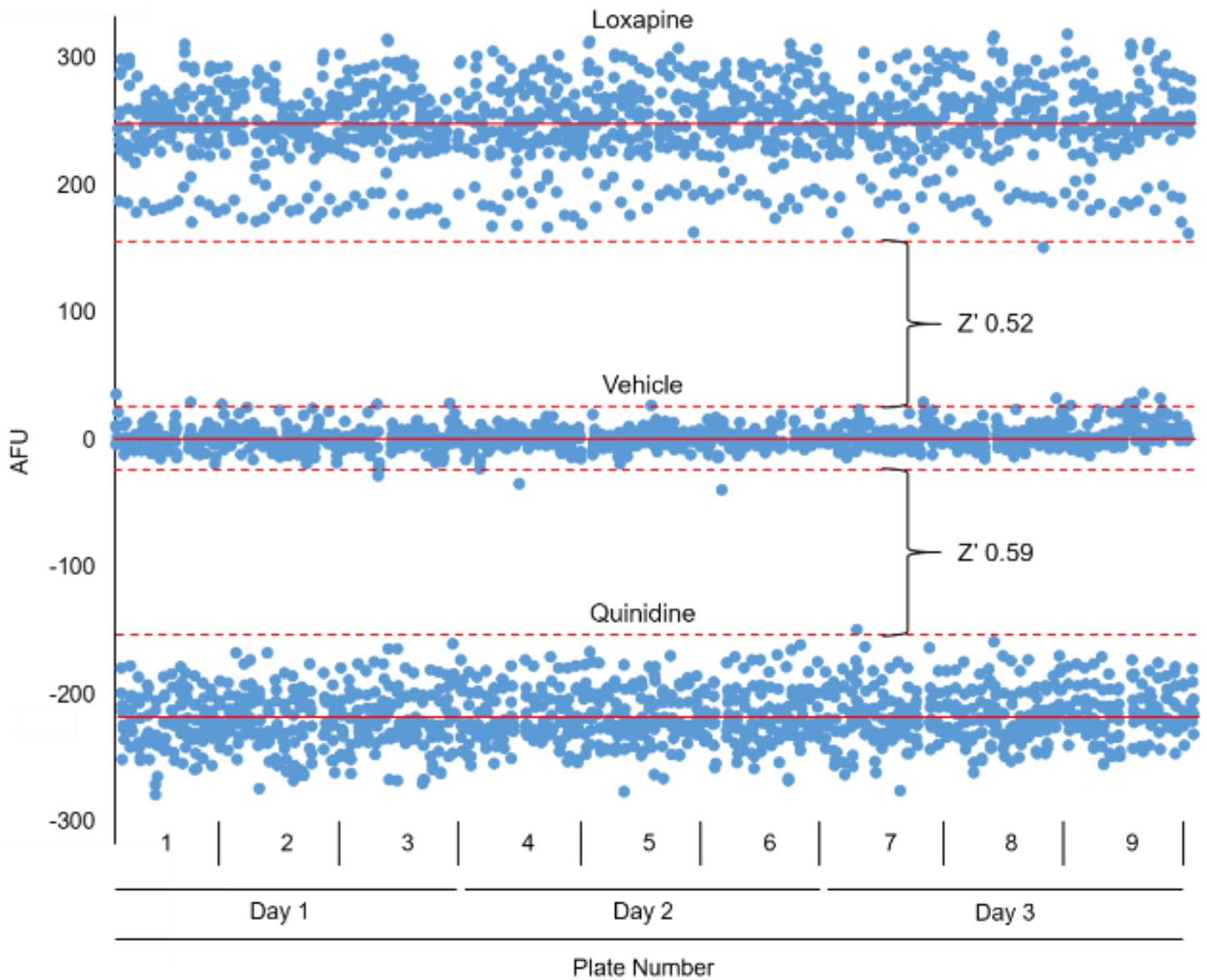


Figure 9: Multi-plate Z' validation. Three, 384-well plates were run per day on three consecutive days using the A934T Slack cell line. Raw fluorescence values were ratioed (F/F_0), vehicle control wells were averaged and the average vehicle control wave was subtracted from all waves. Vehicle, 30 μ M loxapine (activator) and 1 mM quinidine (inhibitor) were evenly spaced across the entire plate.

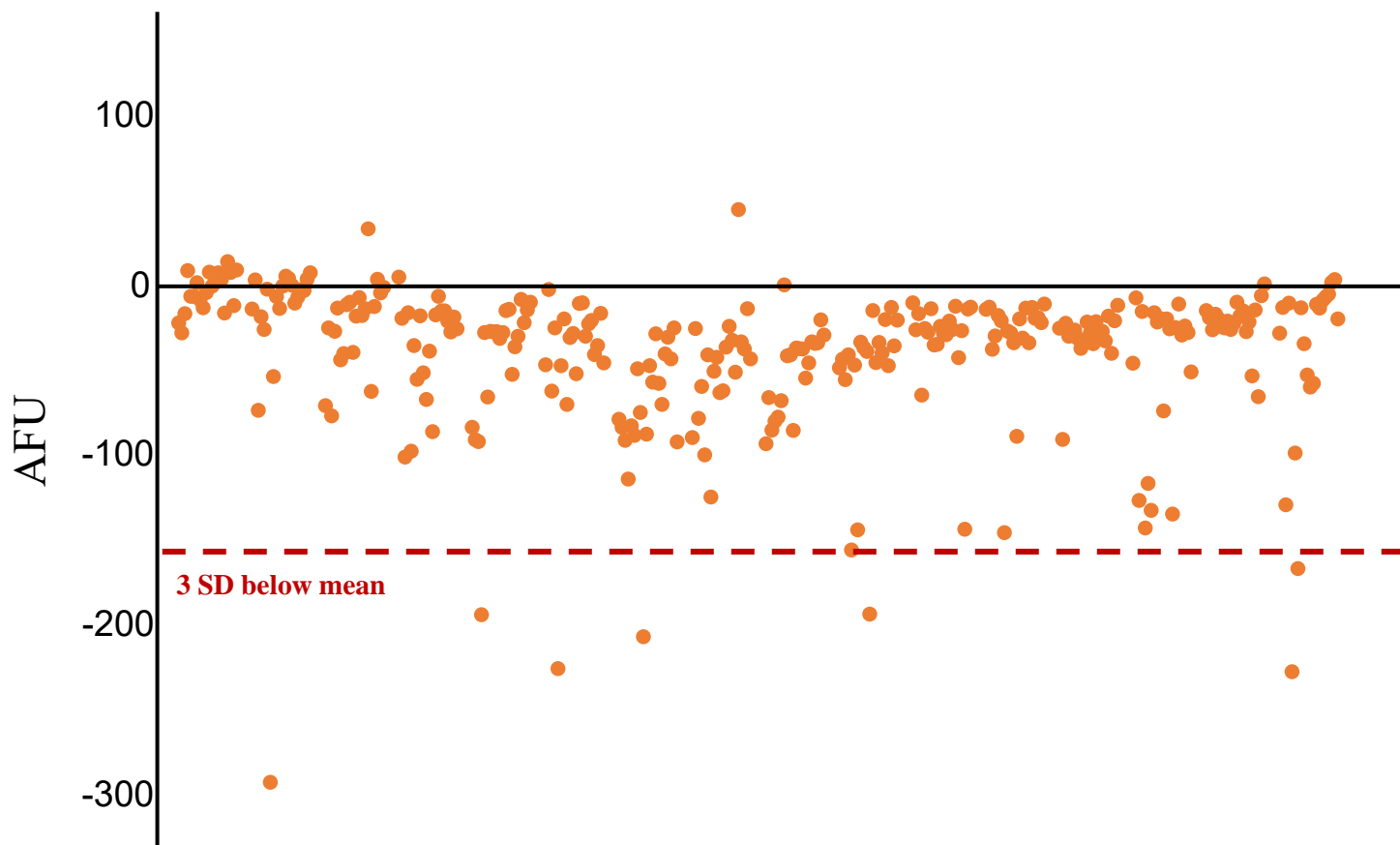


Figure 10: Representative screening plate data for A934T Slack-expressing HEK293 cells. Inhibitor amplitudes plotted as orange dots; hits are classified as being 3 standard deviations (SDs) below the mean of all wells of the plate indicated as being below the red dotted line.

CHANNEL	NUMBER OF HITS
Wild-type Slack	147
G288S Slack	101
R428Q Slack	56
A934T Slack	113

Table 1: Shown are the results of a 4,800-compound screening of WT and three Slack mutants in 384-well plates (60 plates). Hits were identified using an automated (WaveGuide) hit picking algorithm (see methods) supplemented with manual spot-checking. When hits from the WT Slack and A934T mutant Slack channels were combined they accounted for 100% of the hits detected using all four cell lines, therefore the 100,000-compound screen was performed using WT and A934T Slack expressing HEK293 cell lines.

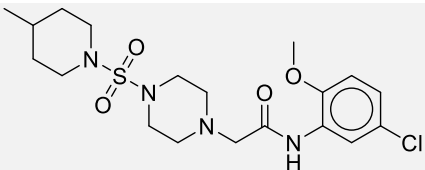
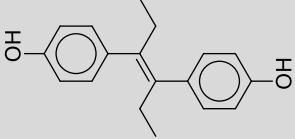
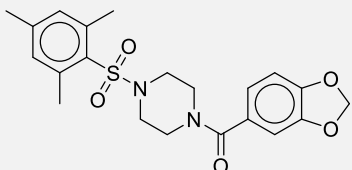
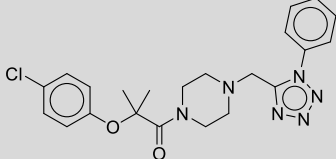
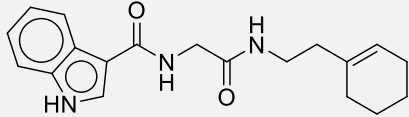
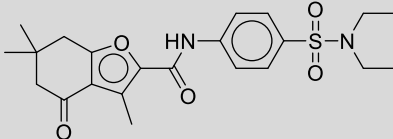
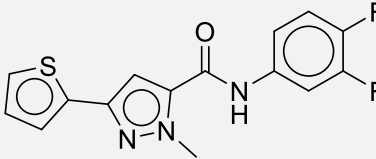
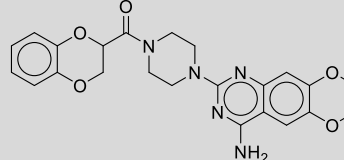
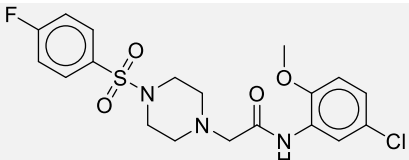
VU number	Structure	WT Slack	A934T Slack
VU0606170		+	++++
VU0243071		NA	++
VU0564634		Activator	++
VU0638793		++	++
VU0527923		NA	+++
VU0610694		+	++
VU0527672		NA	+++
VU0465278		+++	+++
VU0584662		NA	++

Table 2: 9 hits from the Slack channel HTS that inhibited mutant Slack channels or both WT and mutant Slack channels. Efficacy compared to efficacy of 30 μ M quinidine.

CHAPTER 3

CHARACTERIZATION OF VU0606170 ACTIVITY ON SLACK CHANNELS

Introduction

There is currently an unmet need for effective drug therapy to treat MMPSI and numerous other Slack-related epilepsies. Based on a preponderance of evidence for activating mutations in Slack playing a significant role in MMPSI and possibly other epilepsies, we undertook the task to discover selective small molecule Slack inhibitors which will provide the foundation for a novel therapeutic approach. Herein, we describe the evaluation of VU0606170, as an *in vitro* probe. Upon selecting VU0606170 as one of the most promising screening hits, as described in **Chapter 2**, we sought to investigate the activity of this small molecule more thoroughly. In brief, we confirmed the results from our initial screen and counter-screens, explored VU0606170's selectivity against a broader variety of ion channels, studied its ability to modulate Slack channels using EP, and finally investigated VU0606170's activity on the firing rate of cortical neurons *in vitro*. Throughout this chapter we detail the process and logic behind the evaluation of VU0606170's activity using Ti^+ flux assays, automated whole-cell voltage-clamp EP, and Ca^{2+} oscillations in an over-excited neuronal population.

To begin, Dr. Emmitte's lab resynthesized VU0606170 in order for us to confirm the identity and ensure the quality of the molecule. We used this newly synthesized batch of VU0606170 to measure the potency and efficacy of VU0606170 on WT and A934T Slack channels (**Figure 11**). We determined VU0606170's actual potency was much better than previously determined. We attribute this to the quality of compound tested originally from the Vanderbilt compound collection, as the sample could have contained impurities or that it may have degraded over time.

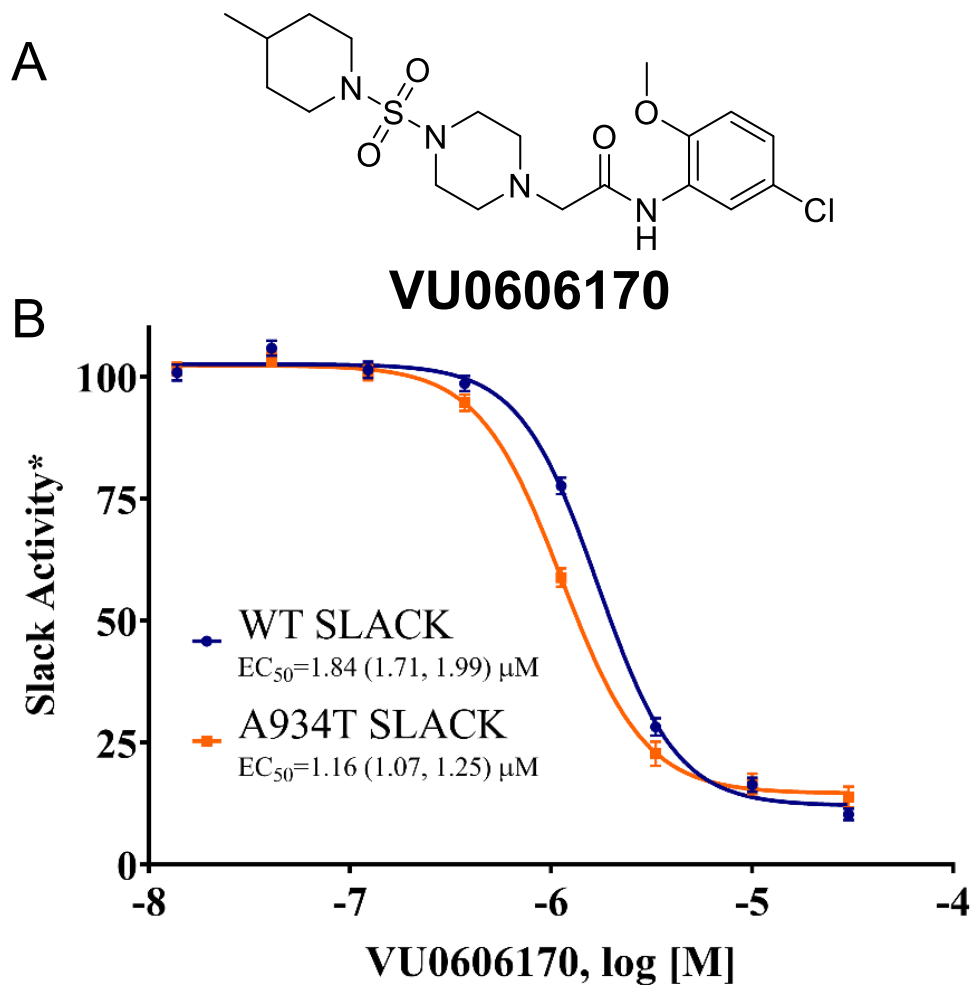


Figure 11: A) Structure of VU0606170. B) Concentration-response curves generated for WT Slack and A934T MMPSI-associated mutant Slack with VU0606170. CRCs arise from Tl^+ flux data obtained from monoclonal cell lines stably expressing WT Slack and A934T mutant Slack in ten separate trials. *VU0606170 data is normalized from E_{max} VU170 (30 μM). Data expressed as mean ± SEM, EC₅₀ (95% CI) values provided, n = 105.

We then investigated whether the activity of VU0606170 we observed in TI^+ flux was replicated using another approach. Patch clamp EP is often referred to as the “gold standard” way to measure the activity of ion channels due in part to the speed and accuracy with which the cellular membrane potential can be controlled. This control enables investigation of a compound’s effects on channel activity that are beyond what can be achieved using TI^+ flux assays. Examples include voltage- and time-dependent effects, effects on channel gating and ionic selectivity. Unfortunately, traditional patch-clamp is a slow, tedious, cell-at-a-time process. Therefore, we utilized automated “planar patch-clamp” electrophysiology to overcome many of the laborious aspects while maintaining many of the advantages of traditional patch-clamp. The SyncroPatch is a high throughput patch clamp instrument recording from up to 384 cells simultaneously, allowing us to more quickly test compounds.

We observed that the potency of VU0606170 measured using planar patch clamp was in close agreement with the value we obtained using the TI^+ flux technique (**Figure 12**). This finding not only confirms the ability of VU0606170 to inhibit Slack-mediated currents, it also lends confidence that the TI^+ flux technique can be utilized for routine measurement of compound potency to speed initial evaluations of newly synthesized compounds. However, additional compounds will need to be tested in both assays to ensure the correlation between rank order potencies and efficacies are consistent.

Furthermore, if it is discovered that potencies between WT and A934T Slack channels vary greatly, further studies will be needed to elucidate its mechanism of action, particularly if the compound exhibits use-dependent/state-dependent inhibition. State-dependent pharmacology refers to a compound preferentially interacting with particular physical state of the channel (e.g. activated or inactivated states). State-dependent pharmacology can result in a compound having drastically different potency depending on what state the channel predominantly occupies⁹⁸. State-dependence has been described in many antiarrhythmic drugs⁹⁸, local anesthetics^{99,100}, and AEDs^{101,102}. This may be of increasing importance if the gain-of-function attributed to Slack mutants is due to the channel being in an activated state for a longer period of time compared to that of WT Slack channels. This could result in a compound exhibiting very different potencies for mutant and WT Slack channels and this, in turn could affect the utility a molecule as a probe or therapeutic.

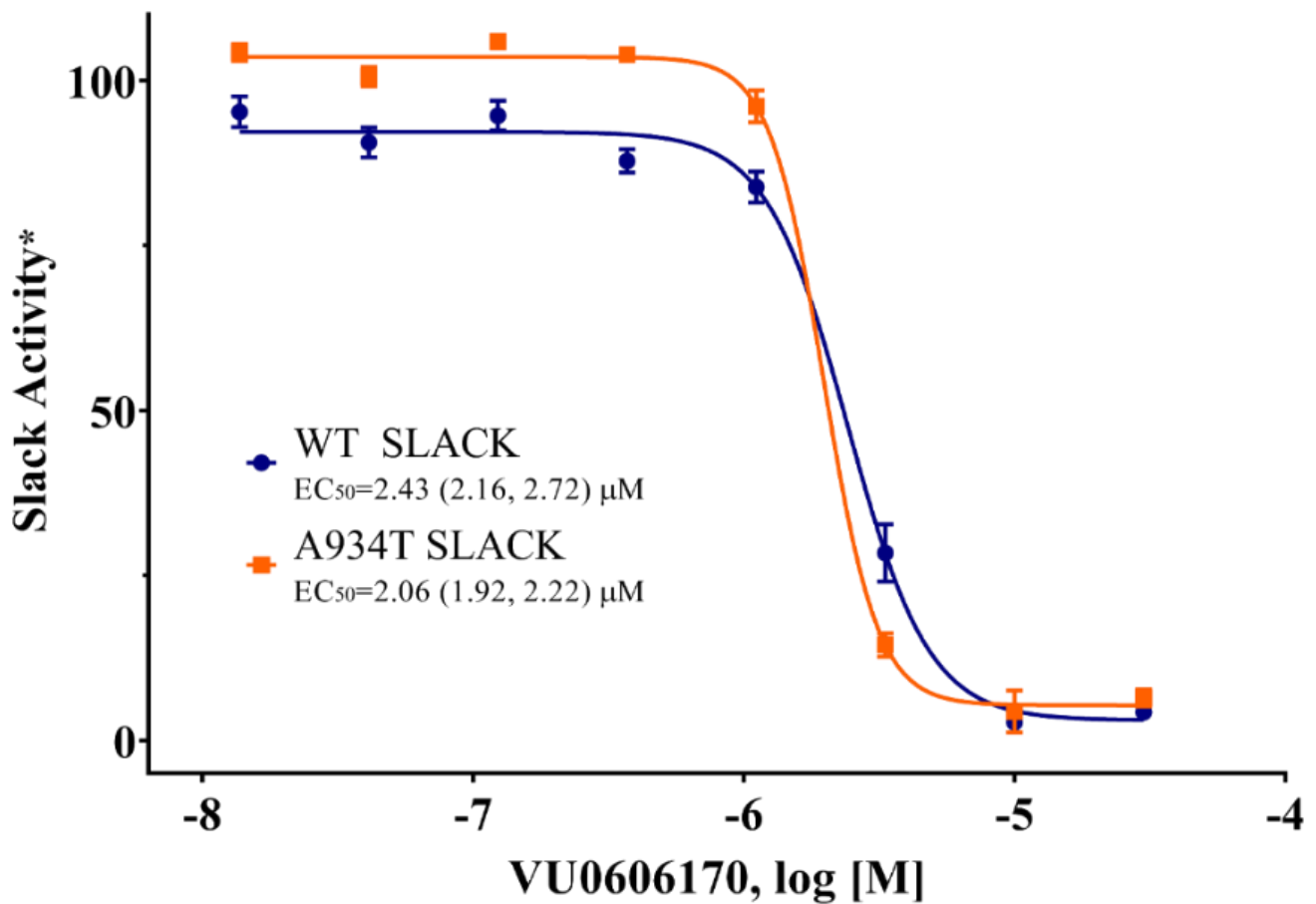


Figure 12: Whole cell automated patch-clamp recordings of WT and A934T Slack expressing HEK293 cells showed a concentration patch-clamp inhibition of currents, response normalized* to zero current by 300 μM (E_{max}) of quinidine, Data expressed as mean ± SEM, n = 12-41, cells per group.

In parallel, we investigated whether a structurally related compound, VU0849686, affected the activity of Slack channels using EP. Identification of this structurally related compound is described in **Chapter 4**. We predicted VU0849686 would be inactive due to a lack of efficacy in our TI^+ flux assay (**Figure 13**). Again, if we determine the effects of VU0849686 on Slack channels tracks between our TI^+ flux and EP assays we can continue to rely on TI^+ flux as the first-tier assay for the discovery and characterization of Slack channel modulators before advancing into more resource consuming experiments.

Next, we aimed to study the selectivity of VU0606170 among a variety of ion channels. We previously discussed how the lack of selectivity of known Slack inhibitors significant limit their use as probes to investigate pathophysiology of Slack channels (**Chapter 1**). We realize that it is not feasible to test its activity against every ion channel; therefore, we chose channels most closely related to Slack (Slick, Slo1, and Slo3) and representatives of major classes of K^+ channels (K_{ir} , K2P and K_{v}). We further evaluated the selectivity of VU0606170 on two ion channels associated with childhood epilepsies, $\text{Nav}1.7$ and $\text{Cav}3.2$. Mutations within the $\text{Nav}1.7$ channel account for 10% of all Dravet Syndrome cases¹⁰³. Dravet Syndrome, like MMPSI, is a severe form of early-onset epileptic encephalopathy with seizures beginning within the first year of life^{104,105}. Mutations within $\text{Cav}3.2$ channels have been linked to several epilepsies, including childhood absence epilepsy¹⁰⁶ and idiopathic generalized epilepsy¹⁰⁷. Additionally, bepridil, a known Slack inhibitor, is a potent inhibitor of $\text{Cav}3.2$ channels¹⁰⁸, making this a particularly relevant channel to assess selectivity of our compounds.

Drug-induced long QT syndrome is a cardiac safety issue that all drugs seeking approval must currently address^{109,110}. Since the long-term objective of this work is to develop new therapeutics for the treatment of MMPSI and other epilepsies we wanted to evaluate VU0606170's activity against hERG ($\text{K}_{\text{v}}11.1$) channels. hERG stands for the human Ether-à-go-go Related Gene, which is a cardiac K^+ channel essential for normal electrical activity in the heart¹¹¹. Inhibition of hERG channels can result in drug-induced long QT syndrome, a heart rhythm condition that can cause fast chaotic heartbeats and can attribute to fainting, seizures and even sudden death¹¹¹. Given that previously identified Slack inhibitors bepridil and quinidine both received black box warnings for their risk of sudden death due to QT prolongation^{112,113} associated with potent hERG inhibition we

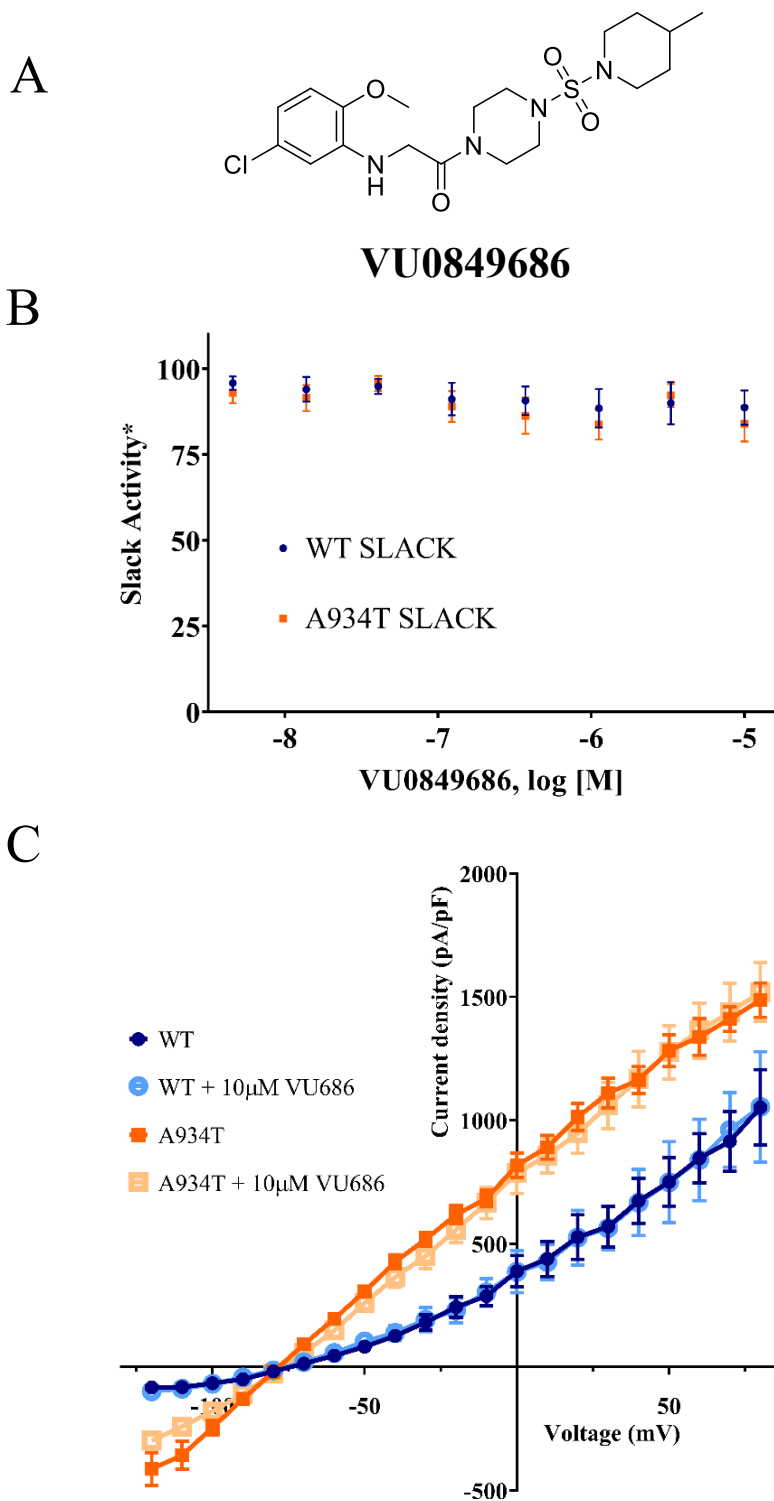


Figure 13: A) Structure of VU0849686 B) Concentration-response curves generated for WT Slack and A934T MMPSI-associated mutant Slack with VU0849686. CRCs arise from TI^+ flux data obtained from monoclonal cell lines stably expressing WT Slack and A934T mutant Slack in ten separate trials. *VU0849686 data is normalized from E_{max} VU170 (30 μM). EC_{50} values could not be calculated, $n = 6$. C) Whole- cell voltage dependent outward Slack current evoked by stepping from -120 mV to +80 mV in 10-mV increments in HEK-293 cells expressing WT or A934T Slack. The IV relationship for WT and A934T Slack were not affected by the addition of 30 μM VU0849686. Data expressed as mean \pm SEM, $n = 8$ -29.

investigated if our hits modulated hERG channels early in the hit evaluation process. Taken together these selectivity studies against this broad range of channels will give us insight into the utility of VU0606170 as a selective probe or if our efforts should focus on another hit scaffold.

The field of epilepsy research is moving from a primary focus on controlling seizures to addressing disease pathophysiology. This requires the implementation of resource- and time-consuming animal models of epilepsy which cannot support the testing of even a moderate number of compounds, in some cases less than one compound per week. Therefore, *in vitro* functional assays of epilepsy are utilized to close the gap between compounds identified through HTS and *in vivo* animal models of human neurological diseases. One such assay is the use of cultured primary neurons to measure epileptiform network activity. This activity is measured using fluorescent probes to monitor the fluctuations of intracellular Ca^{2+} levels that occur upon neuronal depolarization¹¹⁴. When neurons are plated at a high density, they form synaptic connections allowing the population of neurons to undergo synchronized depolarizations resulting in measurable Ca^{2+} oscillations^{114,115}. The rate of oscillations is increased by triggering factors such as incubation in low magnesium buffer, the resulting pattern of recurrent short discharges mimics the hyperexcitability observed during epileptiform activity^{114,116,117}. Furthermore, these spontaneous oscillations have been shown to be sensitive to many anti-epileptic drugs^{114,118} and thus might prove useful as a means to investigate the effect of selective Slack inhibition on neuronal activity.

We were fortunate to have labmate, Francis J. Prael, III, bring this technique to our laboratory. This assay enabled us to study the effect of VU0606170 in a more biologically relevant system. A decrease in the frequency and/or amplitude of the waveform resulting from hyper-synchronous Ca^{2+} oscillations is consistent with an anti-epileptic effect. Again, we investigated the effect of our inactive analog, VU0849686, in parallel. If VU0849686 was found to have no effect in this assay we can infer that the effect in neurons is likely due to Slack inhibition. Herein, we describe the extensive characterization of the first selective small molecule inhibitor of Slack channels.

Methods

Stable Cell Line Generation

WT and A934T cell lines were created as previously described in **Chapter 2**. HEK293 cells stably expressing human Slick channels were generated by transfecting a pCMV6-A-puro vector (Origene, Rockville, MD) with human KCNT2. HEK293 cells stably-expressing human $\alpha 1\beta 2$ Slo1, $\alpha 1\beta 3$ Slo1, and $\alpha 1\beta 4$ Slo1 channels were generated by transfecting a pCMV6-A-puro vector (Origene, Rockville, MD) with human KCNMA1 and a pcDNA3.1(+)/zeo vector (Genscript, Piscataway, NJ) with either human KCNMB2, human KCNMB3 or human KCNMB4, respectively. Similarly, HEK293 cells stably-expressing human $\alpha 1\beta 1$ Slo1 were generated by transfecting pCMV6-A-puro vector (Origene, Rockville, MD) with human KCNMA1 and pCMV6-Entry vector (Origene, Rockville, MD) with KCNMB1. HEK293 cells stably expressing human Kv2.1 were generated by transfecting pIR/ puroR1-1 vector with human KCNB1. HEK293 cells stably expressing human Slo3 and LRRC52 were generated by subcloning human Slo3 and LRRC52 into independent MCS of pBudCE4.1. Stably transfected monoclonal HEK293 cell lines expressing GIRK1/2^{91,119}, GIRK2^{91,119}, GIRK1/4^{91,119}, Na_v1.7⁸⁵, TREK2¹²⁰, hERG¹¹⁹ and Ca_v3.2¹²¹ were generated as previously described by our laboratory or collaborators. Monoclonal cell lines were generated as described in **Chapter 2**.

Synthesis and Purification

Air sensitive reactions were carried out under a nitrogen atmosphere (Airgas Catalog No. NI UHP300). The following solvents were employed for chemical reactions: dichloromethane (99.9%, Extra Dry, AcroSealTM, Acros Organics Catalog No. 610300010), *N,N*-dimethylformamide (Anhydrous, 99.8%, packaged under Argon in resealable ChemSealTM bottles, Alfa Aesar Catalog No. 43997), and tetrahydrofuran (Certified, Fisher Catalog No. T397-500). The following solvents were employed for working up reactions and/or extractions: ethyl acetate (Certified ACS grade, Fisher Catalog No. E145-20), diethyl ether (Anhydrous, BHT stabilized, Certified ACS grade, Fisher Catalog No. E138-4), dichloromethane (Stabilized/Certified ACS, Fisher Catalog No. D37-20), and

isopropyl alcohol (Certified ACS, Fisher Catalog No. A416P-4). Anhydrous sodium sulfate (Fisher Chemical Catalog No. S421-500) was employed for drying organic extracts. Thin layer chromatography (TLC) was conducted on glass plates coated with Silica Gel 60 F₂₅₄ from Millipore Sigma (Catalog No. 1057150001). Normal phase flash chromatography was carried out on either a CombiFlash[®] EZ Prep or CombiFlash[®] Rf+ automated flash chromatography system, both from Teledyne ISCO. Normal phase flash chromatography was carried out using RediSep[®] Rf normal phase disposable flash columns (40-60 micron) from Teledyne ISCO (Catalog Nos. 69-2203-304, 69-2203-312, and 69-2203-324) or SiliaSep normal phase disposable flash columns (40-63 micron) from SiliCycle, Inc. (Catalog No. FLH-R10030B-ISO04 or FLH-R10030B-ISO12). The following solvents were employed for TLC and normal phase chromatography: hexanes (Certified ACS grade, Fisher Chemical Catalog No. H292-20), ethyl acetate (Certified ACS grade, Fisher Catalog No. E145-20), dichloromethane (Stabilized/Certified ACS, Fisher Catalog No. D37-20), and methanol (HPLC grade, Fisher Catalog No. A452-4).

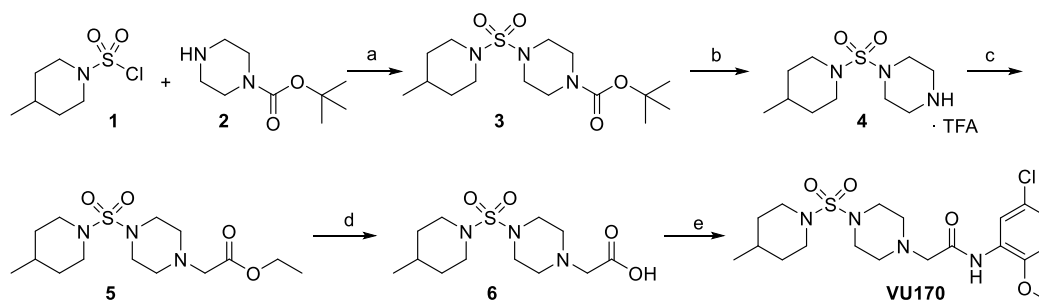
Characterization

All NMR spectra were recorded on a 300 MHz Bruker Fourier 300HD NMR spectrometer equipped with a dual ¹H and ¹³C probe with Z-Gradient and automatic tuning and matching, full computer control of all shims with TopShim[™], 24-sample SampleCase[™] automation system, and TopSpin[™] software. All NMR samples were prepared with either chloroform-d with 0.03% TMS (99.8+ atom % D, Acros Organics Catalog No. 209561000) or deuterium oxide (99.8 atom % D, ACROS Organics Catalog No. 166300100). ¹H and ¹³C chemical shifts are reported in δ values in ppm downfield. Data are reported as follows: chemical shift, multiplicity (s = singlet, d = doublet, t = triplet, q = quartet, br = broad, m = multiplet), integration, coupling constant (Hz). High resolution mass spectrometry was conducted on an Agilent 6230 Accurate-Mass Time-of-Flight (TOF) LC/MS with ESI source equipped with MassHunter Walkup software. MS parameters were as follows: fragmentor: 175 V, capillary voltage: 3500 V, nebulizer pressure: 35 psig, drying gas flow: 11 L/min, drying gas temperature: 325 °C. Samples were introduced via an Agilent 1260 Infinity UHPLC comprised of a G4225A HiP Degasser,

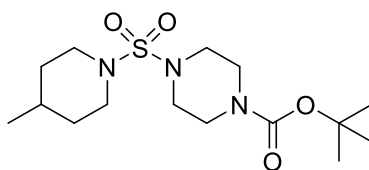
G1312B binary pump, G1367E ALS, G1316A TCC, and G1315C DAD VL+ with a 5 μ L semi-micro flow cell with a 6 mm path length. UV absorption was observed at 220 nm and 254 nm with a 4 nm bandwidth. Column: Agilent Zorbax SB-C18, Rapid Resolution HT, 1.8 μ m, 2.1 x 50 mm. Gradient conditions: Hold at 5% CH₃CN in H₂O (0.1% formic acid) for 1.0 min, 5% to 95% CH₃CN in H₂O (0.1% formic acid) over 5 min, hold at 95% CH₃CN in H₂O (0.1% formic acid) for 1.0 min, 0.5 mL/min.

Preparation of *N*-(5-chloro-2-methoxyphenyl)-2-((4-methylpiperidin-1-yl)sulfonyl)piperazine-1-yl)acetamide (VU170).

Compound **VU170** was prepared via the route pictured immediately below.

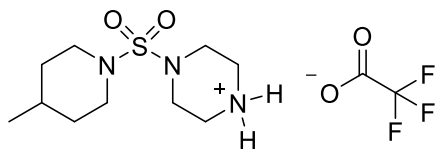


Reagents and conditions: (a) DIEA, CH₂Cl₂, 81%; (b) TFA, CH₂Cl₂, 97%; (c) Ethyl bromoacetate, K₂CO₃, DMF, 40 °C, 92%; (d) LiOH·H₂O, H₂O, THF, 99%; (e) 5-Chloro-2-methoxyaniline, HATU, DIEA, DMF, 48%.

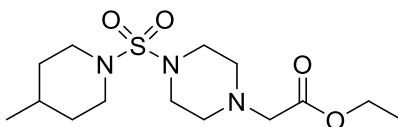


***tert*-Butyl 4-((4-methylpiperidin-1-yl)sulfonyl)piperazine-1-carboxylate (3).** 4-Methyl-piperidine-1-sulfonyl chloride (**1**) (1.00 g, 5.06 mmol, 1.0 eq) was dissolved in CH₂Cl₂ (5 mL), and added dropwise to a solution of *tert*-butyl piperazine-1-carboxylate (**2**) (1.04 g, 5.58 mmol, 1.1 eq) and DIEA (1.67 mL, 9.59 mmol, 1.9 eq) in CH₂Cl₂ (10 mL). The reaction was stirred for 16 h at room temperature. The reaction was quenched with water and extracted with CH₂Cl₂. The organic layer was dried over Na₂SO₄, filtered, and concentrated *in vacuo*. Purification by flash chromatography on silica gel afforded 1.43 g (81%) of the title compound as a white solid.

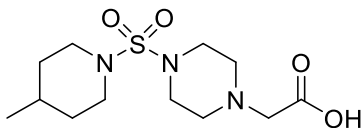
^1H NMR (300 MHz, CDCl_3) δ 3.67 (m, 2H), 3.48 (m, 4H), 3.18 (m, 4H), 2.79 (td, $J = 12.36, 2.55$ Hz, 2H), 1.69 (dd, $J = 12.84, 2.92$ Hz, 2H), 1.54 – 1.40 (m, 10H), 1.21 (ddd, $J = 24.87, 11.91, 4.23$ Hz, 2H), 0.95 (d, $J = 6.51$ Hz, 3H); ^{13}C NMR (75 MHz, CDCl_3) δ 154.44, 80.34, 46.77, 46.17, 33.74, 30.42, 28.37, 21.61 ppm.



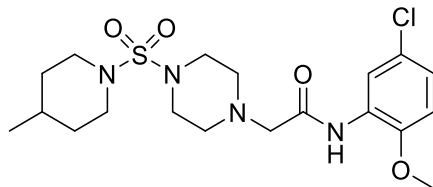
4-((4-Methylpiperidin-1-yl)sulfonyl)piperazin-1-ium 2,2,2-trifluoroacetate (4). Trifluoro-acetic acid (8 mL) was added dropwise to a solution of intermediate **3** (1.43 g, 4.12 mmol, 1.0 eq) in CH_2Cl_2 (8 mL) at 0 °C. The reaction was allowed to warm to room temperature and stirred for 2 h. The reaction was concentrated *in vacuo*, and the solid residue was triturated with diethyl ether to afford 1.44 g (97%) of the title compound as white solid. ^1H NMR (300 MHz, D_2O) δ 3.60 (m, 2H), 3.48 (m, 4H), 3.31 (m, 4H), 2.87 (td, $J = 12.36, 2.26$ Hz, 2H), 1.67 (dd, $J = 13.35, 2.04$ Hz, 2H), 1.49 (m, 1H), 1.14 (ddd, $J = 24.36, 12.42, 4.11$ Hz, 2H), 0.89 (d, $J = 6.55$ Hz, 3H); ^{13}C NMR (75 MHz, D_2O) δ 46.60, 42.97, 42.92, 33.06, 29.48, 20.76 ppm.



Ethyl 2-(4-((4-methylpiperidin-1-yl)sulfonyl)piperazin-1-yl)acetate (5). Intermediate **4** (1.40 g, 3.87 mmol, 1.0 eq), K_2CO_3 (1.17 g, 8.47 mmol, 2.5 eq), and DMF (20 mL) were added to a reaction vessel. Ethyl bromoacetate (0.86 mL, 7.8 mmol, 2.0 eq) was added dropwise, and the reaction was heated at 40 °C for 16 h. The reaction was quenched with water and extracted with ethyl acetate, and the organic layer was washed with brine. The combined organic layer was dried over Na_2SO_4 , filtered, and concentrated *in vacuo*. Purification by flash chromatography on silica gel afforded 1.20 g (93%) of the title compound. ^1H NMR (300 MHz, CDCl_3) δ 4.19 (q, $J = 7.14$, 2H), 3.67 (m, 2H), 3.31 (m, 4H), 3.26 (s, 2H), 2.79 (td, $J = 12.33, 2.47$ Hz, 2H), 2.66 (m, 4H), 1.68 (dd, $J = 12.90, 2.18$ Hz, 2H), 1.47 (m, 1H), 1.32 – 1.13 (m, 5H), 0.95 (d, $J = 6.50$ Hz, 3H); ^{13}C NMR (75 MHz, CDCl_3) δ 169.88, 60.80, 58.91, 52.24, 46.79, 46.11, 33.73, 30.39, 21.59, 14.21 ppm.



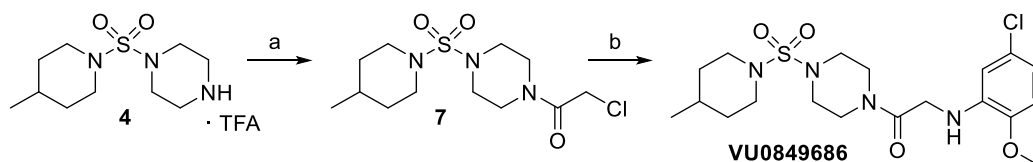
2-(4-((4-Methylpiperidin-1-yl)sulfonyl)piperazin-1-yl)acetic acid (6). A lithium hydroxide monohydrate (86 mg, 2.0 mmol, 2.0 eq) solution in H₂O (3 mL) was added dropwise to a solution of intermediate **5** (341 mg, 1.02 mmol, 1.0 eq) THF (4 mL). The reaction was stirred at room temperature for 1 h. Solvents were removed under vacuum, then the reaction pH was brought to ~3 by a gradual addition of 1 N HCl solution. The acidified mixture was extracted with a 3:1 mixture of CH₂Cl₂ and isopropyl alcohol, and the organic layer was washed with brine. The organic layer was dried over (Na₂SO₄), filtered, and concentrated *in vacuo*, to afford 307 mg (99%) of the title compound as a pale-yellow solid. ¹H NMR (300 MHz, D₂O) δ 3.52 (m, 2H), 3.17 (m, 4H), 2.94 (s, 2H), 2.79 (td, *J* = 12.33, 2.32 Hz, 2H), 2.52 (m, 4H), 1.61 (dd, *J* = 12.96, 2.06 Hz, 2H), 1.42 (m, 1H), 1.07 (ddd, *J* = 24.45, 12.51, 3.82, 2H), 0.82 (d, *J* = 6.55 Hz, 3H); ¹³C NMR (75 MHz, D₂O) δ 177.33, 61.18, 51.60, 46.58, 45.53, 33.04, 29.47, 20.75 ppm.



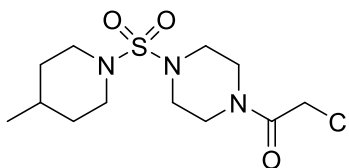
N-(5-chloro-2-methoxyphenyl)-2-(4-((4-methylpiperidin-1-yl)sulfonyl)piperazin-1-yl)acetamide (VU170). Intermediate **6** (50.0 mg, 0.164 mmol, 1.0 eq), HATU (91.7 mg, 0.241 mmol, 1.5 eq), and DIEA (50 μL, 0.29 mmol, 1.8 eq) were dissolved in DMF (2 mL), and stirred for 15 minutes. A solution of 5-chloro-2-methoxyaniline (26.5 mg, 0.168 mmol, 1.0 eq) in DMF (1 mL) was added. The reaction was stirred at room temperature for 16 hours. The reaction was quenched with water and extracted with ethyl acetate, and the organic layer was washed with brine. The combined organics were dried over (Na₂SO₄), filtered, and concentrated *in vacuo*. Purification by flash chromatography on silica gel afforded 34 mg (47%) of the title compound as a white solid. ¹H NMR (300 MHz, CDCl₃) δ 9.80 (br s, 1H), 8.43 (d, *J* = 2.56 Hz, 1H), 7.02 (dd, *J* = 8.67, 2.57 Hz, 1H), 6.79 (d, *J* = 8.75 Hz, 1H), 3.90 (s, 3H), 3.70 (m, 2H), 3.30 (m, 4H), 3.20 (s, 2H), 2.80 (td, *J* = 12.30, 2.56 Hz, 2H), 2.68 (m, 4H), 1.71 (dd, *J* = 12.96, 2.28 Hz, 2H), 1.50 (m, 1H), 1.23 (ddd, *J* = 24.81, 11.97, 4.01 Hz, 2H), 0.97 (d, *J* = 6.51 Hz, 3H);

^{13}C NMR (75 MHz, CDCl_3) δ 167.65, 146.78, 127.95, 126.08, 123.34, 119.48, 110.78, 61.75, 56.15, 52.74, 46.64, 46.45, 33.71, 30.42, 21.62 ppm; LCMS $R_T = 5.33$ min; HRMS, calculated for $\text{C}_{19}\text{H}_{30}\text{ClN}_4\text{O}_4\text{S}^+ [\text{M}+\text{H}]^+$, 445.1671; found 445.1684.

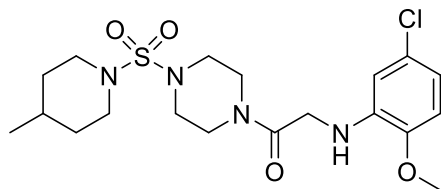
Preparation of 2-((5-chloro-2-methoxyphenyl)amino)-1-(4-((4-methylpiperidin-1-yl)sulfonyl)piperazin-1-yl)ethan-1-one (VU0849686). Compound **VU0849686** was prepared via the route pictured immediately below.



Reagents and conditions: (a) ClCOCH_2Cl , NEt_3 , DMF, 73%; (b) 5-chloro-2-methoxyaniline, K_2CO_3 , NMP, μwave , 130°C , 75 min, 27%.



2-Chloro-1-(4-((4-methylpiperidin-1-yl)sulfonyl)piperazin-1-yl)ethan-1-one (7). Intermediate **4** (400 mg, 1.11 mmol, 1.0 eq) and triethylamine (0.46 mL, 3.3 mmol, 3.0 eq) were dissolved in DMF (5 mL). Chloroacetyl chloride (0.18 mL, 2.2 mmol, 2.0 eq) was added dropwise, and the reaction was stirred for 16 hours at room temperature. The reaction was quenched with water, and extracted with ethyl acetate (2x). The combined organic layers were dried over Na_2SO_4 , filtered, and concentrated *in vacuo*. Purification by flash chromatography on silica gel afforded 0.264 g (73%) of the title compound. ^1H NMR (300 MHz, CDCl_3) δ 4.08 (s, 2H), 3.73 – 3.63 (m, 4H), 3.59 (m, 2H), 3.28 (m, 4H), 2.80 (td, $J = 12.36, 2.57$ Hz, 2H), 1.70 (dd, $J = 12.96, 2.31$ Hz, 2H), 1.50 (m, 1H), 1.22 (ddd, $J = 24.93, 12.18, 4.27$ Hz, 2H), 0.97 (d, $J = 6.51$ Hz, 3H); ^{13}C NMR (75 MHz, CDCl_3) δ 165.25, 46.82, 46.36, 46.03, 45.97, 41.71, 40.67, 33.71, 30.38, 21.59 ppm.



2-((5-chloro-2-methoxyphenyl)amino)-1-(4-((4-methylpiperidin-1-yl)sulfonyl)piperazin-1-yl)ethan-1-one (VU0849686). Intermediate **7** (50 mg, 0.15 mmol, 1.0 eq), 5-chloro-2-methoxyaniline (47.3 mg, 0.30 mmol, 2.0 eq), K_2CO_3 (62.2 mg, 0.45 mmol, 3.0 eq), and NMP (0.5 mL) were added to a G4 microwave reaction vial, and heated in the microwave (Anton Paar Monowave 200) at 130 °C for 75 minutes. The reaction was cooled to room temperature, quenched with water, and extracted with ethyl acetate (2x). The combined organic layers were dried over Na_2SO_4 , filtered, and concentrated *in vacuo*. Purification by flash chromatography on silica gel afforded 18 mg (27%) of the title compound as a white solid. 1H NMR (300 MHz, $CDCl_3$) δ 6.69 – 6.60 (m, 2H), 6.42 (d, J = 2.01 Hz, 1H), 5.41 (br s, 1H), 3.87 (s, 2H), 3.84 (s, 3H), 3.78 – 3.63 (m, 4H), 3.53 (m, 2H), 3.34 – 3.20 (m, 4H), 2.80 (td, J = 12.33, 2.32 Hz, 2H), 1.70 (dd, J = 12.84, 2.05 Hz, 2H), 1.49 (m, 1H), 1.22 (ddd, J = 24.51, 12.03, 3.88 Hz, 2H), 0.96 (d, J = 6.51 Hz, 3H). ^{13}C NMR (75 MHz, $CDCl_3$) δ 167.31, 145.81, 138.24, 126.06, 116.04, 110.12, 109.75, 55.71, 46.86, 46.30, 46.12, 44.88, 44.10, 41.65, 33.72, 30.38, 21.59 ppm; LCMS R_T = 5.69 min; HRMS, calc'd for $C_{19}H_{30}ClN_4O_4S^+$ $[M+H]^+$, 445.1671; found 445.1697.

Cell Culture Conditions and Preparation for Tl^+ and Ca^{2+} Flux Experiments

Cell culture and cell plate preparation for all Tl^+ and Ca^{2+} flux experiments described herein were conducted as described in **Chapter 2**.

Modifications to Tl^+ Flux Experiments for Counter-Screens

To better observe activity of certain channels, assay parameters were varied from as follows. Slo-expressing cells were tested using a Tl^+ stimulus buffer containing 3 μM ionomycin, which elevated intracellular Ca^{2+} and promoted channel activity, enabling activators and inhibitors to be identified. $K_v2.1$ -expressing cells were tested using a modified Tl^+ stimulus buffer (87.5 mM $NaHCO_3$, 37.5 mM $KHCO_3$, 1.8 mM $CaSO_4$, 1

MgSO₄, 5 mM glucose, 4 mM Tl₂SO₄, and 20 mM HEPES pH 7.3) containing an elevated K⁺ concentration to promote channel activity. Slick-expressing cells were tested using a modified Tl⁺ stimulus buffer (125 mM NaHCO₃, 1.8 mM CaSO₄, 1 MgSO₄, 5 mM glucose, 24 mM Tl₂SO₄, and 20 mM HEPES pH 7.3) containing an elevated Tl⁺ concentration to promote channel activity. GIRK-expressing cells were tested using a modified Tl⁺ stimulus buffer (125 mM NaHCO₃, 1.8 mM CaSO₄, 1 MgSO₄, 5 mM glucose, 4 mM Tl₂SO₄, and 20 mM HEPES pH 7.3) containing an elevated Tl⁺ concentration to promote channel activity. hERG-expressing cells were tested using a modified Tl⁺ stimulus buffer (145 mM K⁺-gluconate, 1.3 mM CaSO₄, 0.9 MgSO₄, 5.6 mM glucose, 11.25 mM Tl₂SO₄, and 10 mM HEPES pH 7.3) containing an elevated K⁺ concentration to promote channel activity. Controls for assay validation and comparison of VU0606170's efficacy were as follows: hERG – mibefradil^{122,123}, Nav1.7 – TC N-1752⁸⁵, GIRK – SCH-23390¹²⁴⁻¹²⁶. Quinidine was used as an inhibitor for all other channels. All controls were purchased through Sigma-Aldrich. Data was prepared for analysis as described in **Chapter 2**, with normalization of the data, followed by subtracting each wave by the mean of VHL-treated wells, and finally the minimum amplitude following Tl⁺ stimulus buffer addition is recorded. The efficacy of VU0606170 was expressed as a percent to E_{max} of each cell line's respective control using Excel (Microsoft, Redmond, WA).

T-type Calcium Channel Cell-based Ca²⁺ Flux Assay

For use in Ca²⁺ flux experiments, monoclonal HEK293 cells engineered to express Cav3.2 were grown and plated as described for Tl⁺ flux experiments. The Tl⁺ flux assays were conducted largely as previously described¹²⁷ with modifications described herein. Known Cav3.2 channel modulator bepridil, an inhibitor, was used as a control compound to compare efficacy of VU0606170. Cells were loaded with Calcium Dye Loading Solution consisting of Fluo-8AM (AAT Bioquest, Sunnyvale, CA) in Calcium Assay Buffer (140 mM NaCl, 5 mM KCl, 1 mM MgCl₂, 0.5 mM CaCl₂, 10 mM glucose, 10 mM HEPES pH 7.3) in ambient conditions. Dye loading solution was replaced with calcium assay buffer after a one-hour dye incubation at room temperature. Cell plates were then loaded onto the WaveFront Biosciences Panoptic (Franklin, TN). Data were acquired at 5

Hz (excitation 482 ± 35 nm, emission 536 ± 40 nm) for 10 s, at which time 20 μL /well of test compounds was added and allowed to incubate for 600 s. Next, 10 μL /well of Ca^{2+} stimulus buffer (65 mM NaCl, 5 mM KCl, 1 mM MgCl_2 , 50 mM CaCl_2 , 5 mM glucose, 10 mM HEPES pH 7.3) was added. Imaging was concluded after an additional 120 s. Fluorescence data was collected using WaveFront Biosciences WaveGuide and analyzed using Microsoft Excel. Data reported are the averages of at least 3 independent experiments. Compound activity was extracted from normalized and control-subtracted fluorescence waves generated over 720s of imaging. The wave for each well was normalized by dividing the average fluorescence from the first 5 s of imaging (F/F_0). Next, each wave was control-subtracted, and the minimum wave amplitude due to stimulus buffer addition was calculated. Efficacy of VU0606170 was calculated as a percentage of E_{max} bepridil using Excel.

Compound Plate Preparation for Concentration-Response TI^+ Flux Experiments

For all concentration response experiments, 10 μL aliquots of VU0606170 or VU0849686 dissolved in DMSO in 384-well, Echo qualified, low dead volume microplates (Labcyte, Sunnyvale, CA) were transferred using an Echo555 plate reformatter (Labcyte, Sunnyvale, CA) to generate 8-concentration, 3-fold dilution series in 384-well, round-bottom, polypropylene microplates (compound plates; Greiner, Monroe, NC). Compounds were similarly diluted with assay buffer to twice the final assay concentration. Compounds were used within 30 min of preparation, and the final DMSO concentrations were 0.6% (v/v), with the exception of 100 μM which had a final DMSO concentration of 1.9%. Our laboratory has found that DMSO concentrations $>10\%$ (v/v) inhibit Slack channels (unpublished data). DMSO concentrations were matched to 0.6% (v/v).

Data Analysis for Concentration-Response TI^+ Flux Experiments

ΔA values measuring VU0606170 or VU0849686 activity were normalized to an E_{max} of VU0606170 (30 μM) activity for experiments using Slack channel expressing cell lines. ΔA values for each compound at different concentrations were used to generate fits to a four-parameter variable-slope nonlinear regression model

using GraphPad Prism 8 (GraphPad Prism Software, San Diego, CA), data is presented as mean \pm standard error of the mean (SEM) with potencies (EC_{50}) given as mean (95% CI).

Cell Preparation for Automated Electrophysiology

Cells cultured as described for TI^+ flux experiments. These cells were grown to reach approximately 70% confluence on the day of experimentation. To prepare cells for automated electrophysiology, culture medium was removed from flasks, flasks were washed twice with PBS (Thermo Fisher Scientific, Waltham, MA) then treated using TrypLE Express (Thermo Fisher Scientific, Waltham, MA) for 15 min to dislodge cells, and single-cell suspensions were created through trituration with Dulbecco's Modified Eagle's Medium/Nutrient Mixture F-12 Ham (DMEM/F12) (Thermo Fisher Scientific, Waltham, MA). Cells were then centrifuged at 200xg for 4 minutes, supernatant was removed and cells were then diluted to 100,000 cells/mL with external solution (see below), and allowed to recover 30 minutes at 15°C while shaking on a rotating platform at 200 rpm.

Automated Patch-clamp Electrophysiology

Automated patch clamp recording was performed using the Syncropatch 768 PE platform (Nanion Technologies, Munich, Germany). Single-hole, 384-well recording chips with medium resistance (2-4 $M\Omega$) were used in this study. All whole-cell recordings were performed at room temperature. External solution contained (in mmol/L) 140 NaCl, 4 KCl, 1 $MgCl_2$, 2 $CaCl_2$, 10 HEPES. Internal solution contained (in mmol/L) 40 NaCl, 60 KF, 20 KCl, 1 $MgCl_2$, 10 EGTA, 20 HEPES, 0.5 Na-GTP, 1 NAD^+ (free acid) titrated to a pH of 7.2 and osmolarity of 300 mOsm/kg. Pulse generation and data collection were carried out with PatchController384 and DataController384 software (Nanion Technologies). Pulse generation was performed with PatchControl software, and whole-cell currents were acquired at 5 kHz and filtered at 1 kHz. Fast and slow capacitances were compensated using internal algorithms within PatchControl software. For I-V curves, whole-cell currents were measured from a holding potential of -80 mV and elicited with depolarizing steps (2000 msec) from -120 to +180 mV (10 mV steps). The cells were included for analysis if the whole-cell capacitance measured at -80 mV was

less than 100 pF, the holding current was not more negative than -500 pA, the seal resistance was greater than 0.5 G Ω , and the access resistance was less than 200 M Ω . Analysis of the effect of 10 μ M VU0606170 or 10 μ M VU0849686 on the current-voltage relationships of WT and A934 Slack cell lines was performed using repeated measures ANOVA with Bonferroni post hoc test with significance at $p = 0.05$. The mean current density at each voltage was compared to the current density following compound addition. Sources of variation were voltage, individual cells, treatment with compound and voltage x cells. The significance of the treatment with compound term is reported with significance level of $p=0.05$, and when significant is followed by post-hoc comparison of individual voltages corrected for multiple comparisons. Normality distribution was tested by Shapiro-Wilk test. Slack channel current response to varying doses of VU0606170 were normalized to “full block” of current by 300 μ M quinidine (Sigma-Aldrich, St. Louis, MO), data is presented as mean \pm standard error of the mean (SEM) with potencies given as mean (95% CI) generated using a four-parameter variable slope nonlinear regression model using GraphPad Prism 8.

Rat Husbandry

Time pregnant Sprague Dawley dams were purchased through Taconic Biosciences. Rats were housed at Vanderbilt University which is fully accredited by the Association for Assessment and Accreditation of Laboratory Animal Care. Experiments involving animals were approved by the Vanderbilt Institutional Animal Care and Use Committee; protocol number M1900117-00.

Primary Neurons

Cortical cultures were prepared from rat embryos at 17-19 days postcoitum. Brain cortex was collected in ice-cold HBSS and dissociated in 0.25% trypsin (Invitrogen) for 20 min at 37°C. Trypsin activity was then stopped by adding neuron plating medium containing neurobasal (ThermoFisher), 1% penicillin-streptomycin (Sigma Aldrich), 2% B27 (ThermoFisher), 0.25% glutamax (ThermoFisher) and 10% normal horse serum (Invitrogen). Following trypsin inactivation, tissue was pelleted using centrifugation for 5 min at 100xg. Supernatant was

removed via vacuum aspiration, then 1 mL of neuron plating medium per 3 embryos was added in order to transfer to a 1.5 mL microcentrifuge tube. Cells were titrated to ensure a single cell suspension. Viable cells were counted and diluted to 50,000 cells/well in neuron plating medium for plating in poly-L-lysine coated 96-well plates (Greiner). Four hours after plating, the medium was changed to serum free maintenance medium based on neurobasal-B27. Three days after plating, half of the medium was renewed and the cultures were maintained with two media changes per week. For all pharmacological studies, cultures were used after 14 days *in vitro* (DIV).

Calcium Imaging of Primary Neurons

Incubation with Fluo-8 was performed according to recommendations from the manufacturer (AAT Bioquest, Sunnyvale, CA). Briefly, a vial of Fluo-8 AM was resuspended in 50 μ L of Pluronic F-127 6.67% in DMSO then dissolved into HBSS (Corning, Corning, NY), HEPES 20 mM (Corning, Corning, NY) containing 100 μ L probenecid (Sigma-Aldrich, St. Louis, MO) and cultures were incubated in 90 μ L of Fluo-8 per well for 1 hour at room temperature. For imaging, the Fluo-8-containing HBSS was replaced by 100 μ L of Neuron Assay Buffer consisting of calcium and magnesium-free HBSS (Corning, Corning, NY) supplemented with 0.1 M MgCl₂ (Sigma-Aldrich, St. Louis, MO) and 2 mM CaCl₂ (Sigma-Aldrich, St. Louis, MO). Cultures were imaged in this medium.

For calcium imaging, cell plates were loaded onto the WaveFront Biosciences Panoptic (Franklin, TN). Data were acquired at 5 Hz (excitation 482 ± 35 nm, emission 536 ± 40 nm) for 10 m, at which time 50 μ L/well of test compounds was added and imaged for an additional 20 m. Matching vehicles (0.1 to 0.3% final DMSO in Neuron Assay Buffer) were used to monitor a potential injection effect in the calcium oscillations read out. Changes in calcium oscillations in response to compound treatment were quantified by comparing calcium spike rates 5m before compound addition to spike rates for 10m after compound incubation for 10m. Our data analysis, which was engineered by our labmate Francis J. Prael, III, workflow consisted of: (a) trace flattening, (b) separation of baseline and post-addition datasets, (c) spike counting, and (d) spike rate calculation and normalization. (a) trace flattening: to normalize for baseline drift and facilitate the counting of calcium spikes,

fluorescent traces were flattened by calculating a smoothed version of each trace, and then subtracting the smoothed trace from the original trace. Specifically, smoothed traces were calculated using a mean filter generated by iterative convolutions of a 100-frame and a 200-frame averaging kernel over the timeseries data; afterwards, the smoothed trace was subtracted from the overlapping region of the original trace. (b) data set splitting: flattened traces were separated into baseline (pre-addition) and post-compound addition segments by hand. (c) spike counting: peaks were counted separately in the baseline and post-compound addition segments via counting local maxima by comparison to neighboring values. A threshold and minimum distance between peaks were manually set to prevent noise from being counted as a calcium oscillation, and to prevent a single peak from being counted multiple times, respectively. (d) spike rate counting and normalization: spike rates were calculated by dividing the calcium spike counts over time for each dataset. Lastly, post-addition spike rates were normalized as a percentage of the baseline spike rate. Data is presented as mean \pm standard error of the mean (SEM) with potencies given as mean (95% CI) generated using a four-parameter variable slope nonlinear regression model using GraphPad Prism 8. 30 μ M GABA was used as an inhibitor control to ensure plate to plate reproducibility¹¹⁴.

Immunofluorescence Staining of Primary Neurons

Cortical cultures plated as described for calcium imaging experiments were used for immunofluorescence after 14 days *in vitro* (DIV). Subsequently, medium was removed, and cells were washed 3 times with PBS (Thermo Fisher Scientific, Waltham, MA) and fixed with 4% paraformaldehyde for 20 min at RT. Following fixation cells were washed with PBS then permeabilized with 0.3% Triton X-100 (Sigma-Aldrich, St. Louis, MO) in PBS for 15 m. Again, cells were washed 3 times with PBS prior to blocking with 10% bovine serum albumin (BSA) (Sigma-Aldrich, St. Louis, MO) in PBS for 45 m. Cells were treated with primary antibody against Slack (7 μ g/mL, Origene, TA326566) and GAD65/GAD67 (1:50, Thermo Fisher Scientific, PA5-36080), VGLUT2 (1:100, Sigma-Aldrich, ZRB1170), or GFAP (1:100, Sigma-Aldrich, ZRB2383) in 1% BSA in PBS at 4 °C overnight. Following 3 washes with PBS cells were incubated with goat anti-mouse (1:500, Li Cor, 926-68070)

and goat anti-rabbit (1:500, Thermo Fisher Scientific, A21428) secondary antibodies for 45 minutes at room temperature. Finally, cells were washed with PBS 3 times and stained with Hoechst (1:5,000, Thermo Fisher Scientific, H3570). Images were obtained using ImageXpress Micro XLS system.

Results

Dependence of VU0606170 Activity on Slack Expression

For these experiments, we utilized VU0606170 (**Figure 11**) at various concentrations in order to generate concentration-response curves (CRCs). This enabled measurement of potency and efficacy on a variety of cell types. First, we characterized the ability of VU0606170 to inhibit Slack channels in a dose-dependent manner using TI^+ flux assays. 30 μM VU0606170 was able to inhibit WT and A934T Slack channels to the same extent as 1mM quinidine. Therefore, 30 μM VU0606170 was used as the E_{max} of VU0606170 for normalization of all compound activity from this point forward. VU0606170 inhibited Slack channels in a concentration-dependent manner, with a measured potency (EC_{50}) of 1.84 μM with 95% confidence intervals (95% CI) of (1.71, 1.99) for WT Slack and 1.16 μM (1.07, 1.25) for A934T Slack channels (**Figure 11**). Representative examples of the raw TI^+ flux assay fluorescence traces used to generate concentration response curves are shown in **Figure 14**. Additionally, we tested a structurally similar molecule, VU0849686, and determined it was inactive in our Slack TI^+ flux assay (**Figure 13**).

Influence of VU0606170 on Slack Channels Current-Voltage Relationship Using Automated Whole-cell Voltage-clamp Electrophysiology

After establishing VU0606170's efficacy in TI^+ flux, we further explored the Slack-inhibiting properties of VU0606170 using automated whole-cell voltage-clamp electrophysiology. Here, we utilized the same engineered HEK293 cell lines expressing either WT or A934T Slack channels used for TI^+ flux assays. Currents were recorded in 21 increments of 10 mV, from -120 mV to +80 mV. First, we investigated differences between

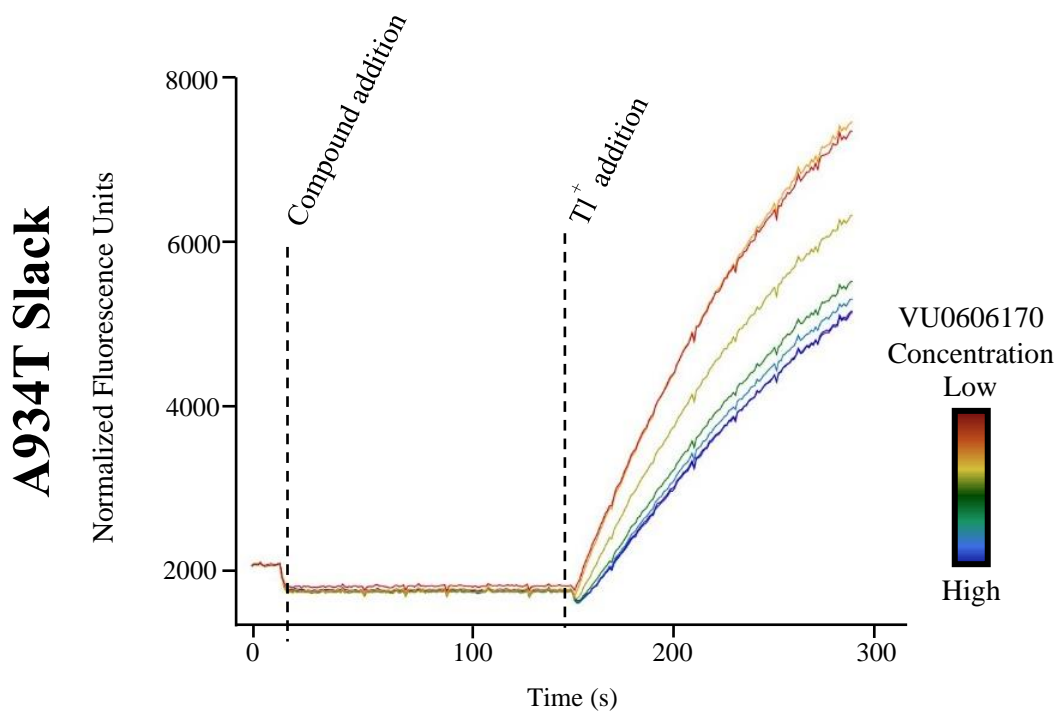
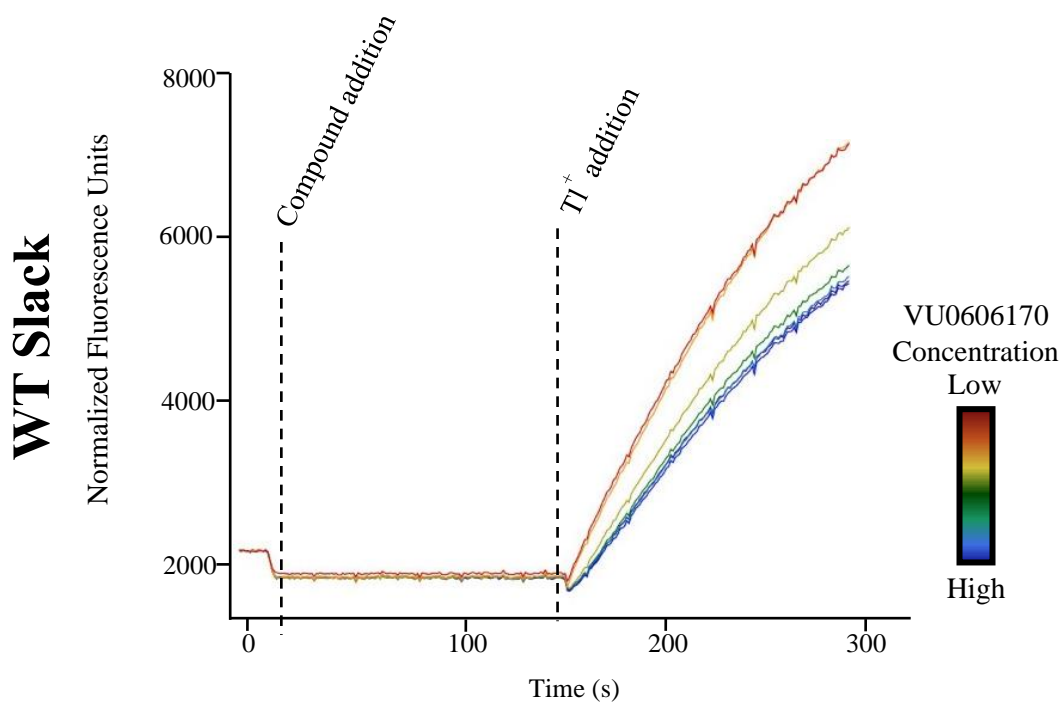


Figure 14: Concentration-dependent efficacy of VU0606170 measured using Tl⁺ flux. VU0606170 concentrations begin at 100 μ M and descend in 3-fold steps. Time of compound and Tl⁺ addition represented as dotted lines.

the two channels. We noted the current density for A934T was significantly larger than WT current densities (**Figure 15**). This result is consistent with our manual patch-clamp data (**Figure 8**) and previous reports^{47,72}. We then investigated the channels' ability to be modulated by bepridil³⁷ and quinidine^{37,69,72}. In agreement with previous reports³⁷, the presence of 10 μ M bepridil reduced current amplitudes of WT or A934T-Slack equal to that of quinidine at 10-fold the concentration. Taken together, these two results gave us confidence we were measuring Slack currents in our EP assay. We then investigated the effect of VU0606170 on the I-V relationship of WT and A934T Slack channels. Recordings demonstrated that inward and outward Slack currents were reduced in the presence of VU0606170 (**Figure 15a, b**). The fold-decrease in current magnitude over basal values upon inhibition with VU0606170 was greater for A934T channels than WT Slack channels (**Figure 15c**).

Additionally, a concentration-response curve of VU0606170 was performed on parallel cell samples, with estimated 50% block of the channel at 2.43 μ M (2.16, 2.72) for WT-Slack and 2.06 μ M (1.92, 2.22) A934T Slack (**Figure 12**). Response was normalized to zero current, or full block, by E_{\max} quinidine. Again, we tested our structurally similar analog, VU0849686, which revealed no change in the I-V relationship of either WT or A934T Slack currents (**Figure 13**). These data corroborated the results observed in our TI^+ flux assay, that VU0606170 activity was concentration-dependent on Slack channels.

Characterization of VU0606170 Selectivity Among Slo Channels

We aimed to determine whether VU0606170 activity was specific to Slack channels or whether this molecule was also capable of inhibiting other channels. We first examined its effect against other members of the *Slo* family of K^+ channels, as they are the most closely structurally related which could increase the risk of the compound being active against these channels. As discussed in **Chapter 1**, the *Slo* family consist of four distinct Slo1 (Maxi-K, BK) channels, Slo1 $\alpha 1/\beta 1$, Slo1 $\alpha 1/\beta 2$, Slo1 $\alpha 1/\beta 3$, Slo1 $\alpha 1/\beta 4$, along with Slick (Slo2.2) and Slo3. We chose to test all 4 Slo 1 channels since each subunit confers a unique expression pattern, change in activation kinetics of the channel and have been identified as individual pharmacologic targets. The $\beta 1$ subunit is primarily expressed in smooth muscle¹²⁸⁻¹³⁰, $\beta 2$ subunit is expressed in the adrenal glands and brain and is the least well

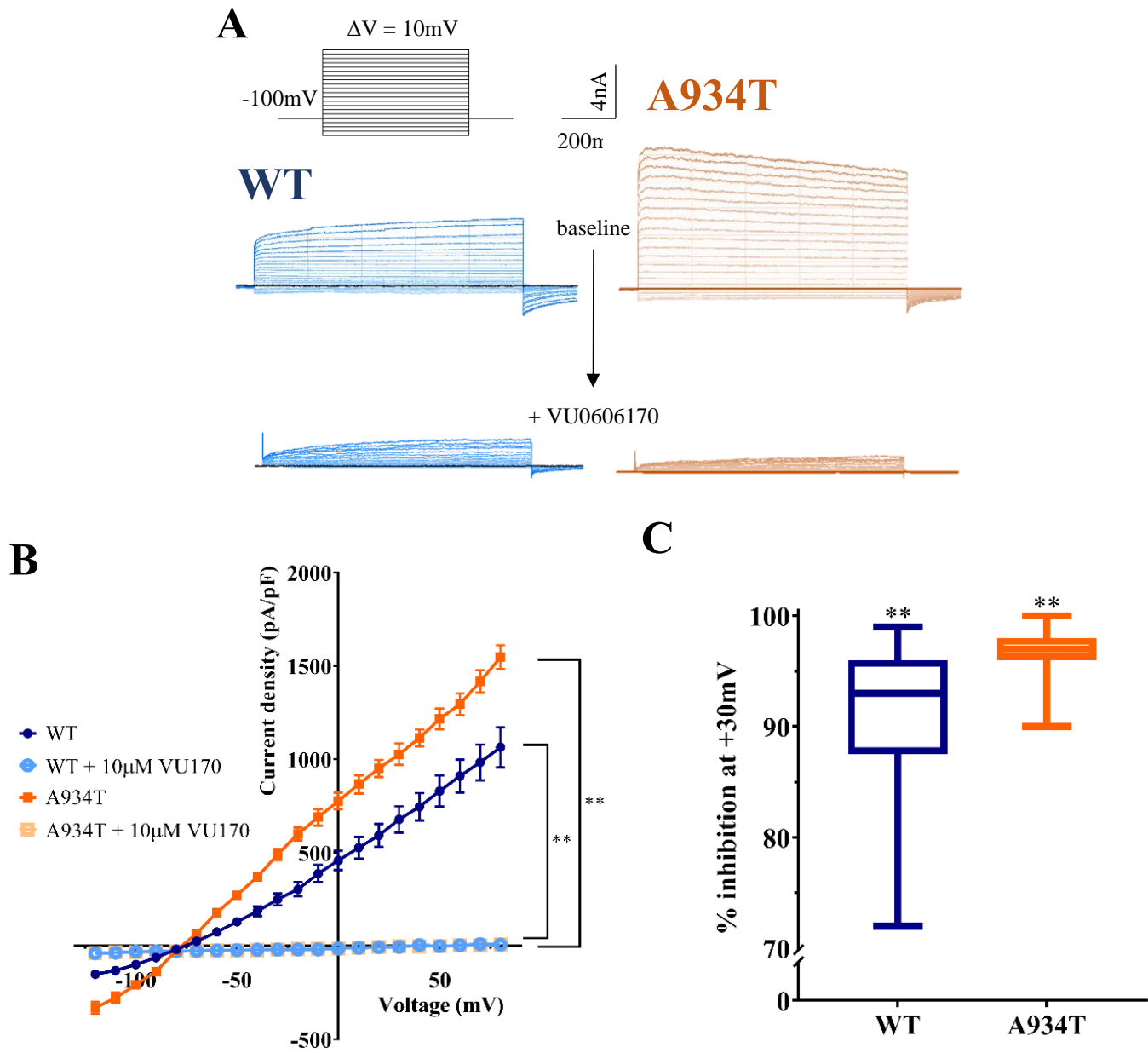


Figure 15: A) Representative whole-cell currents evoked by stepping from -120 mV to $+80\text{ mV}$ in 10-mV increments in HEK-293 cells expressing WT or A934T Slack at baseline and in the presence of $10\ \mu\text{M}$ VU0606170. B) Voltage-dependent outward WT is significantly blocked by $10\ \mu\text{M}$ VU0606170 at all voltages $> -40\text{mV}$ (data expressed as mean \pm SEM, $n = 51$, ** indicates $p < 0.0001$, two-way ANOVA with Bonferroni's post-hoc tests) and A934T Slack current is significantly blocked by $10\ \mu\text{M}$ VU0606170 at all voltages $> -40\text{mV}$ (data expressed as mean \pm SEM, $n = 109$, ** indicates $p < 0.0001$, two-way ANOVA with Bonferroni's post-hoc tests). The addition of $10\ \mu\text{M}$ VU0606170 essentially blocks all outward K^+ current making both compound addition curves overlap. C) Percent Slack current blocked by $10\ \mu\text{M}$ VU0606170 at $+30\text{mV}$ (data expressed as mean \pm SEM, $n = 50\text{-}109$, ** indicates $p < 0.0001$, Mann-Whitney U test).

defined of all the β -subunits¹³⁰, $\beta 3$ is detected in the testis, pancreas and spleen^{131,132} and $\beta 4$ is primarily expressed in the brain^{131,133,134}. This is an especially relevant selectivity target for our studies because selective inhibition of the Slo 1 $\beta 4$ subunit has been reported to reduce the neuronal spiking frequency in hyperexcitable neurons¹³⁵. Additionally, there is evidence that Slick and Slack can form heterotetramers^{32,136-138}, as such we tested for VU0606170 activity in HEK293 cells expressing Slick-Slack heterotetramers. Using Ti^+ flux assays, we observed VU0606170 did not affect Ti^+ influx on HEK293 cells expressing any of the other Slo family members (**Table 3**).

Characterization of VU0606170 Selectivity Among a Broad Variety of Channels

To further investigate the selectivity of VU0606170 we chose representative channels of major classes of K^+ channels (K_{ir} , $\text{K}_{2\text{P}}$ and K_{V}). We determined that VU0606170 was inactive against $\text{K}_{\text{ir}3.1/\text{K}_{\text{ir}3.2}$ (GIRK1/2), $\text{K}_{2\text{p}10.1}$ (TREK2) and $\text{K}_{\text{V}2.1}$ channels in engineered HEK293 cells expressing the channels of interest. We then assessed VU0606170's activity against the neuronal Na^+ channel, $\text{Na}_{\text{V}1.7}$ due to its implications in epilepsies and against $\text{Ca}_{\text{V}3.2}$ channels which have been linked to epilepsies. Additionally, the known Slack inhibitor, bepridil is a potent inhibitor of $\text{Ca}_{\text{V}3.2}$ channels. VU0606170 was inactive against $\text{Ca}_{\text{V}3.2}$ and $\text{Na}_{\text{V}1.7}$.

While both typical Slack inhibitors, bepridil and quinidine inhibit hERG, which lead to their black box warning for the development of long QT syndrome; we determined VU0606170 inhibited hERG, channels only 37% compared to E_{max} of bepridil (**Figure 16**). Proven strategies for further decreasing hERG inhibition in this scaffold may be possible using medicinal chemistry to modify the structure to retain Slack inhibition while reducing activity against hERG channels. Selectivity results for VU0606170, including efficacies at $10\mu\text{M}$, are listed in **Table 3**.

Investigation of Slack Channel Expression in Rat Cortical Neurons

We then investigated VU0606170's effect on Ca^{2+} oscillations mimicking epileptiform activity. Baseline Ca^{2+} oscillations, or spike rate, was recorded for 10 min prior to compound addition. Following compound

Cell Line	10 μ M VU170 Efficacy
Slack, WT ^A	76% (73%, 79%)
Slack, A934T ^A	87% (86%, 89%)
Slack, G288S ^A	82% (78%, 85%)
Slack, R428Q ^A	87% (80%, 93%)
Slick, WT	Inactive
Slo α 1/ β 1	Inactive
Slo α 1/ β 2	Inactive
Slo α 1/ β 3	Inactive
Slo α 1/ β 4	Inactive
Slo3	Inactive
GIRK $\frac{1}{2}$	Inactive
K _v 2.1	Inactive
TREK 1	Inactive
hERG ^B	37% (33%, 41%)
Nav1.7	Inactive
Ca _v 3.2	Inactive
HEK293, UT	Inactive

Table 3: VU0606170 was tested on an array of targets expressed in HEK293 cells. VU0606170 inhibits both WT and mutant Slack channels. VU0606170 inhibits hERG, however; 10 μ M VU0606170 is only 37% effective in blocking hERG in Tl⁺ flux assays. The compound was inactive on all other listed targets. Data is the results of a minimum of three separate trials and a minimum of three replicates per trial; mean (95% CI).

^A Normalized to maximum VU0606170 activity;

^B Normalized to maximum bepridil activity

addition, data were collected for an additional 20 minutes in order to allow for stabilization of oscillations (**Figure 17a**). VU0606170 lead to a decrease in the mean spiking rate with maximum inhibition of 55.58% (50.90, 60.27), and a mean (95% CI) EC₅₀ of 3.70μM (2.80, 4.92) (**Figure 17b**). In order to further explore whether the anti-epileptic activity of VU0606170 was due to inhibition of Slack activity, we investigated the effects of VU0849686 on neuronal Ca²⁺ oscillations. In these studies, we observed a lack of VU0849686 effect on the mean spiking rate (**Figure 18**). Taken together these observations are consistent with the concept that inhibition of Slack currents is able to produce anti-epileptic activity in over-excited neuronal populations.

Discussion

In this chapter, we describe the characterization of the effects of VU0606170 on Slack activity using whole-cell voltage-clamp EP and fluorescent-based assays to help evaluate its potential utility as a Slack-selective small-molecule probe. We observed good correlation with the potency and efficacy for VU0606170 measured using TI⁺ flux and voltage-clamp EP, providing encouragement that TI⁺ flux assays should continue to be used as a first-tier assay for the discovery and characterization of Slack channel inhibitors. We also found that potency of VU0606170 at WT and mutant Slack channels were very similar suggesting that VU0606170 does not appear sensitive to affects the mutation has on the structure and activity of the channel. Additionally, we found that VU0606170 was highly selective for inhibiting Slack channels compared to other channels tested. Of note it did not have activity against the Slick/Slack heterotetrameric channel, providing evidence that this channel could be a pharmacologically distinct target. While VU0606170 did inhibit hERG, its maximum inhibition was significantly lower than that of bepridil. The separation between VU0606170 and hERG activity is promising; however, we would ideally like to see > 100-fold separation between the EC₅₀ of a compound when measured in Slack and hERG channels. Proven strategies for further blunting hERG inhibition in this scaffold may be possible through medicinal chemistry efforts¹³⁹, which will be discussed in **Chapter 4**.

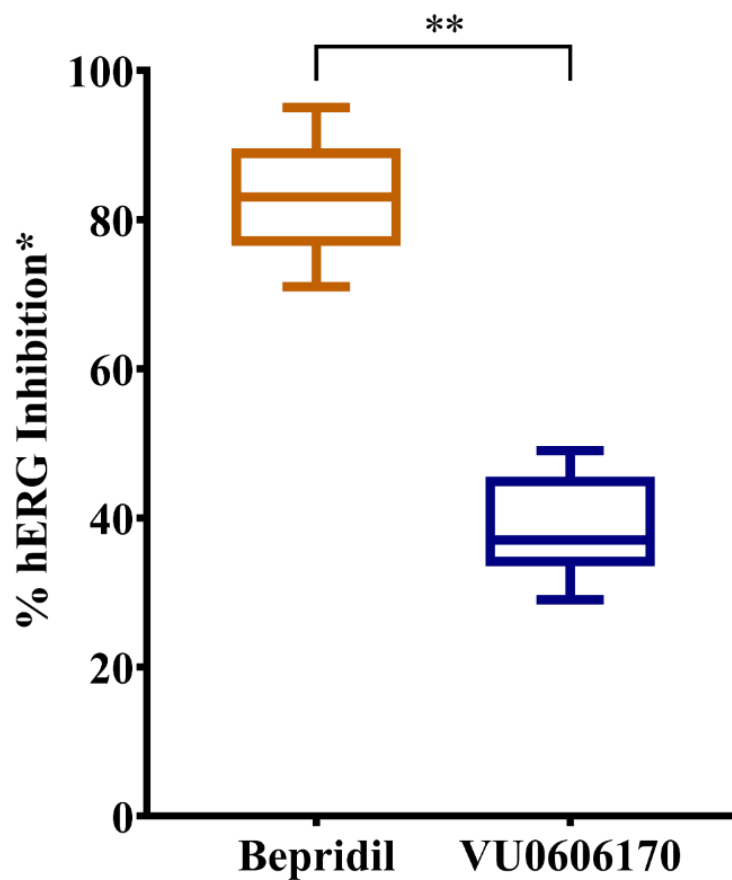


Figure 16: Percent inhibition of HEK-293 cells expressing hERG channels in Ti^+ flux assay, *normalized to E_{max} Bepridil. 10 μM bepridil significantly inhibits hERG to a greater extent than 10 μM VU0606170. Data expressed as mean \pm SEM, $n = 9$, ** indicates $p < 0.0001$, Mann-Whitney U test.

While TI^+ flux and EP assays provide meaningful information regarding the characterization of a molecule, we sought to investigate VU0606170 activity in a more biologically relevant system. The primary neuronal culture assay utilized throughout this work provides an intermediate step towards testing whether inhibition of Slack could have AED-like properties. Indeed, we found that the high-frequency synchronous Ca^{2+} oscillations of these neuronal cultures evoked under low Mg^{2+} concentrations, were significantly decreased following addition of VU0606170 (**Figure 17**). This finding is encouraging because a large number of AEDs are active in this assay¹¹⁴. Critically, we found that a very closely structurally related compound to VU0606170 that demonstrated to be inactive as a Slack inhibitor was also inactive in the neuron assay. This data strongly supports that Slack is the target of VU0606170 leading to Ca^{2+} oscillation inhibition. In the future we will test additional compounds to further investigate the correlation between Slack inhibitory activity and activity in our neuron assay.

Recently, data supporting the mechanism that gain-of-function Slack mutations, such as A934T, lead to epilepsy through inhibitory neuron-mediated mechanisms by prolonging afterhyperpolarization and increasing currents at subthreshold voltages⁴⁶ (detailed in **Chapter 1**). We found that our neuronal cultures contained a mixture of inhibitory and excitatory neurons as well as astrocytes (**Figure 19**) and it is tempting to speculate that the decrease in Ca^{2+} oscillation rate observed when neurons were treated with VU0606170 resulted from increasing inhibitory tone. However, further studies are necessary to elucidate this mechanism, and are described in the **Future Directions** of **Chapter 6**.

We were encouraged by the fact that application of VU0606170 decreased the Ca^{2+} oscillation rate but did not completely suppress neuronal activity. One can imagine that decreasing but not completely eliminating neuronal spiking could mimic normal physiology. Additionally, these data were obtained using WT neurons, suggesting the intriguing possibility that Slack inhibition could prove useful as a therapeutic approach for a broader range of indications, not just epilepsy driven by Slack mutations. While future studies are required to fully understand the effects of VU0606170 on the excitability of these cultured neurons, our observations provide

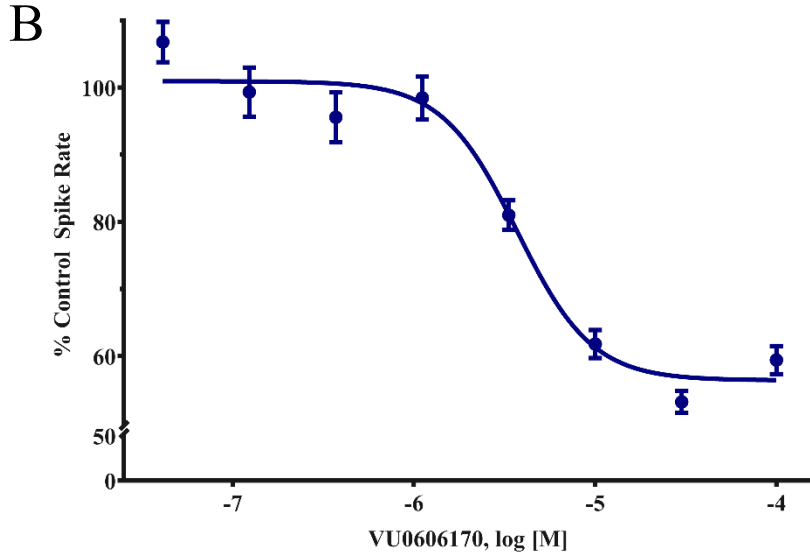
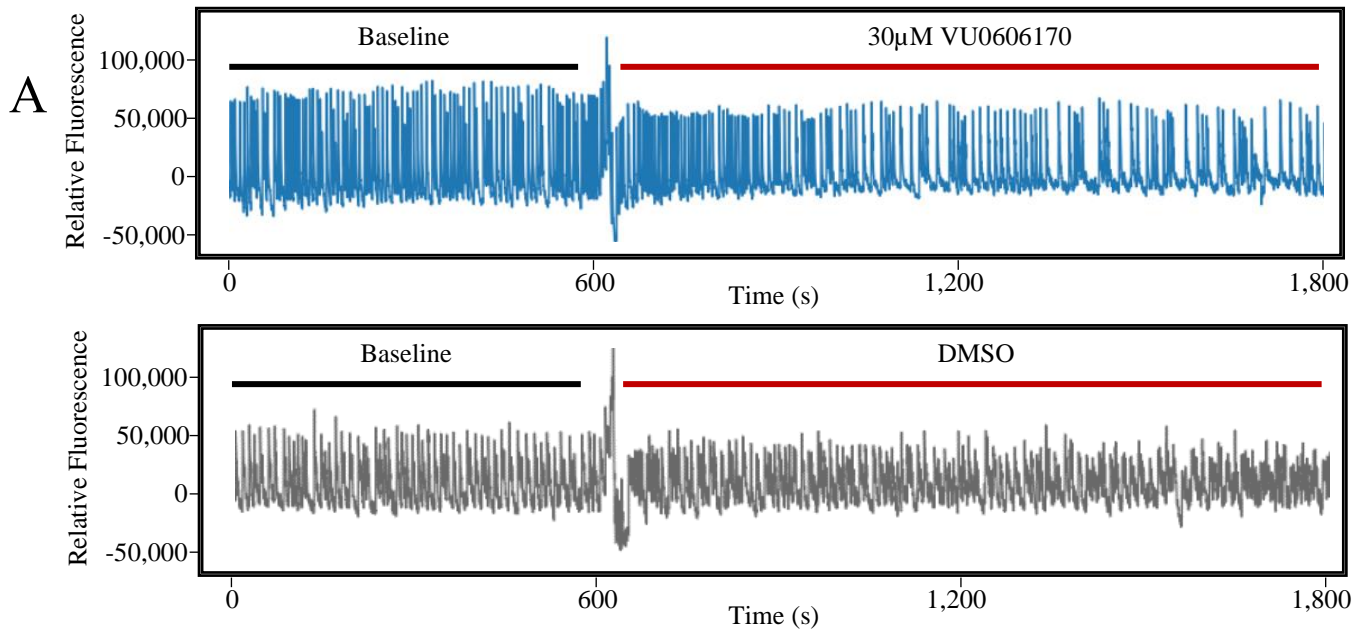
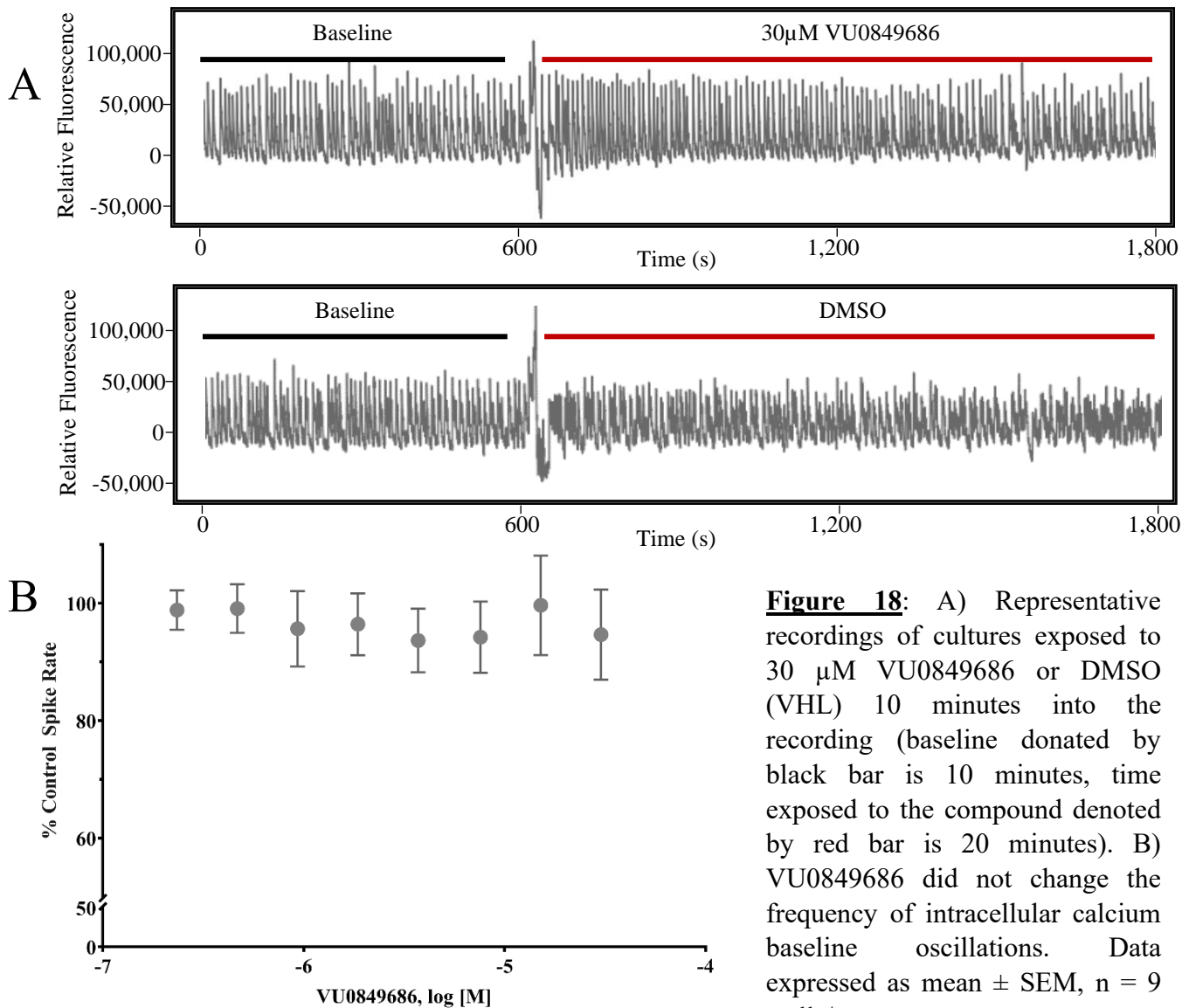


Figure 17: A) Representative recordings of cultures exposed to 30µM VU0606170 or DMSO (VHL) 10 minutes into the recording (baseline denoted by black bar is 10 minutes, time exposed to the compound denoted by red bar is 20 minutes). B) VU0606170 induced a dose-response decrease in frequency of intracellular calcium baseline oscillations. Data expressed as mean \pm SEM, n = 24 wells/group.

the first evidence that selective Slack inhibition may produce anti-epileptic efficacy which, in turn, may begin to pave the way for the development of new therapeutics for the treatment of MMPSI and other epilepsies.



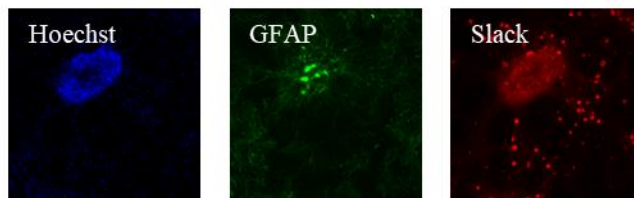
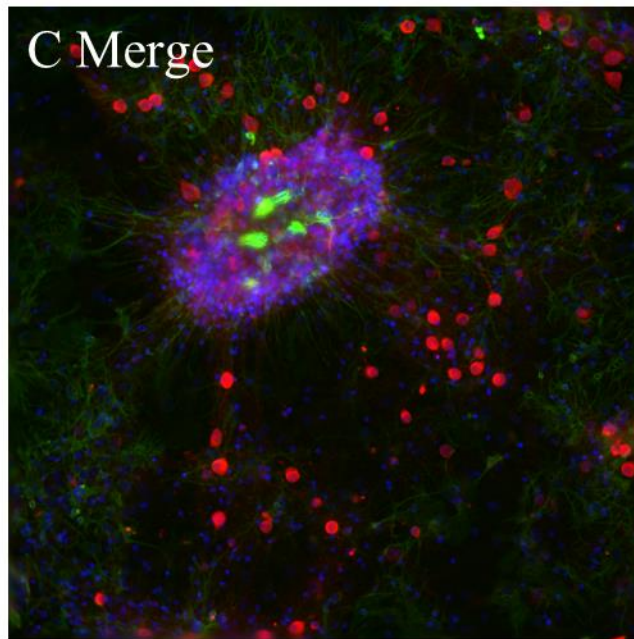
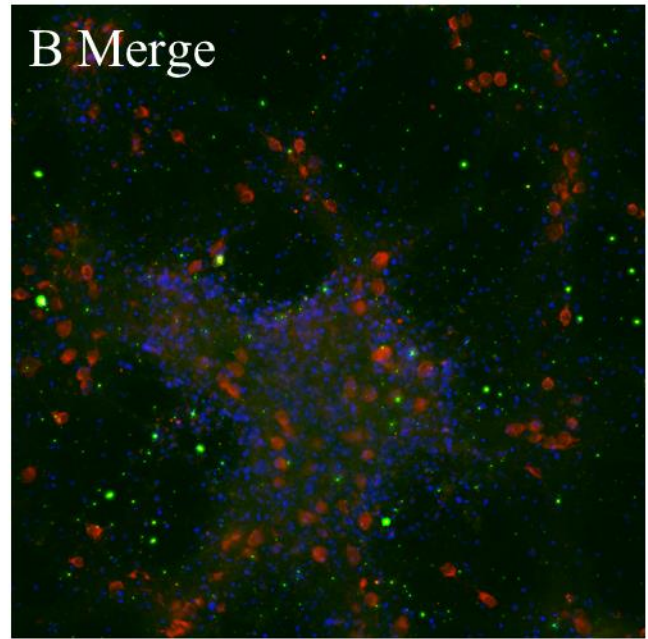
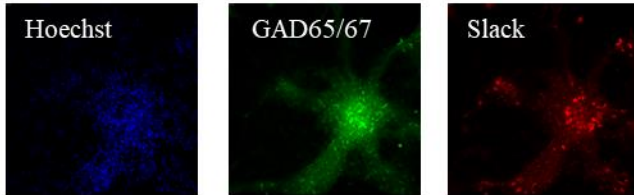
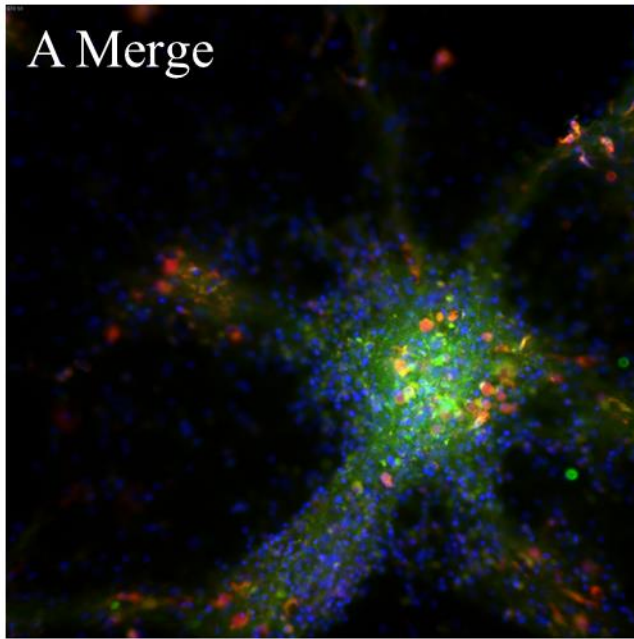


Figure 19: Distribution of Slack channels in rat cortical cocultures. Slack was detected by immunofluorescence in both inhibitory and excitatory neurons but did not colocalized with astrocytes. A) Inhibitory neurons stained with GAD65/67, B) excitatory neurons stained with VGLUT2, C) astrocytes stained with GFAP, nuclei were stained with Hoechst.

CHAPTER 4

CHARACTERIZATION OF VU0606170 ANALOGS

Introduction

VU0606170 provides the first evidence that selective inhibition of Slack channel activity can be achieved with small molecules. However, discovery and characterization of initial hit compounds with *in vitro* pharmacology approaches requires additional validation using animal models to characterize and evaluate *in vivo* exposure, target engagement and therapeutic efficacy of new molecular entities. These *in vivo* studies are performed in an animal modeling the targeted disease, if one is available. However, HTS hits rarely have all the pharmacological and/or pharmacokinetic properties desired for an *in vivo* probe for systemic administration, including selectivity, potency, solubility, brain penetration, and plasma stability, to name a few. We were fortunate that VU0606170 had several favorable properties revealed through our *in vitro* studies, including a suitable selectivity profile, low micromolar potency, and no solubility issues. However, we discovered it is not suitable for systemic administration *in vivo*.

To determine the potential utility of a molecule as an *in vivo* probe, a number of parameters are investigated with drug metabolism and pharmacokinetic (DMPK) properties being two of utmost importance. Drug metabolism refers to the metabolic breakdown, or biotransformation, of drugs by a living organism. The rate of metabolism is particularly important because it determines the duration and efficacy of a drug's pharmacologic action. Pharmacokinetics (PK) describes how the body affects a drug after administration. The drug's movements into, through and out of the body are assessed, these parameters are referred to as absorption, distribution and excretion, respectively. Assays useful for assessing many of these DMPK properties can now be

done *in vitro*. While these cannot completely replace *in vivo* PK studies they do provide advantages such as decreased time and cost of testing individual compounds.

We performed several of these *in vitro* assays to investigate three DMPK parameters of VU0606170. When available assays were run in both human and mouse *in vitro* systems, mouse to test the utility of VU0606170 to be dosed systemically in an animal model of epilepsy and human since the overarching goal of this project is to pave the way for the development of new therapeutics for the treatment of MMPSI and other epilepsies. We examined how quickly VU0606170 would be metabolized, the degree of plasma protein binding, and its permeability across biological membranes. The rate at which a compound is metabolized in the absence of restrictions imposed on drug delivery to the liver by blood flow and protein binding is referred to as intrinsic clearance (CL_{int}), giving insight into the stability of the compound in the test organism. Plasma protein binding is the degree to which a compound will attach, or bind, to proteins within the blood. This affects the compound's efficacy, the less bound a drug is, referred to as free drug, which affects the drug/probe's ability to engage the target. A drug's permeability across biological membranes is a key factor that influences the absorption and distribution. For instance, if a drug is administered orally, it will need to cross the intestinal barrier in order to get out of the gastrointestinal (GI) system and into the circulatory system, where it can travel to its target. In the case of VU0606170 we were interested in how readily the compound crosses cellular membranes and cellular junctions, including the blood brain barrier (BBB) and if would be actively transported back out of the brain. The BBB is a highly selective semipermeable membrane that separates the CNS from the periphery, allowing for passive diffusion and selective transport of some molecule, while restricting the passage of pathogens. Drugs acting in the CNS must cross the BBB to elicit their effect. Assessing transport in both directions, using specific cells that mimic those found on the BBB, enables an efflux ratio to be determined which is a useful predictor of BBB permeability.

Unfortunately, VU0606170 appears to be a poor candidate for systemic administration *in vivo*. We found that VU0606170 is metabolized by both human and mouse liver cells in a matter of minutes, indicating the compound would not be around long enough engage with Slack in the brain. Additionally, VU0606170 showed

extensive binding to human plasma proteins, with only 0.25% free drug reported. We determined the efflux ratio of VU0606170 to be 0.8. Efflux ratios < 1 indicate the compound does not undergo active efflux, meaning it will not be readily transported out of the brain. This allows VU0606170 to remain in the brain in close proximity to its target, neuronal Slack channels. Overall, these DMPK results revealed limitations in the utility of VU0606170 as a systemically administered *in vivo* probe.

While systemic administration is not the only option for evaluating *in vivo* probes, we sought to develop analogs with improved potency, selectivity and pharmacological properties which will allow systemic dosing in animals before exploring more resource intensive options of administration. As such, VU0606170 presents an exciting starting point for the development of analogs, as it has multiple amenable regions (**Figure 20**). Development of these analogs would allow us to explore the structure-activity relationship (SAR) between the compounds and the targeted Slack channels. The analysis of SAR enables the determination of the chemical group(s) responsible for evoking a variety of pharmacologic properties including but not limited to, target biological effect, solubility, DMPK parameters, and selectivity. Our goal is to balance all of these parameters to identify a compound suitable as an *in vivo* probe. Medicinal chemists use the techniques of chemical synthesis to modify the structure of a compound which are then tested for their biological effects.

In collaboration with Dr. Emmitte and members of his laboratory, we have tested the activity of 300 VU0606170 structurally related analogs in our TI^+ flux assay with HEK293 cells expressing WT or A934T Slack channels. We sought to identify structural modifications that retained the efficacy and/or improved potency at Slack channels, while decreasing activity against hERG channels. While VU0606170 did not potently inhibit hERG, we ideally wanted to identify an analog with even lower hERG activity, ideally 100-fold or greater separation in potency compared to Slack. Again, we utilized our TI^+ flux assay to measure each analog's efficacy and potency against HEK293 cells expressing hERG channels. We also tested the selectivity of these compounds against the same ion channels reported for VU0606170 selectivity studies in **Chapter 3**. Additionally, we utilized the neuronal cell culture model as a means of investigating activity of 18 these analogs in a more biologically relevant system.

Through our extensive SAR studies, we revealed several chemical features of VU0606170 that are necessary for Slack inhibition, others that significantly affect potency and other features that contribute to hERG inhibition. These compounds have been grouped into six categories to better identify the portion of the molecule that is being varied. In the **Results** we will report several representatives from each class and how these changes affected the overall activity of the compound. We then sought to determine if Slack-expressing HEK293 cells can predict activity in a more resource and time consuming but also a more native system of cultured cortical neurons. If there is no correlation between the two assays, we would need to explore the reasons behind the compound's mechanism, however; if SAR tracks between Tl^+ flux and neurons we can be more confident that Slack is the major contributor to our compounds' effect in neurons. The overarching themes of our SAR studies will be summarized during the **Discussion** portion of this chapter.

Methods

Cell Culture, Thallium-flux and Calcium-flux Assays

All cell culture, Tl^+ flux assays, and Ca^{2+} assays were performed as previously discussed in **Chapters 2** and **3**. Analogs of VU0606170 were synthesized and their structure confirmed via MS and NMR in the laboratory of Dr. Emmitte.

Drug Metabolism and Pharmacokinetic Assays

DMPK assays were performed by Q² Solutions, including microsomal CL_{int} (mouse and human), fraction unbound (microsomes and plasma), and MDCK II bidirectional permeability assay. Briefly, the microsomal CL_{int} assay was performed according to method Q2-MSIC-001 in which $0.3\mu M$ VU0606170 was incubated in liver microsomes at a protein concentration of 0.25 mg/mL at $37^\circ C$. Two tests were performed, one in the presence of NADPH (+NADPH) and one without (-NADPH). Incubation time points for +NADPH: 0, 5, 15, 30 and 45 min.

The negative control (-NADPH) was used for recovery assessment, the concentration of remaining VU0606170 was taken at 45 min and compared to time 0 to calculate recovery. Samples were analyzed by LC/MS/MS to

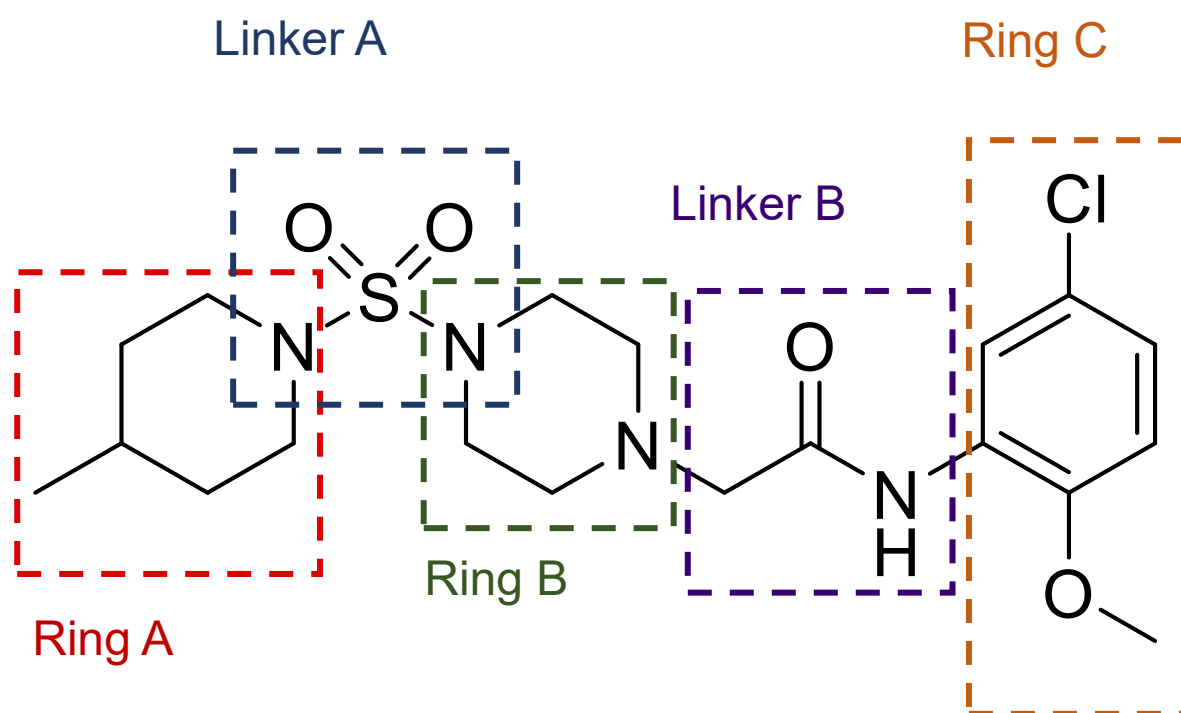


Figure 20: Hit optimization plan for VU0606170 with proposed initial libraries for each region of the scaffold.

acquire a depletion rate calculated by peak area ratio with internal standard (labetalol, imipramine and diclofenac) at each time point relative to time 0. Verapamil was used as a positive control for this assay.

Plasma protein binding was assessed in human and mouse plasma to determine with fraction unbound of VU0606170. Briefly, this assay was performed according to the method Q2-FU-001, in which 1 μ M VU0606170 with 0.5 mg/mL of microsomal protein at 37°C/5% CO₂/95% relative humidity (RH) while shaking at 167 rpm. Samples were taken from buffer and protein sides of the apparatus following a 4.5 hr incubation. Samples were analyzed by LC/MS/MS, the calculation of fraction unbound was calculated using area ratios according to the following equation:

$$Fraction\ Unbound = \left(\frac{[compound]_{buffer}}{[compound]_{protein}} \right) \times 100$$

Again, verapamil was used as a positive control.

Finally, the MDCK II bidirectional permeability assay was used to determine the efflux ratio of VU0606170. This assay was performed according to the method Q2-PERM-001. In brief, 1 μ M was incubated in both A:B and B:A in the presence of Cyclosporin A, a P-glycoprotein (P-gp) inhibitor, at 37°C/5% CO₂/95% RH for 3 hrs. A 9-point concentration curve was prepared for quantitation of samples (2000, 1000, 500, 250, 125, 62.5, 31.3, 15.6, 7.81 nM). Samples were analyzed by LC/MS/MS, with verapamil as a positive control. The ratio of B-A/A-B was calculated as the efflux ratio.

Results

Characterization of VU0606170 Drug Metabolism and Pharmacokinetic Properties

As part of the process of evaluating activity and properties of VU0606170 we tested three parameters to assess the viability of VU0606170 as an *in vivo* tool, which included CL_{int}, plasma protein binding and permeability. Clearance was measured in both mouse and human liver cells containing the drug metabolizing enzymes, known as microsomes, which is used to estimate a compound's metabolic stability. It was determined

that VU0606170 is rapidly cleared with an intrinsic clearance in human liver microsomes of >2763 mL/min/kg. When comparing VU0606170's CL_{int} to normal blood flow to the human liver (21 mL/min/kg), we see that the CL_{int} of VU0606170 is significantly higher than liver blood flow. When CL_{int} is significantly higher than liver blood flow (Q_H), the enzyme so active that the liver removes all or nearly all of the drug presented to it, so the parameter determining the actual hepatic clearance is the rate of supply of the drug to the liver. The same is true when comparing VU0606170's CL_{int} in mouse liver microsomes (>5376 mL/min/kg) and normal Q_H in mice (90 mL/min/kg). Additionally, it was determined that the metabolism of VU0606170 in mouse microsomes was an NADPH-independent mechanism. NADPH is a required cofactor for cytochrome P450 (CYP) enzymes which are the major metabolizing enzymes of the liver. This finding indicates that the enzyme(s) responsible for metabolism of VU0606170 in mice is not a CYP. But the central finding of this assay was that $<1\%$ of VU0606170 remained at the first time point taken during this assay (5 min), indicating the compound is not metabolically stable. Secondly, we had the compound's plasma protein binding tested. The extent of plasma protein binding is inversely proportionate to the percent of drug that is free to interact with biological targets within the body. VU0606170 was found to be highly protein bound in both human and mouse plasma, with a fraction unbound of 0.25% in human and 0.00% in mouse plasma, indicating there is very little drug free available to elicit its biological effect. However, high protein binding does not prohibit drug development. Many commonly used drugs are highly protein bound, including many antibiotics and anti-inflammatories such as ibuprofen.

Lastly, permeability of VU0606170 was tested using a MDCK II bidirectional permeability assay. This particular assay utilizes Madin-Darby Canine Kidney (MDCK) cells expressing the efflux protein P-gp. Assessing transport in both directions across the cells enables an efflux ratio to be determined which provides an indicator as to whether a compound undergoes active efflux, mediated by P-gp. P-gp is overexpressed in both the GI tract and the BBB, compounds that are substrates for P-gp are actively transported back into the intestine for excretion through the urine or feces or out of the brain back into the circulatory system. This is a mechanism by which toxins are removed from of the body. Since our target of interest, Slack, is a neuronal potassium channel it is imperative that our compounds not undergo active efflux out of the brain. VU0606170 had an efflux ratio of 0.8

indicating that the compound does not undergo active efflux by P-gp or other transporters expressed in MDCK cells, meaning it will not be readily transported out of the brain. Taken together these results suggest that VU0606170, while a useful *in vitro* tool, has limited usefulness as a systemically administered *in vivo* probe.

Overview of VU0606170 Structurally Related Analogs

Herein we describe the activity of 300 VU0606170 structurally related analogs synthesized by the Emmitte lab. These analogs are grouped into six distinct generations of compounds based on where in the molecule they are modified from the structure of VU0606170. Representative analogs and their efficacy, potency and selectivity will be discussed, along with generalized conclusions we can draw from each. Throughout these results we will refer to numerous functional groups, which refer to specific substituents or moieties with a molecule that may be responsible for the biological characteristics of that molecule. Note modifications to a molecule are represented as a numbered R, which represents a generic placeholder for a functional group being added.

Characterization of Amide Analogs

Analogs of the amide series refer to changes on the far eastern side of the molecule, shown as **Ring C** in **Figure 20**. These molecules retained the phenyl attached to the amide with varying substituents moved around all positions of the ring. Removal of all substituents, leaving the phenyl alone decreases potency against Slack channels by ~10-fold, and significantly decreases efficacy, as seen with VU0849880. Similarly, a single methyl group at any ring position leads to a significant decrease in efficacy or renders the compound inactive (VU084997). Substituting the 5-chloro with another halogen retains similar potency and efficacy for Slack. This substitution also increases the separation of potency between Slack and hERG, however; compounds are active at other targets. This non-selectivity is exemplified by the 5-fluoro substitution of VU0849693 which is an inhibitor of Slo $\alpha 1/\beta 3$, Slo $\alpha 1/\beta 4$, Slick, Slo 3, GIRK 1/2 and Nav1.7. Removal of the halogen accompanied by the movement of the methoxy around the ring decreases potency by ≥ 10 -fold. Additionally, this change results

in inhibition of Cav3.2 channels, as seen with VU0849968. Lastly, removal of the 2-methoxy group alone leads to a slight decrease in potency but retains efficacy (VU0849883). Data Summarized in **Table 4**.

Characterization of 2,5-Substituted Phenyl Analogs

Analogs of the 2,5-substituted phenyl series involve substitutions at the 2- and 5- positions of the phenyl (**Ring C** of **Figure 20**). VU0849694 replaces the 5-chloro with 5-trifluoro, this substitution slightly increases potency, while efficacy remains the same. This also leads to a larger separation between hERG and Slack potency; however, hERG efficacy is slightly increased at 100 μ M compared to that of VU0606170. Additional carbon chains, often referred to as hydrophobic bulk, added to oxygen at the 2- position decreases potency and slightly decreases efficacy, as seen with VU0854136. Exchanging halogens at the 5- position appears to be well tolerated, retaining efficacy, potency and selectivity, an example of which is VU0849683. Replacing the 2-methoxy with a methyl group results in only a slight decrease in potency (VU0492891). Additionally, exchanging the methoxy for a halogen only slightly decreases potency and efficacy as seen with VU0849695. Data Summarized in **Table 5**.

Characterization of Sulfonamide Analogs

Analogs of this series contain substitutions off of the piperidine ring or exchanging the piperidine for other heterocycles, or substituted phenyls, shown as **Ring A** in **Figure 20**. VU0568747 is the removal of 4-methyl from the piperidine ring, this change decreases efficacy by ~half and causes solubility issues, making it difficult to interpret the actual potency of the compound. Substituting the piperidine with phenyl or cyclohexane significantly decreases compound activity (VU0606126 and VU0849973, respectively). However, when a methyl group is added in the para position, the opposing side of the ring, all activity of the compound is lost, with the exception of inhibition of Cav3.2 channels (VU0492889); however, efficacy is restored when a halogen is added in the para position, as seen with VU0584662. Data Summarized in **Table 6**.

Characterization of XCOR Analogs

These analogs involve replacing the sulfonamide moiety with a variety of substituents, primarily ureas connecting the piperazine to varying heterocycles. There primarily involved changes of **Linker A** with some variations of **Ring A** as well (**Figure 19**). Bulk at the para position of the piperidine ring retains efficacy but decreases potency, as seen with VU0849975 and VU0849983. Other nitrogen containing heterocycles cause a large shift in potency by at least 10-fold (VU0849669). Data Summarized in **Table 7**.

Characterization of Linker Analogs

These analogs consist of compounds variety the linker between the eastern and western sides of VU0606170, shown as **Linker B** in **Figure 19**. Reversing the position of the carbonyl on the linker is not tolerated, as seen with VU0849686. Note this compound was used as our inactive analog for experiments in Chapter 3. Additionally, substitution of the linker with methyl groups is well-tolerated, though stereochemistry seems to make little difference, as seen with VU0857544, VU0857568, VU0857544 and VU0857564. Data Summarized in **Table 8**.

Characterization of Core Analogs

Analogs in this series vary the piperazine core of the molecule, labeled as **Ring B** in **Figure 20**. In general changes to the core lead to a decrease in potency with little effect on efficacy. This is exemplified by VU0858209 and VU0858191. VU0914257 is interesting in that it retains the potency and efficacy of VU0849694, of the 2,5-Substituted Phenyl Analog Series, but decreases the potency at hERG. A similar result is seen with VU0914267, which increases potency compared to the non-methylated piperazine analog, VU0849695, with a decreased hERG potency. Data Summarized in **Table 9**.

Characterization of the SAR of VU0606170 Analogs on Ca²⁺ Oscillations

We were interested in evaluating the correlation in SAR between activity in Slack-expressing HEK cells tested using TI⁺ flux with effect on Ca²⁺ oscillations in neurons to see if the SAR as it applies to Slack inhibition was retained in our Ca²⁺ oscillation assay with cultured primary cortical neurons. In brief, these neurons were shown to express Slack in both excitatory and inhibitory neurons in our cultures isolated from E18 WT rats. These neurons were cultured in vitro for at least 14 days before being assayed with a Ca²⁺ dye, allowing us to visualize the firing rates, or spiking patterns of these neurons and our compounds' effects on this rate. For more information regarding this assay refer to **Chapter 3 Methods**.

We tested the effects of 16 analogs, in addition to VU0606170 and VU0849686 (**Chapter 3**) representing a wide range of pharmacology in our Slack assays. This included compounds with high potency and full efficacy, others that were moderately potent with full efficacy, others with moderate efficacy and still others that were inactive. **Table 10** highlights the compound effect on neuronal firing rates, grouped by their effect in TI⁺ flux.

In general, we determined compounds with moderate efficacy in TI⁺ flux assays had diminished effect in the neuronal assay. Compounds which were inactive in TI⁺ flux were also inactive in this assay, with the exception of VU0849997. While VU0849997 was not active in any of our selectivity screens we cannot rule out that its effect was elicited by inhibition of another channel present in these neurons, further studies are needed to determine the channel(s) or other targets responsible for its effects. VU0849973 and VU0858191 revealed to have the highest potency of any analog we tested, with potencies of 2.92 μ M and 5.78 μ M respectively. Like VU0606170, these potencies were close to that in TI⁺ flux.

Discussion

After identifying VU0606170 and characterizing its activity in a variety of assays, we investigated properties which may affect its utility as an *in vivo* probe. We are most interested in its ability to be used in systemic dosing in mice due to our mouse model of MMPSI which will be discussed in **Chapter 5**. Unfortunately,

VU0606170 is rapidly cleared and is highly protein bound in both human and mouse PK assays. Together these data reveal VU0606170 would not remain in the body long enough to elicit its intended effect if administered as a single systemic dose. However, we were not discouraged by this, it is rare that HTS hits possess all of the properties desired of an *in vivo* probe. VU0606170 is still an excellent probe to study the effects of Slack *in vitro*. Additionally, the structure of VU0606170 has multiple regions amenable to SAR development through the preparation of small libraries of compounds.

We were fortunate to collaborate with Dr. Emmitte for the development of VU0606170 analogs to study its SAR with Slack channels. To date The Emmitte lab has synthesized 300 analogs of VU0606170, which allowed us to examine analogs varying five major areas of the molecule. We discovered relatively quickly that the SAR was quite narrow, meaning even small changes to the compound structure were found to exert a large impact on compound activity, potency or engendered an unanticipated effect. This is exemplified by VU0492889 and VU0849968 which inhibit Cav3.2 channels. We initially chose to screen against Cav3.2 due to bepridil being a potent inhibitor of the channel. The emergence of activity of this scaffold for Cav3.2 is something we will need to be conscious of moving forward.

Initial SAR obtained in the Amide Series was used for the design and synthesis of next generations of analogs that combine optimal features from multiple regions of the scaffold. This “mix-and-match” strategy allowed us to discovery compounds such as VU0914257, which combines the well tolerated 5-trifluoro substitution off the eastern ring (**Ring C**) and a methyl group off the piperazine ring (**Ring B**). VU0914257 retains the efficacy and potency seen with VU0606170 while having a 2-fold decrease in potency against hERG channels (**Table 9**). Overall, we have concluded that 2, 5 substitutions are preferred for inhibition of Slack. Halogens may be substituted at the 5- position but compound loses selectivity.

Furthermore, we investigated the relationship between potency and efficacy of Slack inhibition in Tl⁺ flux and Ca²⁺ oscillation assays. We were particularly interested if the rank order of potency and efficacy in Tl⁺ flux remained true in the Ca²⁺ oscillation assay. Unfortunately, we cannot say conclusively that this is the case. Many of our “high potency” Tl⁺ flux compounds revealed to be less potent than those classified as “moderately potent”.

Additionally, two compounds active in TI^+ flux showed no change in the spike rate of neurons. We did observe a correlation between these two assays in regards to rank efficacy. Most compounds labeled as “moderately efficacious” had a moderate effect in decreasing the baseline spike rate compared to that of compound deemed to have “full efficacy”. While we may not be able to correlate these results to that of TI^+ flux 100% of the time, this assay provides a useful intermediate between *in vitro* and *in vivo* studies. We are currently working to validate this assay with mouse neurons which would enable us to use neurons isolated from our novel MMPSI mouse model to test future analogs of VU0606170. Although derivative of VU0606170 have not proven to dramatically improve potency we retain several other scaffolds to begin medicinal chemistry efforts with and other that are currently underway.

While we chose to pursue development of analogs of VU0606170 in an effort to combat these issues other methods may be employed in future studies to validate Slack inhibition as an antiepileptic target. One such example being continuous systemic dosing, which would eventually saturate the metabolic enzymes responsible for VU0606170’s metabolism allowing for accumulation of VU0606170 in the body. While more studies are required to determine the exact enzyme responsible for VU0606170’s metabolism in mice, once identified an inhibitor of the enzyme could be administered along with VU0606170 leading to a decrease in VU0606170’s clearance. Finally, an intracerebral cannula could be implanted into the mouse allowing for VU0606170 to be administered directly to the brain. These methods may be applied in the future if we are unable to resolve the metabolic instability issues through development of structurally related analogs of VU0606170.

Table 4: Amide Analogs of VU0606170

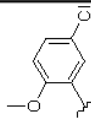
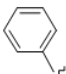
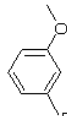
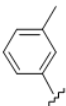
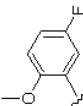
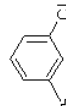
VU Number	R group	WT Slack Potency Efficacy	A934T Slack Potency Efficacy	hERG Potency Efficacy	Slo $\alpha 1/\beta 1$	Slo $\alpha 1/\beta 2$	Slo $\alpha 1/\beta 3$	Slo $\alpha 1/\beta 4$	Slo 3	Slick	TREK 2	Kv2.1	Cav3.2	GIRK 1/2	Nav1.7	HEK UT
VU0606170		1.55 μ M 96%	1.12 μ M 97%	>6.1 μ M -49	NA	NA	NA	NA	NA	NA	NA	NA	NA	NA	NA	NA
VU0849880		>18 μ M -24%	>25 μ M 31%	>18 μ M -61	NA	NA	NA	NA	NA	A	NA	NA	I	NA	NA	NA
VU0849968		>22 μ M 99%	> 20 μ M 96%	>43 μ M -30	NA	NA	NA	NA	NA	NA	NA	NA	I	NA	NA	NA
VU0849997		inactive inactive	inactive inactive	>30 μ M -58	NA	NA	NA	NA	NA	NA	NA	NA	NA	NA	NA	NA
VU0849693		2.68 μ M 106%	1.76 μ M 97%	>15 μ M -66	NA	NA	I	I	I	I	NA	NA	NA	I	I	NA
VU0849883		8.61 μ M 101%	5.98 μ M 106%	>15 μ M -82	NA	NA	NA	NA	NA	A	NA	NA	NA	NA	NA	NA

Table 5: 2,5-Substituted Phenyl Analogs of VU0606170

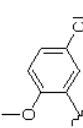
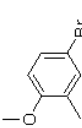
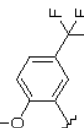
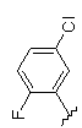
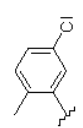
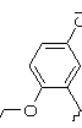
VU Number	R group	WT Slack Potency Efficacy	A934T Slack Potency Efficacy	hERG Potency Efficacy	Slo $\alpha 1/\beta 1$	Slo $\alpha 1/\beta 2$	Slo $\alpha 1/\beta 3$	Slo $\alpha 1/\beta 4$	Slo 3	Slick	TREK 2	Kv2.1	Cav3.2	GIRK 1/2	Nav1.7	HEK UT
VU0606170		1.55 μ M 96%	1.12 μ M 97%	>6.1 μ M 49%	NA	NA	NA	NA	NA	NA	NA	NA	NA	NA	NA	NA
VU0849683		1.99 μ M 88%	1.04 μ M 92%	100 μ M 21%	NA	NA	NA	NA	I	NA	NA	NA	I	NA	NA	NA
VU0849694		1.23 μ M 105%	1.20 μ M 97%	>8.0 μ M 81%	NA	NA	NA	NA	NA	A	NA	NA	NA	NA	NA	NA
VU0849695		3.45 μ M 66%	2.95 μ M 67%	>7.1 μ M 21%	NA	NA	I	NA	NA	A	NA	NA	NA	NA	NA	NA
VU0492891		5.20 μ M 95%	5.34 μ M 96%	>7.4 μ M 87%	NA	NA	NA	NA	NA	I	NA	NA	I	NA	NA	NA
VU0854136		3.20 μ M 84%	2.96 μ M 87%	8.04 μ M 65%	NA	NA	NA	NA	NA	A	NA	NA	NA	NA	NA	NA

Table 6: Sulfonamide Analogs of VU0606170

VU Number	R_group	WT Slack Potency Efficacy	A934T Slack Potency Efficacy	hERG Potency Efficacy	Slo $\alpha 1/\beta 1$	Slo $\alpha 1/\beta 2$	Slo $\alpha 1/\beta 3$	Slo $\alpha 1/\beta 4$	Slo 3	Slick	TREK 2	Kv2.1	Cav3.2	GIRK 1/2	Nav1.7	HEK
VU0606170		1.55 μ M 96%	1.12 μ M 97%	>6.1 μ M 49%	NA	NA	NA	NA	NA	NA	NA	NA	NA	NA	NA	NA
VU0568747		2.24 μ M 44%	1.70 μ M 52%	> 1.7 μ M 27%	NA	NA	NA	NA	NA	I	NA	NA	NA	NA	NA	NA
VU0849973		2.99 μ M 37%	2.06 μ M 88%	2.02 μ M 45%	NA	NA	NA	NA	NA	A	NA	NA	A	NA	NA	NA
VU0606126		1.72 μ M 36%	1.20 μ M 35%	inactive inactive	NA	NA	NA	NA	NA	A	NA	NA	NA	NA	NA	NA
VU0492889		inactive inactive	inactive inactive	inactive inactive	NA	NA	NA	NA	NA	NA	NA	NA	I	NA	A	NA
VU0584662		2.45 μ M 81%	2.62 μ M 83%	> 1.1 μ M 82%	NA	NA	NA	NA	I	NA	NA	NA	A	NA	NA	NA

Table 7: XCOR Analogs of VU0606170

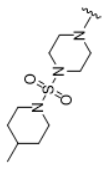
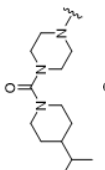
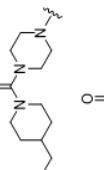
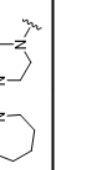
VU Number	R group	WT Slack		A934T Slack		hERG		Slo $\alpha 1/\beta 1$	Slo $\alpha 1/\beta 2$	Slo $\alpha 1/\beta 3$	Slo $\alpha 1/\beta 4$	Slo 3	Slick	TREK 2	Kv2.1	Cav3.2	GIRK 1/2	Nav1.7	HEK
		Potency Efficacy	Potency	Potency Efficacy	Potency	Potency Efficacy	Potency												
VU0606170		1.55 μ M	96%	1.12 μ M	97%	>6.1 μ M	49%	NA	NA	NA	NA	NA	NA	NA	NA	NA	NA	NA	NA
VU0849983		9.30 μ M	117%	7.04 μ M	121%	>9.8 μ M	-05%	NA	NA	NA	NA	NA	I	NA	NA	I	NA	NA	NA
VU0849975		8.60 μ M	108%	7.20 μ M	110%	6.17 μ M	103%	NA	NA	NA	NA	NA	NA	NA	NA	NA	NA	NA	NA
VU0849699		>19 μ M	89%	>17 μ M	93%	>1.5 μ M	93%	NA	NA	NA	NA	NA	I	NA	NA	I	NA	I	NA

Table 8: Linker Analogs of VU0606170

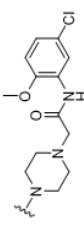
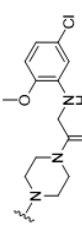
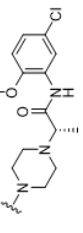
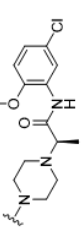
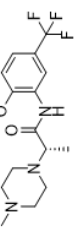
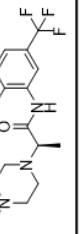
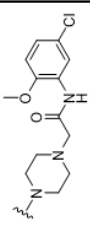
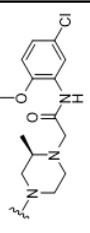
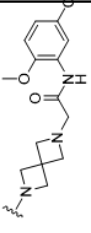
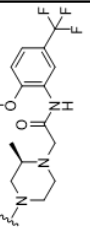
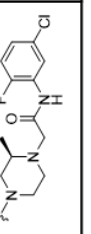
VU Number	R group	WT Slack Potency Efficacy	A934T Slack Potency Efficacy	hERG Potency Efficacy	Slo $\alpha 1/\beta 1$	Slo $\alpha 1/\beta 2$	Slo $\alpha 1/\beta 3$	Slo $\alpha 1/\beta 4$	Slo 3	Slick	TREK 2	Kv2.1	Cav3.2	GIRK 1/2	Nav1.7	HEK
VU0606170		1.55 μ M 96%	1.12 μ M 97%	>6.1 μ M 49%	NA	NA	NA	NA	NA	NA	NA	NA	NA	NA	NA	NA
VU0849686		inactive inactive	inactive inactive	inactive inactive	NA	NA	NA	NA	NA	A	NA	NA	NA	NA	NA	NA
VU0857550		2.38 μ M 87%	2.20 μ M 90%	>12 μ M 69%	NA	NA	NA	NA	NA	NA	NA	NA	NA	NA	NA	NA
VU0857564		2.42 μ M 96%	2.04 μ M 104%	>12 μ M 59%	NA	NA	NA	NA	NA	NA	NA	NA	NA	NA	NA	NA
VU0857544		2.20 μ M 88%	1.98 μ M 87%	>9.0 μ M 69%	NA	NA	NA	NA	NA	NA	NA	NA	NA	NA	NA	NA
VU0857568		2.37 μ M 98%	2.04 μ M 104%	7.79 μ M 63%	NA	NA	NA	NA	NA	NA	NA	NA	NA	NA	NA	NA

Table 9: Core Analogs of VU0606170

VU Number	R group	WT Slack Potency	WT Slack Efficacy	A934T Slack Potency	A934T Slack Efficacy	hERG Potency	hERG Efficacy	Slo $\alpha 1/\beta 1$	Slo $\alpha 1/\beta 2$	Slo $\alpha 1/\beta 3$	Slo $\alpha 1/\beta 4$	Slo 3	Slick	TREK 2	Kv2.1	Cav3.2	GIRK 1/2	Nav1.7	HEK
VU0606170		1.55 μ M	96%	1.12 μ M	97%	>6.1 μ M	49%	NA	NA	NA	NA	NA	NA	NA	NA	NA	NA	NA	NA
VU0858209		2.35 μ M	101%	1.91 μ M	101%	>13 μ M	68%	NA	NA	NA	NA	NA	A	NA	NA	NA	NA	NA	NA
VU0858191		6.81 μ M	100%	6.88 μ M	97%	>14 μ M	65%	NA	NA	NA	NA	NA	NA	NA	NA	NA	NA	A	NA
VU0914257		1.22 μ M	98%	1.22 μ M	102%	>14 μ M	67%	NA	NA	NA	NA	NA	I	NA	NA	A	NA	NA	NA
VU0914267		1.29 μ M	102%	1.32 μ M	111%	>11 μ M	57%	NA	NA	NA	NA	I	A	NA	NA	I	NA	A	NA

COMPOUND	POTENCY	EFFICACY (% CNTR BASELINE SPIKES)
VU0606170	3.89μM	53
HIGH POTENCY WITH FULL EFFICACY VS. WT AND A934T		
VU0849694	29.3 μ M	16
VU0849683	13.6 μ M	8
VU0858209	14.0 μ M	23
VU0914257	27.3 μ M	39
VU0857544	11.0 μ M	37
HIGH POTENCY WITH MODERATE EFFICACY VS. WT AND A934T		
VU0606126	50.7 μ M	64
VU0908660	2.92 μ M	81
VU0584662	INACTIVE	INACTIVE
VU0849973	INACTIVE	INACTIVE
MODERATE POTENCY VS. WT AND A934T WITH FULL EFFICACY		
VU0492891	12.7 μ M	1
VU0849883	12.5 μ M	6
VU0858191	5.78 μ M	0
MODERATE POTENCY VS. WT AND A934T WITH MODERATE EFFICACY		
VU0849880	25.1 μ M	29
INACTIVE VS. WT AND A934T		
VU0849686	INACTIVE	INACTIVE
VU0492889	INACTIVE	INACTIVE
VU0908659	INACTIVE	INACTIVE
VU0849997	17.8 μ M	4

Table 10: Potency and efficacy measurements on Ca²⁺ oscillations of VU0606170 analogs synthesized through SAR studies. n=9, from three replicates per three biological replicates. Efficacy is normalized to the percentage of control baseline spikes at the highest concentration tested (60 μ M).

CHAPTER 5

CHARACTERIZATION OF NEUROLOGICAL EFFECTS OF AN MMPSI-ASSOCIATED SLACK MUTATION IN A MURINE MODEL

Introduction

A major critique of the field of Slack research is the lack of animal models based on *KCNT1* mutations observed in human patients. These models are required in order to accurately analyze the mechanism of these disease-causing mutations. As discussed in **Chapter 1**, there have been several recent attempts to study Slack channels *in vivo*. This includes three Slack KO mice lines, as well as two mouse models expressing MMPSI-associated Slack mutations, P924L and R455H. Taken together, these mouse models support the hypothesis that Slack channels play a role in anxiety-like behaviors⁴⁵ and seizure activity^{50,67}. The loss of Slack function decreased anxiety-like behavior in a variety of assays, showed a deficit in sociability of the animal, and had a protective effect when challenged with pro-epileptogenic stimuli⁵⁰. This is in contrast to the hyperfunction mutation models which exhibited spontaneous seizures^{49,67}. Additionally, *KCNT1*^{+/R455H} mice experienced a great number of seizures when challenged with the pro-epileptic drug, PTZ. However, the effect of these Slack gain-of-function mutations was not investigated in assays assessing anxiety-like behaviors or other Slack-related phenotypes seen in MMPSI patients.

In order to investigate another of these disease-causing mutations, we have, in collaboration with Dr. Eric Delpire, created a mouse line expressing the mouse homologous to the human A934T Slack mutation, A913T. Attributable to Dr. Delpire's expertise in the area of generating genetically modified mice, we were able to produce a heterozygous A913T (*KCNT1*^{+/A913T}) mutant colony founder on our first attempt, allowing us to quickly begin characterizing these mice, to investigate its utility as a model of MMPSI. We sought to perform a variety of neurobehavioral assays investigating changes in gross appearance, anxiety-like behavior, motor activity,

procedural learning, and sensorimotor function. Additionally, we wanted to determine if this mutation induced spontaneous seizures in our mice. We chose to focus on these as assays based on the phenotypes associated with MMPSI in humans and implications of Slack function based on Slack KO mouse models.

At the time we undertook this endeavor, there were no published mutant Slack mouse models therefore, we started with the most basic of assays to examine any gross changes in the animals' appearance or global behavior profile. These tests were especially important because severe physical disabilities could cause false positives in many of the behavioral tasks we planning to utilize in the future. Additionally, observations made during this assay could direct our attention to potential phenotypes to be investigated further. To examine overt difference in our mice, we utilized a modified Irwin assay^{140,141}, comprised of a battery of tests/observations, investigating overall physical appearance, behavior in a novel environment, response to a variety of simple stimuli, and reflexes. A complete list of tests and their scoring can be found in the **Methods** section below.

We then examined any locomotor changes caused by overactivation of Slack. The choice to investigate locomotor activity was two-fold. The first being the lack of muscle tone and regression of motor skills seen in patients with MMPSI^{14,15,20}; the second being that motor dysfunctions could prevent a mouse from active exploration of test environments that require locomotion complicating the assays we chose to investigate anxiety-like behaviors¹⁴². These locomotor tests included inverted screen, locomotor activity chamber and rotarod assays. In brief, together these assays allow for the investigation into grip strength, general locomotor activity levels, endurance, balance, motor coordination and motor skill learning.

Next, we investigated the role of the A913T Slack mutation in a variety of assays assessing anxiety-like behaviors. Behaviors relating to anxiety are of particular interest since Slack KO mice reportedly have a decrease in anxiety-like behaviors across several different assays. Unfortunately, results between assays of anxiety have proved inconsistent; therefore, we chose to investigate anxiety-related behaviors in three separate assays. Animals such as mice display a natural aversion to brightly lit open areas, however; they also have a drive to explore a perceived threatening stimulus. Consequently, decreased levels of anxiety lead to increased exploratory behavior,

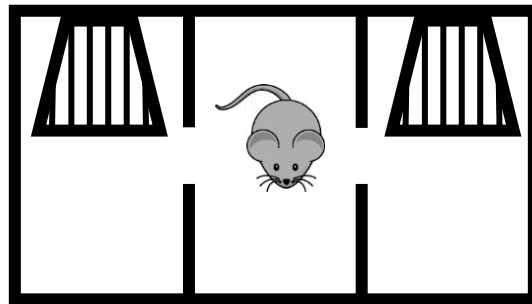
whereas an increase in anxiety will result in less locomotion and a preference to stay in dark, enclosed, or seemingly more protected areas.

Slack dysfunction has been linked to intellectual disability¹⁶, developmental delays commonly seen in autism^{12,14,15,20,21} and FXS⁵⁵⁻⁵⁷ which presents with autistic-like behaviors; this includes alterations in social behaviors. To investigate changes in these parameters associated with a gain-of-function Slack mutation we utilized a three-chamber assay. The three-compartment social approach test (**Figure 21**) is probably the most widely used test for autistic behaviors in mice¹⁴³. In brief, this test measures two aspects of social behavior, sociability and social novelty. As a means to investigate sociability the test mouse is presented with a novel (stranger 1) mouse, normally, mice prefer to spend more time with another mouse which is an indicator of sociability¹⁴⁴. However, in an autism-like phenotype there are no significant differences seen between time spent with the empty cup compared to the cup containing the stranger mouse, indicating impaired sociability of the mouse. As a means of testing social novelty, a second stranger mouse is presented and the test mouse is allowed to interact with now-familiar mouse (stranger 1) or the novel mouse (stranger 2). Mice normally investigate a novel stranger more than a familiar one, indicating intact social memory and preference for novel experiences¹⁴⁴. Impaired sociability and dysregulated social behavior is implicated in many psychiatric disorders, such as autism spectrum disorder¹⁴⁵ and schizophrenia¹⁴⁶.

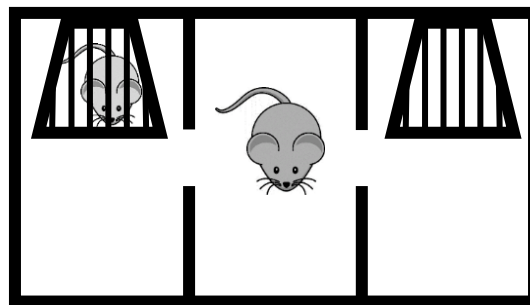
We then investigated whether the A913T Slack mutation leads to abnormalities in sensorimotor gating. Sensorimotor gating refers to the ability of a sensory event to suppress a motor response, which can be measured using prepulse inhibition (PPI) of the startle response. PPI is the ability of a weaker prepulse to inhibit the reaction of an animal to a subsequent pulse or startle stimulus. The reduction of the amplitude of startle reflex reflects the ability of the nervous system to temporarily adapt to a strong sensory stimulus when a preceding weaker signal is given to warn the animal. Deficits in PPI are seen if the animal is unable to filter out unnecessary information, which is considered to be a deficit in sensorimotor gating. Patients with MMPSI have a limited ability to process sensory information making this assay an obvious choice. Additionally, changes in PPI have been linked to a

Overview of 3-Chamber Assay

Phase I: Habituation



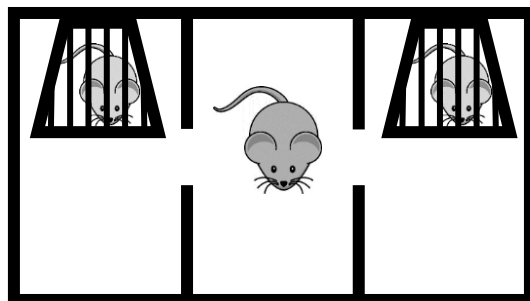
Phase II: Sociability



Stranger

Empty

Phase III: Social Novelty



Familiar

Novel

Figure 21: Depiction of the three phases of the 3-chamber assay used to assess general sociability and interest in social novelty.

variety of neuropsychiatric disorders, including schizophrenia¹⁴⁷⁻¹⁵⁰, autism spectrum disorder¹⁵¹⁻¹⁵³ and Fragile X Syndrome^{154,155}. These correlations led us to investigate if our mouse model exhibited deficits in sensory motor gating utilizing the PPI assay

Spontaneous seizures were observed in the two mutant Slack mouse model previously described^{49,67}. In order to determine if this particular Slack mutant mouse is a model of epilepsy we needed to determine if the mutant mice present with abnormal brain activity, particularly seizure-like activity. In collaboration with Dr. Fiona Harrison's lab, we implanted small telemetry devices in mice and observed their brain activity via EEG for 3-7 days.

Throughout these experiments we used littermates of all three genotypes, wild-type (WT, *KCNT1*^{+/+}), heterozygous (HET, *KCNT1*^{+/A913T}) and homozygous (HOMO, *KCNT1*^{A913T/A913T}) mice, for all of the studies described above. Initially, we analyzed data of males and females separately, however, no sex differences were observed in any assay allowing us to combine both sexes, resulting in a larger sample size. We investigated differences between *KCNT1*^{+/+}, *KCNT1*^{+/A913T} and *KCNT1*^{A913T/A913T} mice in a variety of assays, assessing motor function, anxiety-like behavior, sociability, sensorimotor function, and spontaneous seizure activity. While this covered a large array of assays investigating several phenotypes implicated in MMPSI or Slack function, further studies may be required to fully characterize this novel mouse model.

Methods

Generation of Mouse Line

The *KCNT1* A913T mouse model was generated using CRISPR/CAS9 technology in the laboratory of Dr. Eric Delpire. In brief, a 20 bp sequence (GTTCATGCAGTTCCGTGCCA) located in exon 24 of mouse *KCNT1*, followed by TGG (as protospacer adjacent motif or PAM) was selected to create a target-specific guide RNA molecule. The sequence flanked by BbsI sites was ligated in pX330, a vector expressing the guide RNA under a strong U6 promoter and cas9 under a hybrid chicken β -actin (Cbh) promoter. The vector was injected alongside

a 165 base repair oligonucleotide into 371 mouse embryos. The repair oligo consisted of different size homology arms, 120 and 38 base homology arms, a codon substituting alanine residue 913 to threonine, a unique BsiWI restriction site, and a few additional third-base mutations to prevent retargeting of cas9 to the repaired allele. Out of 371 embryos injected, 262 were transferred to 12 pseudo-pregnant females to generate 31 pups. At weaning, genotyping was done by amplifying a 440 bp fragment followed by sequencing. Two founder males were identified: line #6 which carried the designed mutated allele alongside a randomly repaired and mutated allele, and line 13 which carried the designed mutated allele alongside an allele with a large deletion. Each founder was mated to C57BL/6J females to separate the desired alleles and after sequence confirmation, one line was backcrossed for several generations to eliminate any possible off target events prior to phenotyping.

Animal Care and Housing

All *in vivo* studies were carried out using 6-14-week-old mice, of three genotypes ($KCNT1^{+/+}$, $KCNT1^{+/A913T}$ and $KCNT1^{A913T/A913T}$). These mice were produced by crossing $KCNT1^{+/A913T}$ x $KCNT1^{+/A913T}$ ensuring that WT control animals were of the same genetic background as well as exposed to the same environment. Animals were group-housed under a 12/12-h light-dark cycle (lights on at 6 AM) with food and water available *ad libitum*. All animal experiments were approved by the Vanderbilt University Animal Care and Use Committee, and experimental procedures conformed to guidelines established by the National Research Council's *Guide for the Care and Use of Laboratory Animals*. All efforts were made to minimize animal suffering and the number of animals used.

Irwin Assay

On the day of the experiment, the animals were weighed, followed by a series of observational tests. First animals were placed in a new cage and their behavior was assessed as shown in **Observation of Behavior in a Novel Environment** below. Next, animals **Reflexes and Reactions to Simple Stimuli** were performed. Touch escape was assessed by using a single finger stroke from above, starting light and slowly getting firmer until the

animal has a marked response. Next the animal's struggle response to sequential handling was performed to assess positional passivity. Trunk curl was performed by gripping the tail between the thumb and forefinger and lifting the animal about 30 cm above the cage, the presence or absence of a body curl is marked. Reaching reflex was tested by measuring the extension of forelimbs when the mouse is lowered by the base of its tail from a height of 15cm above the edge of a table. Following, a 90 dB click is administered 30 cm above the mouse and the presence of a head twitch, known as the preyer reflex, was assessed. While the mouse was gently restrained, the tip of a 31-gauge stainless-steel wire probe was used to touch each auditory meatus lightly and the retraction of the ear was assessed for level of pinna reflex. All other assessments as outlined below are performed while the animal was grasped by the neck and lying in the palm of the hand. Animal behavioral changes, neuromuscular, autonomic and sensorimotor signs were recorded according to a standardized observation battery^{140,141}. The parameters included in the observations are given in **Table 11** along with detailed scoring methods.

Inverted Screen Assay

Mice were placed on a square of wire mesh (131 mm × 92 mm) which was gently inverted until mice were hanging upside down approx. 30 cm above an enclosure lined with bedding. Mice were observed until they fell, or the maximum trial time of 60 sec had elapsed.

Rotarod Assay

Rotarod testing was conducted using an accelerating rotarod (Ugo Basile, Italy) that increased in speed from 4 to 40 RPM over the course of 4 min with a maximum trial time of 5 min. Three trials were conducted per day, on three consecutive days. The time taken to fall from the apparatus was recorded automatically.

Open Field Assay

Locomotor activity was recorded in square activity chambers (27.5 cm × 27.5 cm) contained within individual sound-attenuating chambers (MedAssociates, Fairfax, VT, USA). Mice were placed in the center of

the chamber and permitted to explore for 60 min. Activity was recorded via the breaking of infra-red beams (MedAssociates ENV-510 software). Time spent in the periphery was calculated for exploration in the edge versus a central square (19.05 cm × 19.05 cm).

Light/Dark Assay

Anxiety behaviors were assessed using a light/dark chamber. Locomotor activity was recorded in square activity chambers (27.5 cm × 27.5 cm) contained within individual sound-attenuating chambers (MedAssociates, Fairfax, VT, USA), modified by inserting a specialized, opaque Dark Box Insert (MedAssociates, Fairfax, VT, USA) to enclose two equal-sized chambers, connected *via* small passage, with one section illuminated and the other one darkened. Activity was recorded via the breaking of infra-red beams (MedAssociates ENV-510 software). At the start of the experiment, the animal was positioned in the bright section and allowed to explore freely both sections for 5 min. Since mice instinctively avoid the brightly lit chamber, percentage of time spent in the lit area, number of crossings between chambers and latency to enter the dark chamber were recorded and used as experimental indices of anxiety.

Elevated Zero Maze

A single 5 min trial was conducted using a standard white elevated zero maze (width 5 cm; diameter 50 cm; wall height 15 cm, Stoelting Co. IL). Mice were video-recorded using a ceiling-mounted camera and viewed remotely by the experimenter in an adjacent room. Position and movements of the mice were analyzed using AnyMaze (Stoelting Co., Wood Dale, IL, USA). Analysis parameters were set so that 80% of the mouse needed to be present in a zone for an entry into that zone to be registered.

Three-Chamber Assay

A three-part trial was conducted using an apparatus consists of a 60 × 42 × 22 cm box divided into 3 equal-sized compartments. In the first portion of the test, the test mouse was introduced into the central chamber of a 3-

chamber cage with the gates open, allowing free movement between the chambers for 5 min for the mouse to habituate. Each side chamber contains a small wire cup. During the second portion of the test, an unfamiliar WT mouse was introduced under the wire cup of one chamber, and the opposite side chamber contains an empty wire cup as a control. In the second portion of the test, the now-familiar WT mouse was reintroduced in a wire cup in one side chamber. A novel WT mouse was present in the cup in the opposite side chamber. Portions two and three of the test are recorded for 7 min each. Behavior in all three portions of the test are videotaped and coded blindly for dependent variables including transitions between chambers, time in each chamber and time spent in close proximity (less than 1 mouse length) to the cup.

Prepulse Inhibition Assay

The test began following a 5 min acclimation period. Nine rounds of pseudorandomized presentations of the following trials: no stimulus, startle pulse alone (120 dB, 40-msec broadband noise burst), and four varying prepulses (70, 76, or 82, or 88 dB; 20 msec) followed by a startle pulse (120 dB, 40-msec broadband noise burst, 50 msec interstimulus interval). The intertrial interval varied randomly between 9 and 21 seconds. Background noise of 65 dB was presented continuously. Percent PPI was calculated as $100 \times (\text{mean acoustic startle reflex [ASR]} - \text{mean ASR in prepulse plus pulse trials}) / \text{mean ASR in startle pulse trials}$. Data are expressed as mean \pm SEM and analyzed using one-way ANOVA with a Bonferroni post-hoc test comparing HET and HOMO groups to WT.

Intracranial Electrode Placement

In order to determine if the A913T Slack mutation affects neuronal firing a small animal telemetry device (HD-X02, Data Sciences, Inc.) was implanted. Before implantation the device was hydrated for at least 30 minutes by adding sterile saline to the sterile container in which it was kept. The animal was placed on the surgery table with the head placed in stereotaxic equipment. For the device implant a 1.5-2 cm incision was made through the skin and the abdominal wall along the ventral midline. A head incision of up to 3 cm through the skin along the

dorsal midline from the posterior margin of the eyes to a point midway between the scapulae. To ensure a pocket was formed, a 3-cc syringe filled with warm, sterile saline was used to irrigate the area. A small (< 4 g) telemetry device is subcutaneously implanted. EEG leads (2) exit through the dorsal neck incision. Using a 0.7 mm micro drill bit the skull was perforated in each hemisphere above the cortex relative to bregma and lambda sutures. Specialized screws (012011-001, Data Sciences, Inc.) were inserted into the skull perforations. Test lead/wire was coiled around the screw and the screw was advanced until fully inserted into the skull and the lead was secure. The skull was then dried and a small amount of dental acrylic was used to maintain the position of the wire. EMG wires (2) were inserted into the cervical trapezius muscles. A 20-gauge syringe needle was used to tunnel through approximately 4 mm of muscle tissue perpendicular to the long axis of the fiber bundles. The EMG lead wire was passed into the lumen of the needle so that, as the needle is withdrawn, the lead wire is left embedded in the muscle. A small silicon tip was placed over the end of the wire to secure it. Non-absorbable sutures were used to close the subcutaneous and skin layers. After postoperative analgesia and a minimum of 72 h recovery, mice were individually housed in transparent home cages in a 12/12-h light-dark cycle (lights on at 6 AM), temperature, and humidity-controlled chamber with *ad libitum* access to food and water before EEG monitoring began.

Electroencephalogram Recordings

Recordings of EEG via telemetry were obtained while mice are in the home cage. Implants were turned on or off by holding a magnet next to the animal. The home cage was positioned over a receiver (flat plate) and the device was turned on. Data was acquired automatically. Recordings were obtained for a minimum of 72 hours and up to 7 days. Food and water are available *ad libitum* throughout the procedure. One-channel video-EEG was recorded between the two electrodes. EEG (500 Hz), core body temperature, and locomotor activity (50 Hz) were continuously sampled over a period of 3-7 days along with time-registered videos.

Table 11: Modified Irwin Assay and Scoring**Physical factors and gross appearance**

Presence of whiskers		Wounds	
0	None	0	None
1	A few	1	Signs of previous wounding
2	Most, but not a full set	2	Slight wounds present
3	A full set	3	Moderate wounds present
		4	Extensive wounds present
Piloerection (hairs standing on end)		Patches of missing fur on face	
0	None	0	None
1	Most hairs standing on end	1	Some
		2	Extensive
Patches of missing fur on body		Appearance of fur	
0	None	0	Ungroomed and disheveled
1	Some	1	Somewhat disheveled
2	Extensive	2	Well-groomed (normal)

Observation of behavior in a novel environment

Transfer behavior		Body position	
0	Coma	0	Completely flat (on stomach)
1	Prolonged freeze (>10 sec.), then slight movement	1	Lying on side
2	Extended freeze, then moderate movement	2	Lying on back
3	Brief freeze (a few seconds), then active movement	3	Sitting or standing
4	Momentary freeze, then swift movement	4	Rearing on hind legs
5	No freeze, immediate movement	5	Repeated vertical leaping
6	Extremely excited ("manic")		
Spontaneous activity		Respiration rate	
0	None, resting	0	Gasping, irregular
1	Casual scratch, groom, slow movement	1	Slow, shallow
2	Vigorous scratch, groom, moderate movement	2	Normal
3	Vigorous, rapid/dart movement	3	Hyperventilation
4	Extremely vigorous, rapid/dart movement		
Piloerection (hairs standing on end)		Tremor	
0	None	0	None
1	Coat stood on end	1	Present
Pelvic Elevation		Gait	
0	Markedly flattened	0	Normal
1	Barely touches	1	Fluid but abnormal
2	Normal (3mm elevation)	2	Limited movement only
3	Elevated (more than 3mm elevation)	3	Incapacity
Palpebral Closure (eyelid closure)		Tail Elevation (during forward motion)	
0	Eyes wide open	0	Dragging
1	Eyes 1/2 closed	1	Horizontally extended
2	Eyes closed	2	Elevated (Straub tail)
Urination		Defecation	
0	None	count the number of fecal boli emitted during the 3-min. period	
1	Little		
2	Moderate amount		
3	Extensive		

Reflexes and reactions to simple stimuli

Touch escape		Positional passivity	
0	No response	0	Struggles when restrained by tail
1	Mild (escape response to firm stroke)	1	Struggles when restrained by neck (finger grip, not scruffed)
2	Moderate (rapid response to light stroke)	2	Struggles when held supine (on back)
3	Vigorous (escape response to approach)	3	Struggles when restrained by hind legs
		4	Does not struggle
Toe pinch		Reaching reflex	
0	None	0	None
1	Slight withdrawal	1	Upon nose contact
2	Moderate withdrawal, not brisk	2	Upon vibrassee contact
3	Brisk, rapid withdrawal	3	Before vibrassee contact (18mm)
4	Very brisk repeated extension and flexion	4	Early vigorous extension (25mm)
Body tone		Pinna reflex	
0	Flaccid, no return of cavity to normal	0	None
1	Slight resistance	1	Active retraction, moderately brisk flick
2	Extreme resistance, board like	2	Hyperactive, repetitive flick
Preyer reflex		Trunk curl	
0	None	0	Absent
1	Active retraction, moderately brisk flick	1	Present
2	Hyperactive, repetitive flick		

Measures recorded during supine restraint

Skin color		Heart Rate	
0	Blanched	0	Slow, bradycardia
1	Pink	1	Normal
2	Bright, deep red flush	2	Fast, tachycardia
Limb Tone		Abdominal Tone	
0	No resistance	0	Flaccid, no return of cavity to normal
1	Slight resistance	1	Slight resistance
2	Moderate resistance	2	Extreme resistance, board like
3	Marked resistance	Righting Reflex	
4	Extreme resistance	1-10	Number of seconds required to right
Provoked Salivation		Air Righting Reflex	
0	None	0	No impairment
1	Slight margin of sub-maxillary area	1-10	Number of seconds required to right
2	Wet zone entire sub-maxillary area	Provoked Biting	
		0	Absent
		1	Present

Grip strength, motor coordination, and locomotor activity

Grip strength	
0	None
1	Slight grip, semi-effective
2	Moderate grip, effective
3	Active grip, effective
4	Unusually effective

Results

Characterization of Gross Physical and Behavioral State of Mutant Slack Mice

To characterize the overall appearance and gross neurologic function of *KCNT1*^{+/^{A913T}}, which will be referred to as HET, and *KCNT1*^{A913T/A913T}, which will be referred to as HOMO herein, mice we utilized a modified Irwin assay. This enabled us to compare physical appearance, behavior in a novel environment, response to a variety of simple stimuli, and reflexes of these mutant animals to that of *KCNT1*^{+/⁺}, which will be referred to as WT henceforth. We did not observe any physical differences between the three genotypes. Slight variations in weight were observed, with HOMO mice tending to be lower in body weight at the time of the assay; however, these results were not statistically significant. Upon introducing the animal in a novel environment, I noted a slight decrease in HOMO animals' spontaneous activity, they appeared more cautious when exploring their new environment and did so at a slower pace than that of WT animals. However, this was an observation assay and these parameters could not be quantified. Similarly, we observed a larger percentage of HOMO mice presented with a tremor (25%) compared to either WT or HET animals (7%, 6%, respectively).

Furthermore, we investigated each group's response to simple stimuli and reflexes. When presented with a finger stroke from above, known as touch escape, HET and HOMO mice attempted to escape upon approach more often than escaping upon touch. Tests investigating the presence or degree of reflex to a variety of stimuli including, being lowered into a cage, touch of the outer ear, presence of a 30 dB sound, or righting themselves when placed on back, revealed no differences between genotypes. Overall, we found no significant differences between our mutant Slack mice and WT mice; however, several observations including, increased presence of a tremor, more cautious exploration and heightened response to simple stimuli all point to a potential anxiety-like phenotype.

Characterization of Mutant Slack Mice Motor Function

After establishing baseline characteristics of our mutant mouse line, we sought to characterize any changes in motor function due to Slack hyperfunction. Beginning with the inverted screen assay, we investigated differences in grip strength between the 3 genotypes by having the mouse grab onto mesh wire before the apparatus is turned upside down, the measurement being latency to fall, with a maximum time of 60 sec. We did not observe any statistically significant differences between genotypes, however; there was a gene-dose dependent decrease in latency to fall. Meaning as the number of copies of mutant Slack channel increased the latency to fall decreased, with WT holding on for longer time than HETs and HETs holding on for longer than HOMO animals. There was also a gene dose-dependent decrease in the percentage of animals able to hold on for the maximum time of 60 sec (WT: 27.8%, HET: 25.8%, HOMO: 23.3%). We then utilized the locomotor activity chamber to gauge overall locomotor levels. Mice are placed in an open, brightly lit, novel square box and allowed to explore for 1 h. Their movements are tracked over this period and indicators of locomotor activity including total distance traveled, mean speed, and stationary time are measured. We observed no differences in these parameters between mutant Slack mice and WT controls. Our final locomotor assay, the rotarod performance test, evaluated balance, grip strength, motor coordination and motor skill learning. This assay consists of a mouse being placed on a rotating rod suspended above a cage floor, the rod accelerates from 0 rotations per min (RPM) to 40 RPMs over the course of 5 min. The ability for the mouse to remain on the rod is analyzed for endurance. Again, we observed a gene dose-dependent decrease in latency to fall for each trial, **Figure 22**. An interesting note is that there appears to be a ceiling effect for mutant animals around 210 sec for day 1, 230 sec for day 2, and 240 sec for day 3, this ceiling was reached during trail 2 each day and remained constant for trail 3 indicating there may be a slight deficit in A913T mutant Slack animal's endurance. Using this assay, we could also glean insight into deficits in motor skill learning, as the test is performed three times per day over three consecutive days. If motor skill learning is normal, an increase in the latency to fall off of the rod should increase between daily trials and between days, showing an upward trend in latency to fall over the three days of testing¹⁵⁶. All 3 genotypes exhibited the ability to increase their time to fall over the course of the 3-day test; however, mutant

Motor Function Assessment

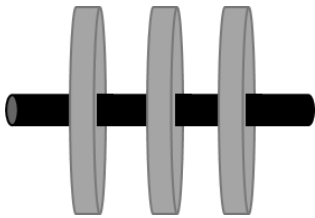
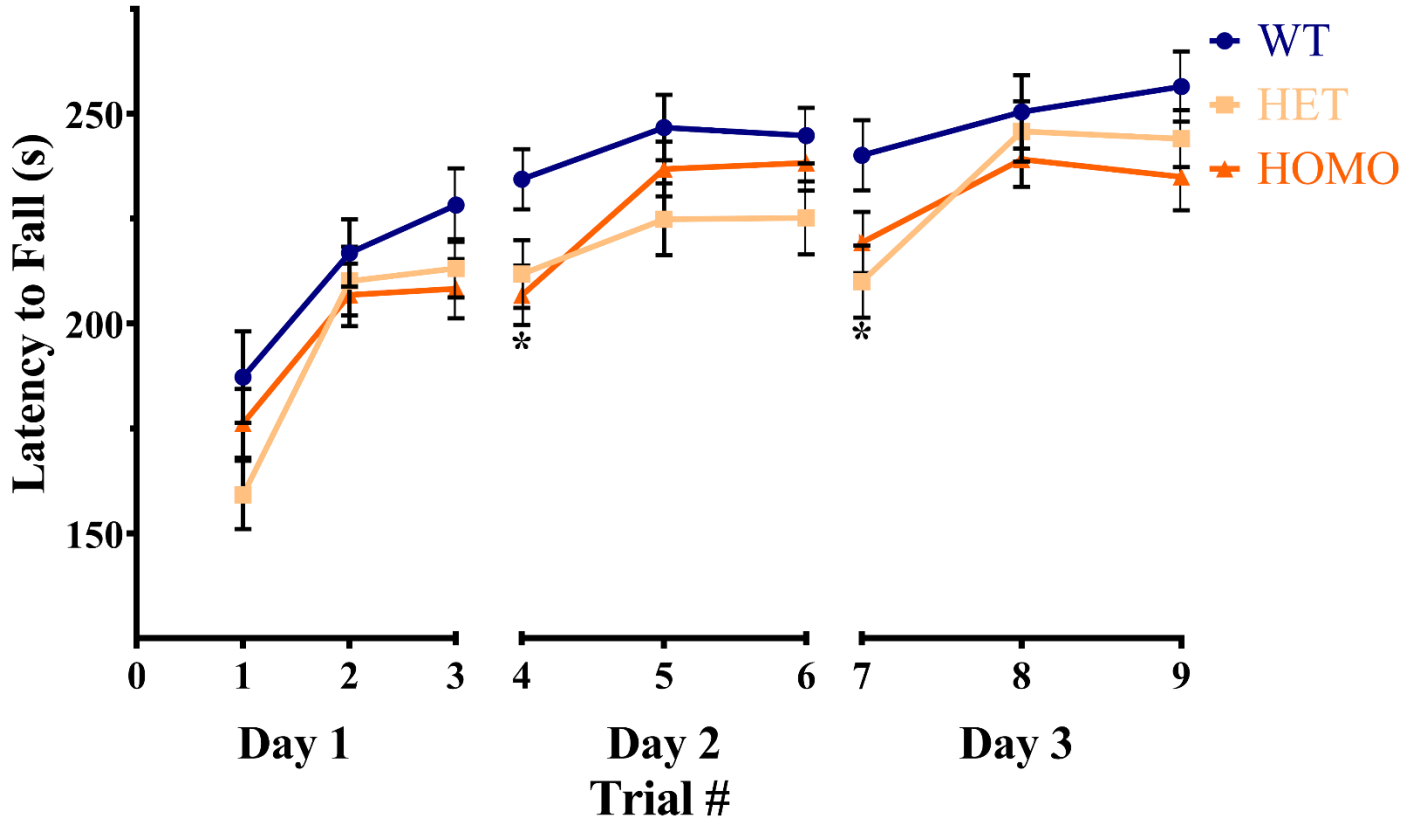


Figure 22: Right: depiction of rotarod apparatus used during this assay. Above: Latency to fall during accelerating rotarod assay. Trial data presented as mean \pm SEM, WT $n = 29$, HET $n = 31$, HOMO $n = 30$. HET animals fell significantly earlier than WT animals during trial 4. HOMO animals fell significantly earlier than WT animals during trial 7, * indicates $p < 0.05$, two-way ANOVA with Bonferroni's post-hoc tests. Note ceiling effect for HET and HOMO animals. Little to no difference is seen in the latency to fall between trials 2 and 3 for a given day.

Slack animals did not retain intrasession (between the final test of one day to the first test of the next day) improvement as seen in WT controls, indicating a slight deficit in motor skill learning. In summary, there were measured differences in motor function, and while none of the individual tests reveal a statistically significant difference between WT and mutant animals, we did observe an overall trend in mutant animals have slight deficits in grip strength, endurance and motor skill learning.

Characterization of Anxiety-like Behaviors in Mutant Slack Mice

Based on the decreased anxiety-like behavior of Slack KO mice, and observations made during the Irwin battery, we sought to investigate these behaviors in our model. We first performed an open field analysis of the data collected during the locomotor chamber assay. This analysis assesses the animal's willingness to explore the center of the chamber compared to the surrounding area. Mice have a natural aversion to brightly lit open spaces, which is characterized by the "center" of the locomotor chamber. The "surrounding", or area closest to the walls of the chamber, is thought to provide a feeling of safety for the animal since it is less exposed. We observed a gene dose-dependent effect on the time it took the animal to enter the surrounding area, with HOMO taking the shortest amount of time, with a mean (95% CI) of 1.55 s (1.09, 2.02), in contrast to WT whose mean (95% CI) latency to enter the surrounding area was 2.47 s (1.74, 3.21) (**Figure 23**).

We then moved to a light-dark chamber assay, in which mice are placed in the same square chamber used for locomotor activity assay with the addition of an insert enclosing half of the chamber, providing the animal with a covered, dark area. Anxiety-like behavior in this assay is expressed as more time spent in the dark chamber, less entries into the light chamber, or a decrease in exploratory behavior such as total distance traveled or rearing to investigate the chamber¹⁵⁷. As seen in open field, we observed a tendency for mutant animals to display anxiety-like behaviors. These included gene dose-dependent trends in an increased resting time, longer duration spent in the dark chamber and a decreased latency to enter the dark chamber; however, these differences did not reach statistical significance.

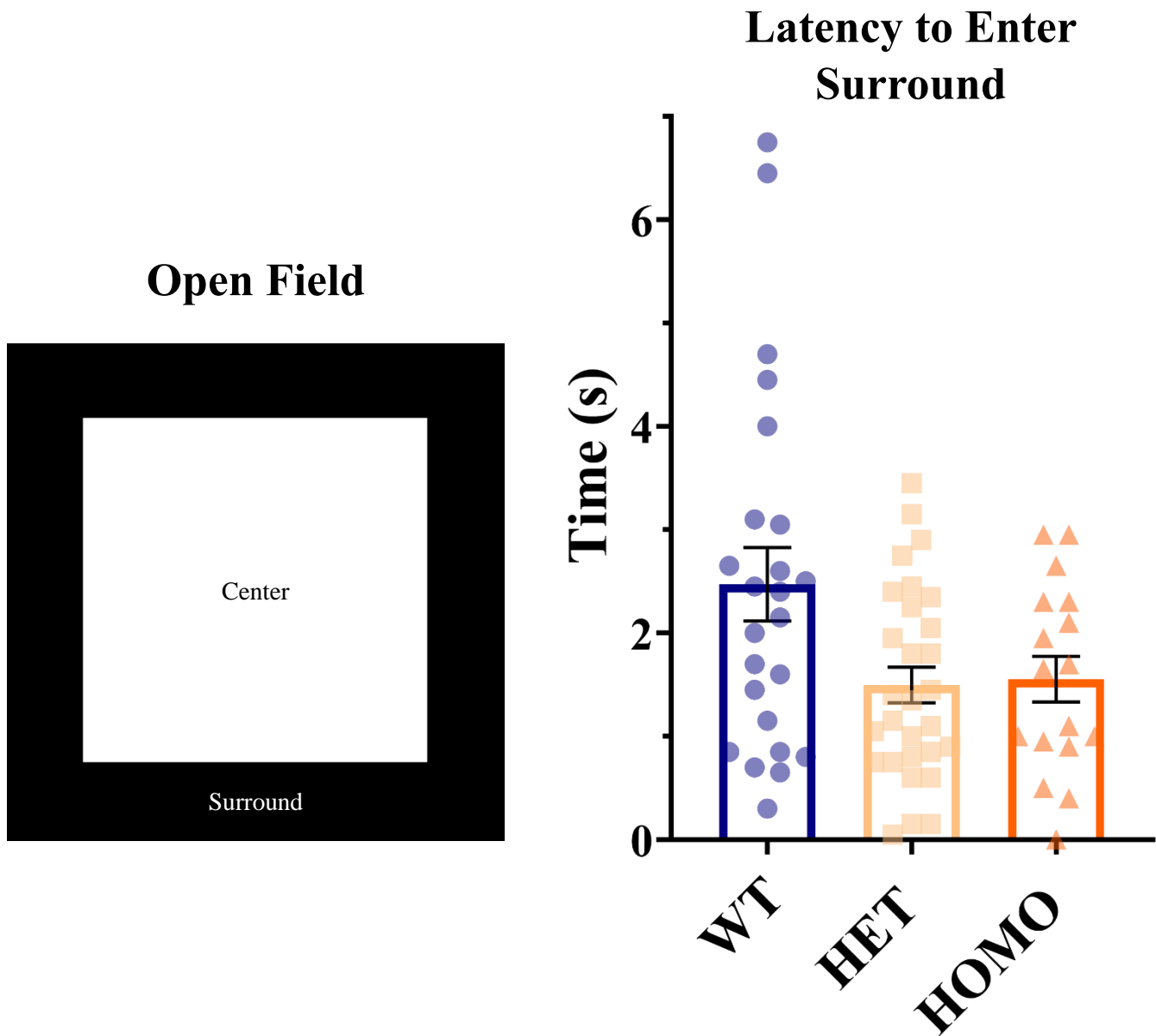


Figure 23: Right: Depicts the two areas, center (white) and surround (black), analyzed during open field. Left: While no statistically significant differences were observed, we noted a trend in mutant Slack animals to enter the surround area quicker than that of WT. Data presented as mean \pm SEM and individual data points as symbols within each bar graph, WT n = 29, HET n = 31, HOMO n = 30.

In our third and final assay investigating anxiety-like behaviors of these animals we conducted a 5 min EZM, in which a mouse is placed on an elevated circular runway with alternating open light areas and enclosed dark areas¹⁵⁸. In this assay, anxiety is expressed by the animal spending more time in the enclosed arms. EZM revealed statistically significant increases in the amount of time HET and HOMO animals spent in the closed arm (**Figure 24a**). Additionally, WT animals traveled a further distance overall and a higher percentage of total distance traveled in the open arms (**Figure 24b, c**). In summary, mutant Slack mice exhibit anxiety-like behaviors, which is clearly illustrated in the EZM assay.

Investigation of Social Interaction in Mutant Slack Mice

We used a 3-chamber social test to quantify sociability and social novelty preference in mutant Slack mice, which are both shown to have deficits in animal models of autism. Testing occurred in three sessions within a three-chambered box with openings between each of the chambers. The first phase began with a 5 min habituation, allowing the test animal to become familiar with its surroundings. In the second phase, a stranger mouse was placed under a wire cup in one chamber and an empty wire cup is placed in the opposing chamber. In this assay the middle chamber remains empty throughout the entire experiment. The test animal was then allowed to investigate for 7 min, the time spent with the other mouse compared to the empty chamber is recorded along with other parameters. The stranger mouse being placed under the cup is particularly important because it allows the test mouse to sniff and explore their new surroundings without direct interaction with the stranger mouse decreasing interference of putative aggressive behavior and other confounding factors⁶⁴. Regardless of genotype, mice spent slightly more time in the chamber containing the stranger mouse over the empty cup (**Figure 25a**). All groups showed greater than 50% preference for exploring the novel mouse over the empty cup (**Figure 25b**). The third and final phase, is designed to estimate social novelty and social memory¹⁴⁴. The test animal encounters the first stranger, now considered a familiar mouse, as well as a second stranger (novel) mouse under the previously empty cup. Again, the animal is allowed to explore all three chambers for 7 min and the time spent in

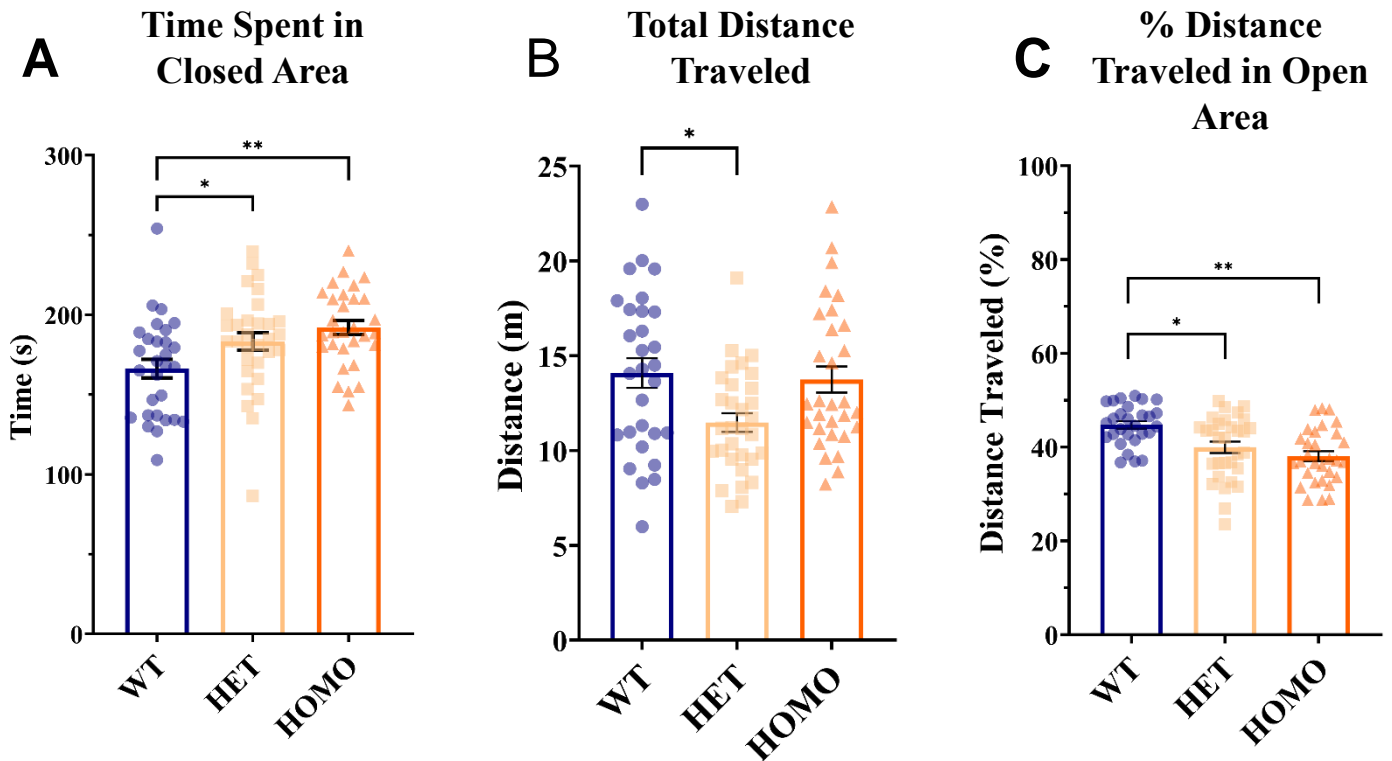
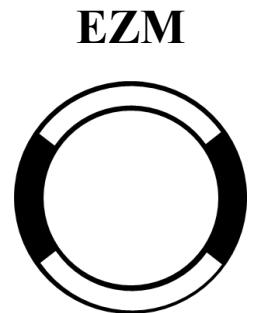


Figure 24: A) Time spent in closed area of EZM, B) total distance traveled and C) distance traveled in open area as a percentage of total distance traveled by WT, HET, and HOMO mice. Mutant Slack mice spent significantly more time in the closed areas and traveled less distance in the open areas of the maze. Data presented as mean \pm SEM and individual data points as symbols within each bar graph, WT n = 29, HET n = 31, HOMO n = 30, * indicates $p < 0.05$, ** indicates $p < 0.0001$ two-way ANOVA with Bonferroni's post-hoc tests. Left: Depiction of an EZM with the open areas in white and closed areas in black.



each chamber. All three genotypes spent slightly more time in the chamber containing the novel mouse (**Figure 25c**) and showed a preference for investigating the novel mouse over the now familiar mouse (**Figure 25d**). While the results of this assay were not statistically significant, this data indicate that A913T mutant Slack mice have no deficits in sociability or social novelty compared to WT controls.

Characterization of Mutant Slack Mice Sensorimotor Function

We utilized an acoustic PPI assay to investigate alterations in sensorimotor gating. Briefly, the acoustic PPI assay consists of three main parts, prepulse, startle stimulus and startle reflex. Mice are placed in a tube on top of a sensing plate that serves as a motion sensor for recording the startle reflex. Animals are habituated to the chamber for 5 min, followed by the start of the session. The session begins with 120 dB, 40 ms burst of sound followed by acoustic startle trials. Four prepulse stimulus intensities are used: 70, 76, 82 and 88 dB, as well as startle stimulus (120 dB) alone and no stimulus. The stimuli are 20 ms in duration and are presented in a pseudorandomized order, followed by the startle stimulus (120 dB).

The startle response is a basic behavioral reaction to a strong auditory stimulus. Analysis of startle reflex amplitudes for the startle stimulus (120 dB) alone trials revealed significantly higher startle amplitudes for HOMO mice compared to WT (**Figure 26b**). The ratio of startle amplitudes between the prepulse and startle stimulus, indicated as PPI, was compared. The PPI of startle describes a phenomenon by which a non-startling sound preceding the startling sound by a few milliseconds reduces the amplitude of the startle response. All three genotypes displayed increased inhibition of startle with increasing prepulse intensity (**Figure 26c**). HOMO animals showed statistically significant decreases in PPI at 76 and 82 dB prepulse intensities, shown in **Figure 26c**. Overall, we observed a gene dose-dependent decrease in PPI at each prepulse intensity, indicating a deficit in sensorimotor gating.

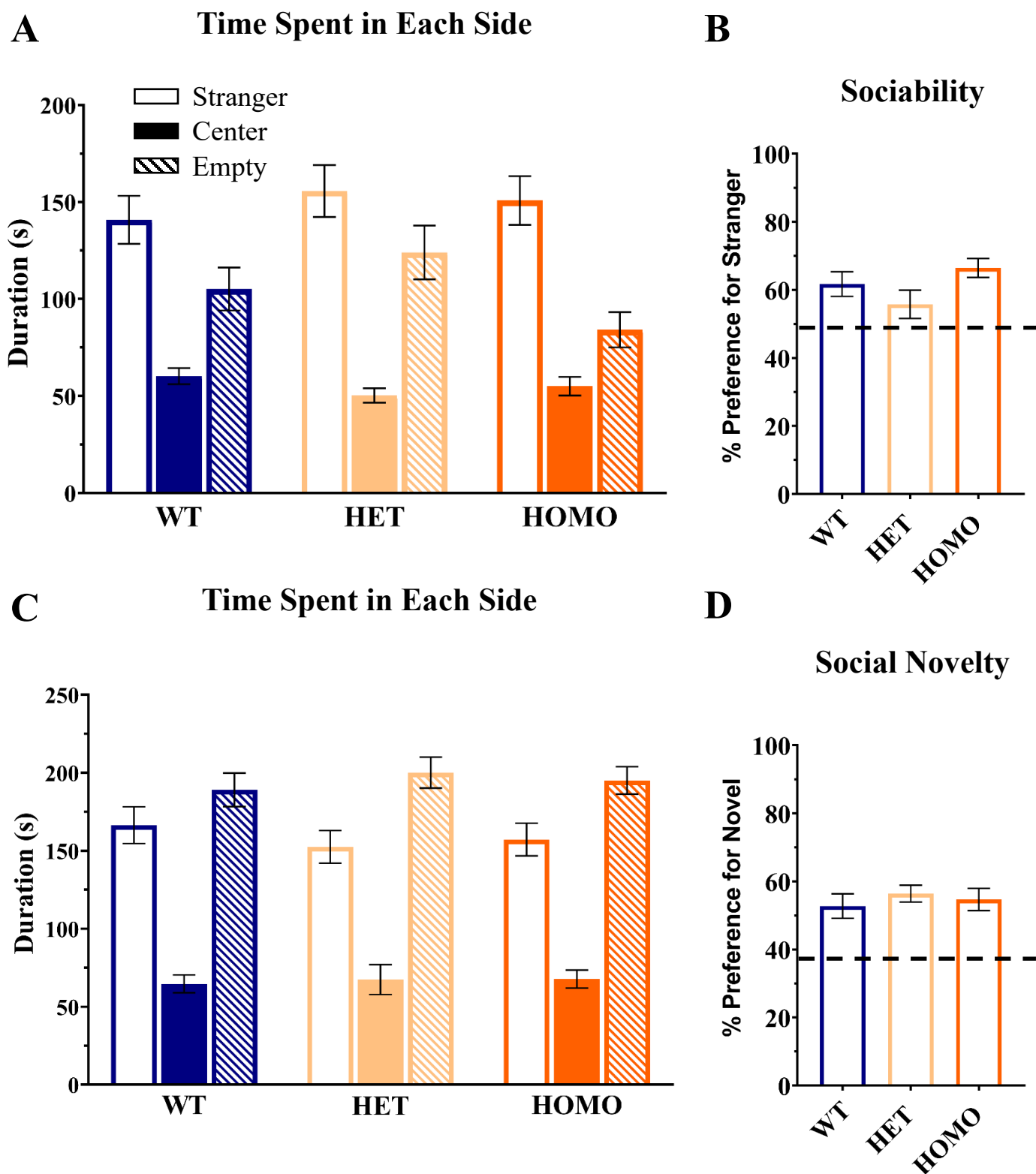


Figure 25: All genotypes show sociability and preference for social novelty in three-chamber tests. A) Time spent in each chamber containing a stranger mouse or empty wire cup, or the center chamber, B) Preference for stranger mouse, calculated as $[(\text{time spent exploring stranger mouse})/(\text{total time spent exploring stranger mouse and empty cup})] \times 100\%$. C) Time spent in each chamber containing the now familiar mouse or novel mouse, or the center chamber. D) Preference for novel mouse, calculated as $[(\text{time spent exploring novel mouse})/(\text{total time spent exploring familiar mouse and novel mouse})] \times 100\%$. Data presented as mean \pm SEM, WT n = 29, HET n = 31, HOMO n = 30.

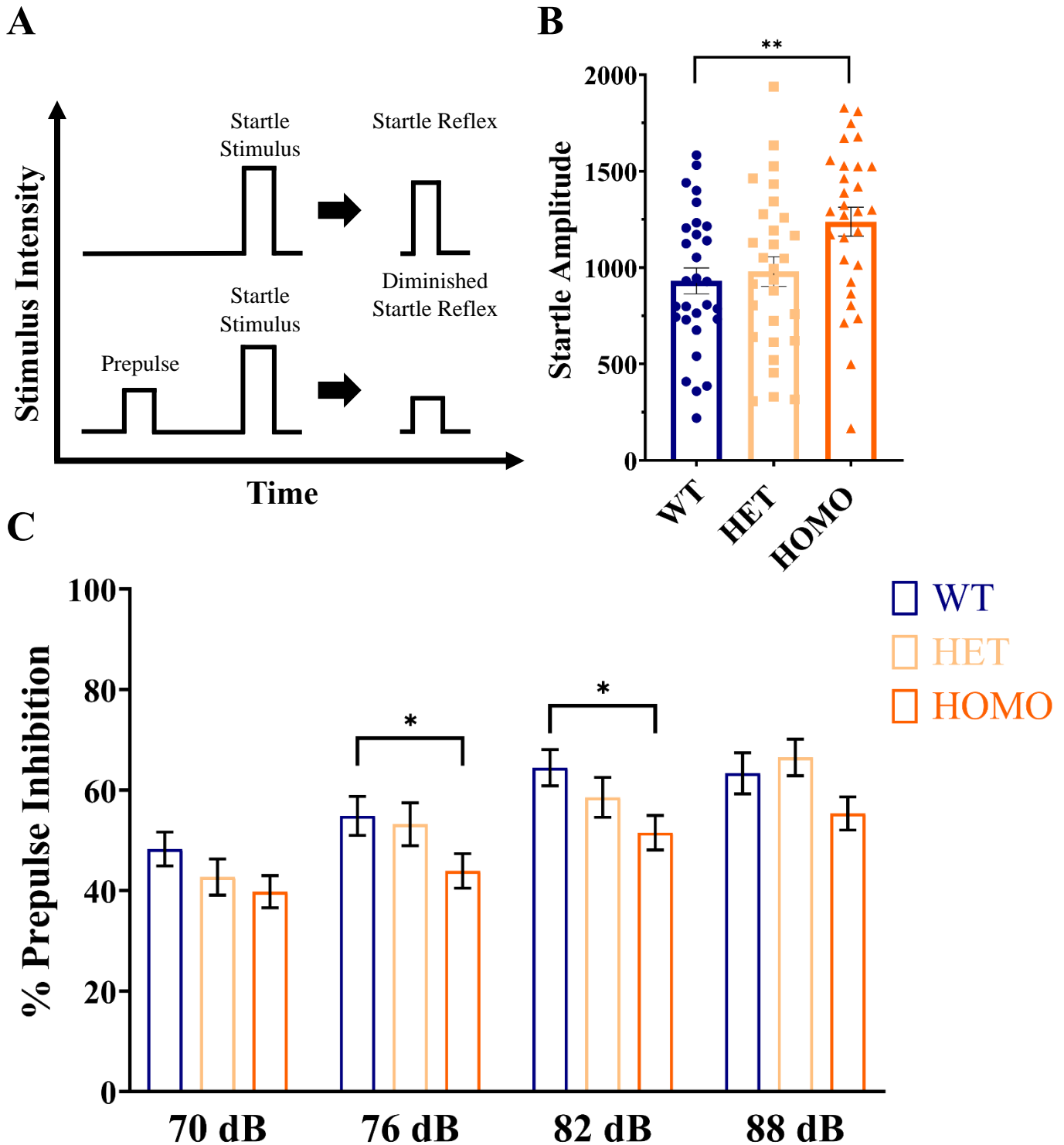


Figure 26: PPI reflects the % decrease in startle to a sound when preceded by a quieter prepulse sound. A) Graphical depiction of prepulse inhibition B) HOMO mice showed startle responses (arbitrary unit) significantly above those of WT control mice. Data presented as mean \pm SEM, * indicates $p < 0.05$ two-way ANOVA with Bonferroni's post-hoc tests. C) Mutant Slack mice showed a deficit in prepulse inhibition of startle compared to WT control mice, however; only 76 dB and 82 dB were statistically significant for HOMO mice compared to WT. Data presented as mean \pm SEM and individual data points as symbols within each bar graph, WT $n = 29$, HET $n = 31$, HOMO $n = 30$. ** indicates $p < 0.001$ one-way ANOVA with Bonferroni's post-hoc tests.

Investigation of Spontaneous Seizure Activity in Mutant Slack Mice

Gain-of-function Slack mutations have been linked to a variety of epilepsies, for this reason we investigated the brain activity of our mutant Slack mouse. A brief description of the surgical and recording methods follow, additional details can be found in **Methods**. The small (< 4 g) telemetry device was implanted into the subcutaneous space above the right rear hindlimb and was able to be turned on and off with a magnet, allowing recordings to take place over several days to months if necessary. The device transmits to a plate receiver placed underneath the animal's cage. Using this approach, the animal remained free to roam about their home cage, unlike older systems in which the animal was tethered to the device. Two stainless steel screws were placed on either side of the skull midline and EEG wires were wrapped around the screws as electrodes to record brain activity. Two additional electrodes were placed in the neck muscle for electromyography (EMG) recording to compare with EEG spikes, since large EMG spikes, or movements of the animal, can result in false EEG spikes. We obtained between 72 and 168 h of EEG/EMG recordings and simultaneous video recordings for 27 mice (WT n=7, HET n=10, HOMO n= 10). We have observed spontaneous seizures in mutant animals but thus far have not observed overt seizure activity in WT controls. However, at this time we are continuing to refine our automated analysis parameters to allow us to quantitatively compare the EEG and EMG recordings of mutant and WT animals. A representative EEG trace is provided in **Figure 27**, showing spontaneous seizure activity noted thus far.

Discussion

Within the last two years three groups, including our own, have begun to characterize mouse models with MMPSI-associated Slack mutations. It is important to note that all three groups have generated mouse lines expressing three separate Slack mutations. The first two groups outlined the epileptic phenotype of their mutant mice, however; they did not fully investigate additional phenotypes associated with hyperfunction of Slack channel, including increased anxiety, deficits in motor skills and altered social function. For this reason, we

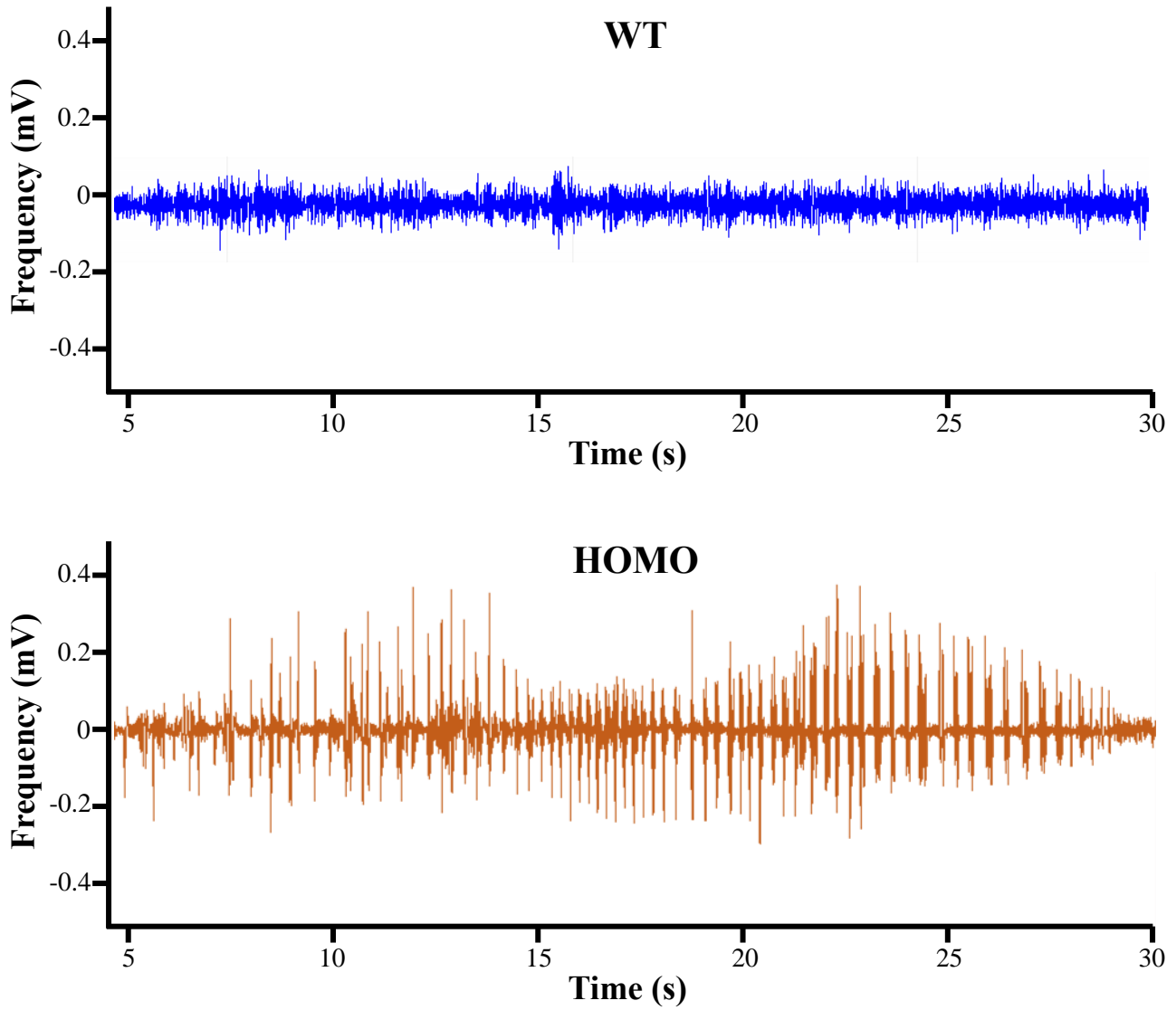


Figure 27: WT EEG activity over 30 sec interval (blue), compared to representative spontaneous seizure recorded from a HOMO mouse EEG (orange).

characterized our A913T mutant Slack mouse model in a variety of assays to investigate a broad range of behaviors.

After determining both *KCNT1*^{+/A913T} (HET) and *KCNT1*^{A913T/A913T} (HOMO) mice were able to survive into adulthood and breed normally, we began by characterizing the overall appearance and gross behaviors of the animals. We compared both HET and HOMO characteristics to that of *KCNT1*^{+/+} (WT) animals from the same litters. Using littermate controls ensures that WT control animals are of the same genetic background and exposed to the same environment as the experimental animals. Mutant Slack mice did not appear to have any outward physical differences compared to WT animals. However, we noted that mutant animals appeared to have slight decreased body weight, this discrepancy appears larger in infants (< 3 weeks) and young juveniles (3-5 weeks). Further studies are needed to assess changes in growth of mutant Slack mice.

Next, we tested the animals' response to simple stimuli. Mutant animals showed no differences in their response to tactile stimulation of the ear or toe, audiogenic stimulation with a 30 dB click, or reaching out when lowered into their cage. We did note a slight decrease in HOMO animals' spontaneous activity, they appeared explore their new environment at a slower pace than that of WT animals, although actual speed was not quantified in this observational assay. This was particularly interesting because mice have a natural tendency to explore a new environment to determine the presence of any threatening stimuli, therefore, a decrease in exploratory behaviors is a marker of anxiety-like behavior in mice. Additionally, we observed a larger percentage of HOMO mice presented with a tremor compared to WT controls. The higher incidence of tremor and lack of exploration led us to hypothesize mutant Slack mice had a higher incidence of anxiety-like behaviors and needed to be explored in assays specifically addressing anxiety.

Before beginning these anxiety-related tests we sought to determine if this observed decrease in exploratory behavior was due to a deficit in motor function rather than increased anxiety. We tested mice in a series of three locomotor function assays: inverted screen, locomotor activity and rotarod. We recorded a slight deficit in grip strength using an inverted screen. We did not observe differences in our Slack mutant mice in the locomotor activity assay. We then moved to an accelerating rotarod assay, in which we tested the mice in 3

separate trials over the course of 3 consecutive days. This assay allows several parameters to be measured including balance, grip strength, motor coordination, and endurance. Additionally, insights into motor skill learning may be gained from this particular assay¹⁵⁹. Throughout this assay we observed a decrease in mutant animals' latency to fall, this difference was greatest during trial 1 of each testing day, indicating the mutant animals has a slight deficit in motor skill learning, since they did not show improvement between testing day (indicated by trials 3 – 4 and 6 – 7 in **Figure 21**). We also observed that the mutant animal's intersession improvement diminished, suggesting a ceiling effect. As shown in **Figure 21**, there is essentially no improvement between trials 2 and 3 for each testing day in both HET and HOMO groups. Taken together, these assays show a slight decrease in motor function in our mutant Slack mice, particularly endurance, as indicated by the ceiling effect in rotarod and decreased latency to fall in inverted screen, and motor skill learning, as indicated by the lack of intrasession improvement at the beginning of the next day's session. We did not detect large motor functions in our mutant mice; therefore, differences we observe in anxiety-like behaviors are not attributed to motor function deficits, allowing us to draw conclusions regarding Slack mutations' association with anxiety-like phenotypes without confounding variables.

While conducting the Irwin assay we noted an increased incidence of tremor and decreased exploration of a new environment, provoking us to investigate behaviors related to anxiety further. Anxiety is defined as a negative emotional state associated with the perception of potential or ambiguous threat¹⁵⁷. It is characterized by a feeling of apprehension, uncertainty, worries, uneasiness or tension stemming from the anticipation of potential threat or negative outcomes. While we cannot directly measure anxiety in animals as we can humans by having them reveal their thoughts, we are able to correlate rodent behaviors to anxiety. Anxiety-related assays exploit the animals' natural aversion to open, brightly lit spaces with the assumption that anxiety involves a conflict between the drive to avoid and the drive to explore these open/lit areas^{60,157}. An increase in time spent in the closed or dark areas compared to WT controls is considered a marker of anxiety-like behavior or a hypersensitivity to light⁶⁰. However, numerous reviews have reported the lack of consistency and reliability between measures of anxiety-related behaviors^{157,160,161}; therefore, we took a broad-based approach and investigated these behaviors

using three typical tests of anxiety, open field analysis of locomotor activity, Light-Dark chamber and EZM. We began by analyzing our locomotor activity chamber data by separating parameters measured into two areas, one being the center, or the open, middle area, of the chamber and the second being the surrounding, or perceived protected area closest to the walls of the chamber. While we did not observe statistically significant differences in the time spent, or distance traveled in either area between genotypes, we did observe a gene dose-dependent trend in mutant animals entering the surrounding area more quickly than WT controls. Similarly, when mice were introduced to the same activity box with half enclosed in a dark, covered box we observed a gene dose-dependent trend in an increased amount of stationary time, longer duration in the dark chamber and a decreased latency to enter the dark chamber by mutant animals. As discussed previously, animals naturally explore a new environment making a decrease in distance traveled and decreased ambulatory time markers of anxiety-like behavior⁶⁰. In an EZM mice are allowed to explore the circular track which alternates between areas of light and dark, time spent in each area, as well as distance traveled are measured. This assay provided the most insight into our mutant Slack mouse model's anxiety-like behaviors. We observed a significant increase in the amount of time mutant mice spent in the closed areas. Similarly, mutant mice exhibited a decrease in the total distance traveled, having been stationary in the closed areas for longer periods of time. We also observed a significant difference in the ratio of distance traveled in open vs closed areas. WT animals traveled at a higher percentage in the open areas of the maze compared to that of mutant Slack animals, indicating their desire to explore the lit, exposed area to a greater degree than mutant animals. Taken together, these assays, especially EZM, indicated an increase in anxiety-like behaviors in mutant Slack mice.

Mutations within Slack have been linked to intellectual disability¹⁶, motor deficits^{12,14,15,20} typical in autism and FXS⁵⁵⁻⁵⁷, which are all associated with alterations in social interactions. For this reason, we investigated the effect of Slack hyperfunction on social interaction in our mouse model, utilizing a 3-chamber social test. We did not observe alterations in sociability or social novelty in these tests, indicating mutant Slack mice display normal social interactions.

Utilizing the PPI assay, we measured deficits in sensorimotor gating in our mutant Slack animals. Deficits in sensorimotor gating have also been associated with autism¹⁵¹⁻¹⁵³ and FXS^{154,155}. Additionally, increased startle amplitudes have been associated with anxiety¹⁶² and autism¹⁶³. We observed a significant increase in the startle reflex amplitude of HOMO animals compared to WT controls. Increased startle responses are excessive or evoked by stimuli that would not be effective in most animals. We detected reduced PPI in our mutant animals in a gene dose-dependent manner, suggesting that Slack contributes to normal sensorimotor gating. Additionally, deficits in PPI have been associated with neonatal epilepsy¹⁶⁴. While we have not tested for, or observed seizures in our mutant mice as neonates, we have documented spontaneous seizures in our mutant animals as early adults, making it within reason to think our mutant Slack mice are having seizures at a young age contributing to their deficits in PPI and abnormal sensorimotor gating.

Our most relevant finding supporting the use of our A913T mutant Slack mice as a model of MMPSI, is the occurrence of spontaneous seizure activity. We have documented seizures via EEG in both our HET and HOMO mutant Slack mice. Additionally, we are analyzing these recordings for single spike epileptiform discharges (EDs) and spike wave discharges (SWDs). These discharges present as individual spikes or a cluster of spikes in an EEG recording but do not last long enough to be considered as a seizure¹⁶⁵. Both EDs and SWDs are abnormal EEG findings associated with epilepsies^{166,167}. Data analysis of these recordings is currently underway; however, we are encouraged by our findings thus far. We would ideally like to find a robust epileptic phenotype in order to evaluate future compounds in vivo. If this phenotype is not observed in our spontaneous seizure assay then we will move to seizure-threshold models. These utilize increasing electroshock intensities or increasing doses of pro-epileptic drugs, such as PTZ, to determine the threshold at which the animal has a tonic seizure that can be observed. These models are based on general observation of the animal and do not require the use of the EEG system, making it less resource intensive. It is worth mentioning that genetic background may be important in the development of epilepsies in humans⁹ and mice^{168,169}. C57BL6 mice are generally regarded to be fairly seizure resistant^{168,169}; therefore, it might be worth breeding the A913T Slack mutation into other background possibly revealing more robust phenotype.

In summary, we have shown our A913T *KCNT1* mouse line is a sufficient and relevant model of MMPSI. We documented several phenotypes associated with MMPSI patients and opposing phenotypes to the KO Slack mice, which were not reported by the two previous mutant Slack mouse models. We revealed an increase in anxiety-like behaviors, slight decreases in motor function associated with motor skill learning, deficits in sensorimotor functioning and spontaneous epileptiform behavior. This model presents yet another advance in the field of Slack and MMPSI research. We are eager to use this model for *in vivo* testing of selective Slack inhibitors in the future.

CHAPTER 6

CONCLUSIONS AND FUTURE DIRECTIONS

Conclusions

MMPSI is a rare, devastating form of epilepsy most commonly associated with gain-of-function mutations in the K⁺ channel, Slack. Not only is this condition almost completely pharmacoresistant, there are not even selective drug-like tools available to evaluate whether inhibition of these over-activated, mutant Slack channels may represent a viable path forward toward new anti-epileptic therapies. Therefore, the overarching goal of my research was to discover and characterize novel Slack channel inhibitors. Additionally, we sought to generate and characterize the utility of a mutant Slack mouse as an *in vivo* model of MMPSI.

In order to discover Slack inhibitors, we used a high-throughput Tl⁺ flux assay to screen a drug-like, 100,000-compound library in search of inhibitors of both WT and disease-associated mutant Slack channels, which is described in **Chapter 2**. Using this approach, we discovered VU0606170, a selective Slack channel full effective inhibitor with low μM potency. Several compounds have been shown to modulate Slack currents *in vitro*, most notably quinidine^{32,47,68-71}, bepridil^{15,37,71} and recently BC1-BC17⁷¹ have been shown to reduce current amplitudes. Unfortunately, each of these compounds are known to modulate multiple other targets^{51,68,72,73} or their selectivity profile has yet to be investigated. In **Chapter 3**, we demonstrate VU0606170's ability to selectively inhibit Slack channels among a diverse group of ion channels.

Critically, VU0606170 also proved effective at significantly decreasing the rate of Ca²⁺ oscillations in over-excited, spontaneously firing cortical neuron cultures. This represents the first pharmacologic evidence that inhibiting Slack channels can produce an AED-like effect, demonstrating that there is hope for conventional pharmacologic approaches for the treatment of MMPSI. While this is an important first step, its PK profile was not suitable for use as an *in vivo* probe. In **Chapter 4** we report the results of our efforts to improve the druglike

qualities of VU0606170 using medicinal chemistry. Although we were unable to significantly improve potency or metabolic stability in these early efforts, we were able to further resolve Slack inhibition from hERG inhibition. We anticipate that continued studies to expand our understanding of SAR related to Slack inhibition will yield further improvements in the drug-like properties of our Slack inhibitors. Taken together, our data provide compelling evidence that selective inhibition of Slack channel activity can be achieved with small molecules and that inhibition of Slack channel activity in neurons produces efficacy consistent with an anti-epileptic effect.

In **Chapter 5**, we discuss the characterization of a novel mutant Slack mouse line, expressing the A913T mutation. At the time this project began there were no *in vivo* models of disease-associated Slack mutations. In order to further investigate the activity of selective Slack inhibitors as therapeutics for MMPSI and other Slack-induced epilepsies, models of these diseases are required. We explored brain activity of these mice to examine the presence of epileptiform behavior. This presented the most relevant finding regarding MMPSI; we observed spontaneous seizure activity in both heterozygous and homozygous mutant mice. Additionally, we investigated the motor function, anxiety-like behaviors, phenotypes related to autism including social behaviors and sensorimotor gating. These assays were chosen for their connection to MMPSI phenotypes or phenotypes associated with Slack KO animals. Our A913T Slack mouse line presented with anxiety-like behaviors, deficits in sensorimotor function, and a slight decline in motor function. All together these data confirm a neurologic phenotype associated with the A913T mutant Slack mouse which will be useful for evaluating the *in vivo* efficacy of Slack inhibitors, the next critical step in helping determine whether inhibition of Slack channels may be a productive approach for the treatment of MMPSI.

The identification of VU0606170 and development and characterization of a mutant Slack mouse provide much-needed tools for advancing our understanding of the role of the Slack channel in normal physiology and disease as well as its potential as a target for therapeutic intervention. In addition, our data demonstrating VU0606170's AED-like effect in WT neurons provides the first intriguing data that Slack inhibition may have broader utility as an AED beyond Slack-associated epilepsies. All in all, these studies provide a promising

foundation for the drug discovery efforts for these important channels and provide a framework for evaluating Slack inhibitors *in vivo*.

Future Directions

Understanding the Mechanism of Action of VU0606170

Going forward, the mechanism by which VU0606170 inhibits Slack channels needs to be elucidated. Our neuronal assay investigating compound activity in over-excited neuronal populations consist of mixed cortical neurons, containing excitatory neurons, inhibitory neurons, and astrocytes. While our data, at least superficially, support the idea that Slack's effect is primary seen in inhibitory neurons, it would be desirable to investigate this more directly. This can be investigated by infecting neurons with a genetically encoded Ca^{2+} signaling dye under a neuron subtype-specific promoter. This would enable us to observe inhibitory neurons alone and the effect of VU0606170. Several variations of these sensors are readily available as recombinant adeno-associated viruses (AAVs) under pan-neuronal and excitatory specific neuronal promoters. AAV vectors are used similarly to plasmids in order to insert new genetic material into the sample at hand. jRCaMP7f is a sensitive Ca^{2+} sensor which is available under the Syn promoter by Addgene (catalog #104488-AAV1) which can subsequently be subcloned into a vector containing the inhibitory neuron specific promoter, h56d. This general process is outlined by Mehta et al.¹⁷⁰. Alternatively, we can explore VU0606170's effect on GABA release using the GABA biosensor, GABase (Sigma Aldrich catalog # G7509). GABase can also be used in brain slices, which would be particularly useful to measure a compound's effect on GABA release in our A913 mutant Slack mouse model.

Investigating Other Slack Inhibitor Scaffolds

Extensively described in **Chapter 4**, VU0606170 does not possess the PK properties to be dose systemically in an animal model of MMPSI. While we have tested 300 structurally related analogs through our SAR studies (**Chapter 4**), we have been unable to produce a significantly more potent, effective and selective compound. For this reason, we have begun investigating a secondary chemical scaffold based on the compound

VU0531245, another hit discovered through the first half of our HTS with low μM potency. CRCs for VU0531245 in Ti^+ flux, along with its chemical structure can be found in **Figure 28**. In collaboration with the Emmitte lab we have already synthesized and tested 85 structurally related analogs in our Ti^+ flux assay. These compounds have not been extensively characterized, however; we recently identified VU0915290 as the most potent compound to date, with an EC_{50} of $1.30\mu\text{M}$ with 95% CI of (0.78, 2.42) for WT Slack and $0.52\mu\text{M}$ (0.44, 0.61) for A934T Slack channels (**Figure 29**). Additionally, this compound showed maximum efficacy (6% (3, 9)) at the mutant channel but only moderate inhibition of WT channels (47% (40, 53)). Efficacy of VU0915290 was compared to E_{max} ($100\mu\text{M}$) of VU0531245. CRCs for VU0915290 in Ti^+ flux, along with its chemical structure can be found in **Figure 29**. Our lab will continue to pursue characterization of the top VU0531245 analogs in an effort to discover a Slack inhibitor suitable for systemic dosing.

We have recently completed the second half of the HTS, providing many additional hits. Once their activity has been confirmed, our lab should begin narrowing down this list of hits by investigating the stability of these compounds in the microsomal intrinsic clearance assay described in **Chapter 4**. Additionally, screening against hERG earlier in the discovery process would allow us to quickly pursue hits with a large separation between Slack and hERG activity.

Further Characterization of A913 Mutant Slack Mice

Future work may involve further characterization of the A913T mutant Slack mouse line, primarily with regards to seizure activity. Models of acute seizures would be useful in determining the mutant animals' susceptibility to seizure induction. The two most extensively studied and well-established animal seizure models are maximal electroshock-induced seizure threshold (MEST) and PTZ-induced seizure threshold. MEST refers to inducing tonic convulsions by applying a low-intensity electrical current of high frequency (50 to 60 Hz) and short duration (0.2 sec), the intensity is slowly increased until all animals have a response. Animals more susceptible to seizures will undergo tonic convulsions at a lower current intensity. The second model of PTZ-induced seizure threshold is essentially performed the same way but with increasing doses of the pro-epileptic

drug PTZ. Again, animals that have a lower seizures threshold will undergo tonic seizures at a lower PTZ dose. With both of these methods seizures are able to be documented by observation, making them less time and resource intensive than the EEG telemetry recordings. Once a validated seizure assay is decided upon, this model or the spontaneous seizure model can be used to validate compounds as an antiepileptic.

If there is no difference in seizure threshold or epileptiform behavior recorded by EEG then the anxiety-like phenotype could be used as a means of testing *in vivo* probes. Once a Slack inhibitor with a PK profile allowing for systemic dosing is identified, it will be used to investigate the reversal of the A913T mouse model's anxiety-like phenotype. The anxiety-like behaviors revealed through EZM provide the most robust phenotype of the mouse model thus far. This would provide a relatively quick and cheap assay to test our hypothesis that Slack inhibition reverses phenotypes associated with gain-of-function Slack mutations. We believe Slack inhibition may be useful for a broader range of epilepsies, for this reason it would be fitting to test Slack inhibitors in a variety of epilepsy models, including the NINDS Epilepsy Therapy Screening Program.

Interpretation and Impact

MMPSI and other Slack related epilepsies have a devastating impact on patients and their families. While the relation of Slack mutations to the development of MMPSI was identified 8 years ago, little progress has been made in understanding the pathophysiology or treatment of the disease until very recent. Shore et al. identified the gain-of-function mutations in Slack lead to a prolonged hyperpolarization in inhibitory neurons. This imbalance between excitatory and inhibitory input leads to the development of seizures. However, seizures are not the only issue these patients face. After speaking with parents and caregivers of MMPSI patients at the KNCT1 Epilepsy Foundation Conference in 2019, I realized that seizures were just a part of what they go through on a day to day. Many of them discussed feeding issues due to a total loss of muscle tone or the devastating fact that they will never hear their child speak or see them take their first steps. It is difficult to put into words how much stories like these affected me and my passion for this research. I came back from the conference with a newborn

sense of focus and drive to identify Slack inhibitors and investigate the phenotype of our mutant Slack mouse model.

Combining both the pharmacologic and genetic approaches of this work we were able to make significant advances in the field of Slack channel and MMPSI research. We have identified the first selective Slack channel inhibitor. Moreover, we showed this compound exhibits an effect similar to antiepileptic drugs when tested in a native system of cultured neurons. We also have characterized several phenotypes in our mutant Slack mouse which will be used to test small molecule Slack channel inhibitors in the future. Though we are still a long way from having a drug to treat MMPSI, this work has provided a leap forward in the development of compounds that may one day lead to a treatment for this devastating disease.

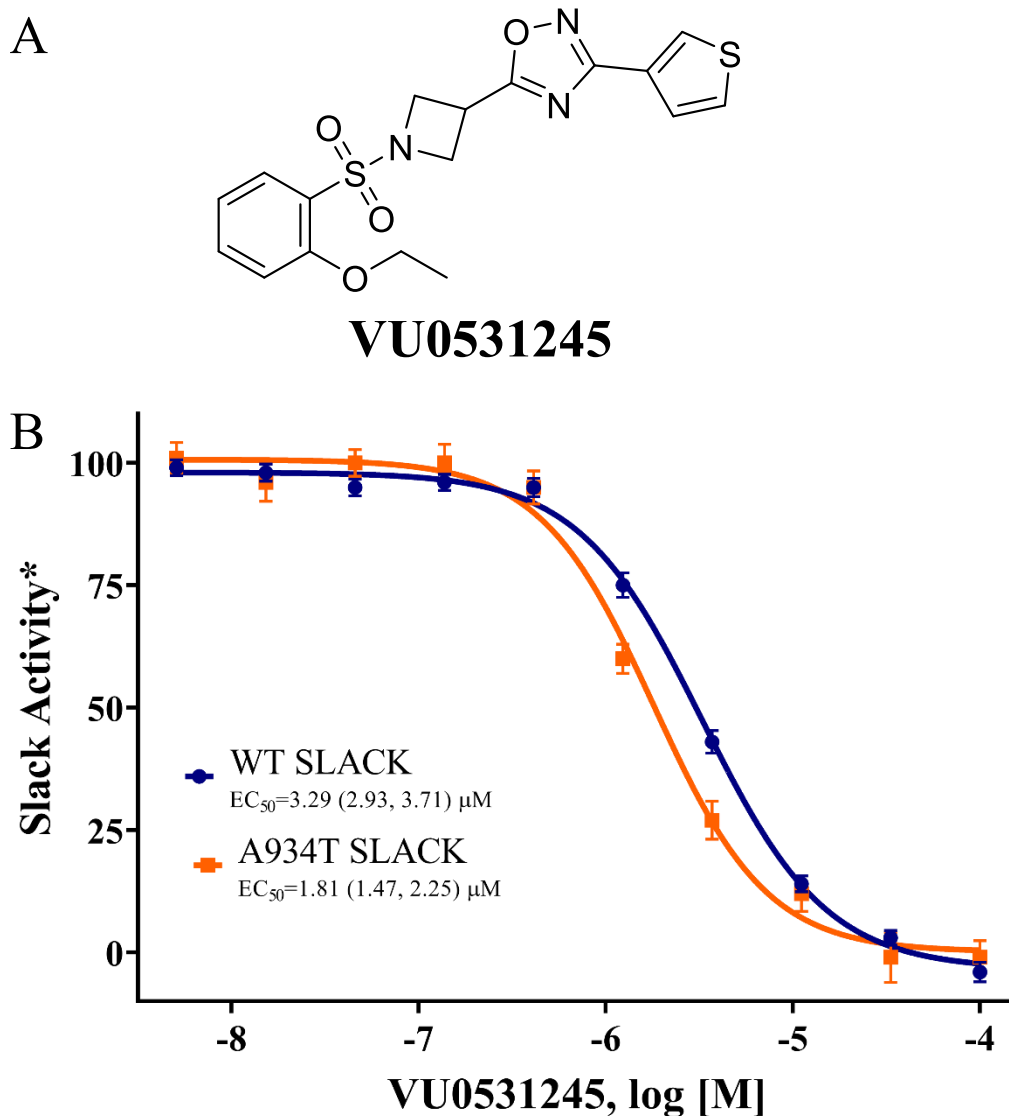


Figure 28: A) Structure of VU0531245. B) Concentration-response curves generated for WT Slack and A934T MMPSI-associated mutant Slack with VU0531245. CRCs arise from Tl^+ flux data obtained from monoclonal cell lines stably expressing WT Slack and A934T mutant Slack in three separate trials. * VU0531245 data is normalized from E_{max} VU245 (100 μ M). EC_{50} (95% CI) values provided, data presented as mean \pm SEM, $n = 19$.

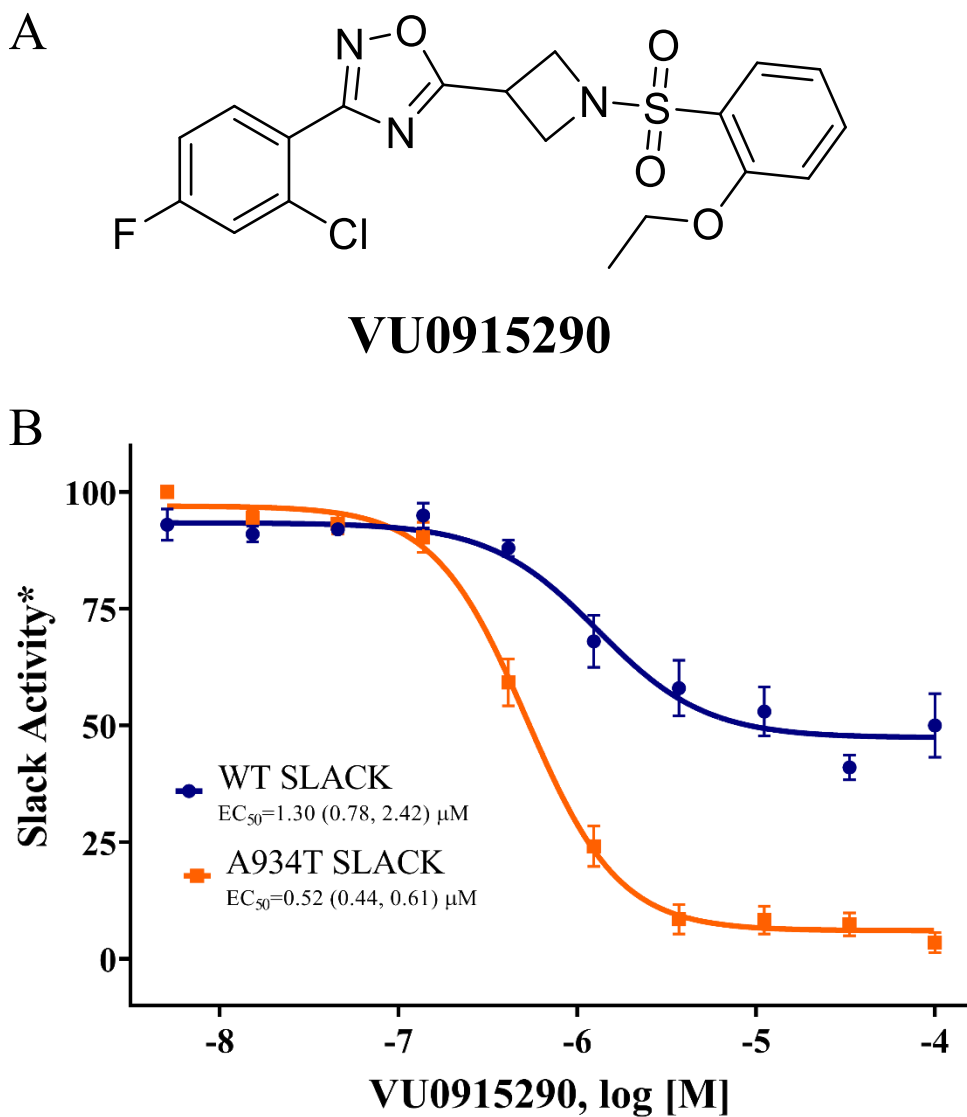


Figure 29: A) Structure of VU0915290. B) Concentration-response curves generated for WT Slack and A934T MMPSI-associated mutant Slack with VU0915290. CRCs arise from Ti^+ flux data obtained from monoclonal cell lines stably expressing WT Slack and A934T mutant. * VU0915290 data is normalized from E_{max} VU245 (100 μM). EC_{50} (95% CI) values provided, mean \pm SEM, $n=3$.

REFERENCES

- 1 Epilepsy Foundation. *About Epilepsy: The Basics*, <<https://www.epilepsy.com/learn/about-epilepsy-basics>> (2020).
- 2 World Health Organization. *WHO | Infographics on epilepsy*, <<https://www.who.int/mediacentre/infographic/mental-health/epilepsy/en/>> (2017).
- 3 Epilepsy Foundation. *Who Gets Epilepsy?*, <<https://www.epilepsy.com/learn/about-epilepsy-basics/who-gets-epilepsy>> (2020).
- 4 Scheffer, I. E. *et al.* ILAE classification of the epilepsies: Position paper of the ILAE Commission for Classification and Terminology. *Epilepsia* **58**, 512-521, doi:10.1111/epi.13709 (2017).
- 5 Epilepsy Foundation. *Types of Seizures*, <<https://www.epilepsy.com/learn/types-seizures>> (2020).
- 6 Kearney, H., Byrne, S., Cavalleri, G. L. & Delanty, N. Tackling Epilepsy With High-definition Precision Medicine: A Review. *JAMA Neurology* **76**, 1109-1116, doi:10.1001/jamaneurol.2019.2384 (2019).
- 7 EpiPM Consortium. A roadmap for precision medicine in the epilepsies. *The Lancet Neurology* **14**, 1219-1228, doi:10.1016/s1474-4422(15)00199-4 (2015).
- 8 Delanty, N. & Cavalleri, G. Genomics-Guided Precise Anti-Epileptic Drug Development. *Neurochem Res* **42**, 2084-2088, doi:10.1007/s11064-017-2312-y (2017).
- 9 Steinlein, O. K. Genetics and epilepsy. *Dialogues Clin Neurosci* **10**, 29-38 (2008).
- 10 Wang, J. *et al.* Epilepsy-associated genes. *Seizure* **44**, 11-20, doi:10.1016/j.seizure.2016.11.030 (2017).
- 11 Perucca, P. Genetics of Focal Epilepsies: What Do We Know and Where Are We Heading? *Epilepsy Currents* **18**, 356-362 (2018).
- 12 Barcia, G. *et al.* De novo gain-of-function KCNT1 channel mutations cause malignant migrating partial seizures of infancy. *Nat Genet* **44**, 1255-1259, doi:10.1038/ng.2441 (2012).
- 13 Coppola, G. *et al.* Mutational scanning of potassium, sodium and chloride ion channels in malignant migrating partial seizures in infancy. *Brain Dev* **28**, 76-79, doi:10.1016/j.braindev.2005.05.002 (2006).
- 14 Rizzo, F. *et al.* Characterization of two de novo KCNT1 mutations in children with malignant migrating partial seizures in infancy. *Mol Cell Neurosci* **72**, 54-63, doi:10.1016/j.mcn.2016.01.004 (2016).
- 15 McTague, A. *et al.* Migrating partial seizures of infancy: expansion of the electroclinical, radiological and pathological disease spectrum. *Brain* **136**, 1578-1591, doi:10.1093/brain/awt073 (2013).
- 16 Kim, G. E. & Kaczmarek, L. K. Emerging role of the KCNT1 Slack channel in intellectual disability. *Front Cell Neurosci* **8**, 209, doi:10.3389/fncel.2014.00209 (2014).
- 17 Coppola, G., Plouin, P., Chiron, C., Robain, O. & Dulac, O. Migrating partial seizures in infancy: a malignant disorder with developmental arrest. *Epilepsia* **36**, 1017-1024, doi:10.1111/j.1528-1157.1995.tb00961.x (1995).
- 18 Coppola, G. *et al.* Temporal lobe dual pathology in malignant migrating partial seizures in infancy. *Epileptic Disord* **9**, 145-148, doi:10.1684/epd.2007.0106 (2007).
- 19 Lim, C. X., Ricos, M. G., Dibbens, L. M. & Heron, S. E. KCNT1 mutations in seizure disorders: the phenotypic spectrum and functional effects. *J Med Genet* **53**, 217-225, doi:10.1136/jmedgenet-2015-103508 (2016).
- 20 McTague, A. *et al.* Clinical and molecular characterization of KCNT1-related severe early-onset epilepsy. *Neurology* **90**, e55-e66, doi:10.1212/WNL.0000000000004762 (2018).
- 21 KCNT1 Epilepsy Foundation. *What We Know about KCNT1 Epilepsy*, <<https://kcnt1epilepsy.org/kcnt1-epilepsy>> (2020).
- 22 Moller, R. S. *et al.* Mutations in KCNT1 cause a spectrum of focal epilepsies. *Epilepsia* **56**, e114-120, doi:10.1111/epi.13071 (2015).
- 23 De Filippo, M. R. *et al.* Lack of pathogenic mutations in six patients with MMPSI. *Epilepsy Res* **108**, 340-344, doi:10.1016/j.epilepsyres.2013.11.007 (2014).
- 24 Ohba, C. *et al.* De novo KCNT1 mutations in early-onset epileptic encephalopathy. *Epilepsia* **56**, e121-128, doi:10.1111/epi.13072 (2015).
- 25 Heron, S. E. *et al.* Missense mutations in the sodium-gated potassium channel gene KCNT1 cause severe autosomal dominant nocturnal frontal lobe epilepsy. *Nat Genet* **44**, 1188-1190, doi:10.1038/ng.2440 (2012).

- 26 Ishii, A. *et al.* A recurrent KCNT1 mutation in two sporadic cases with malignant migrating partial seizures in infancy. *Gene* **531**, 467-471, doi:10.1016/j.gene.2013.08.096 (2013).
- 27 Vanderver, A. *et al.* Identification of a novel de novo p.Phe932Ile KCNT1 mutation in a patient with leukoencephalopathy and severe epilepsy. *Pediatr Neurol* **50**, 112-114, doi:10.1016/j.pediatrneurol.2013.06.024 (2014).
- 28 Hille, B. *Ion Channels of Excitable Membranes*. 3rd edn, (Sinauer Associates, Inc., 2001).
- 29 Ion Channels. *Br J Pharmacol* **164**, S137-174, doi:10.1111/j.1476-5381.2011.01649_5.x (2011).
- 30 Potassium. *Br J Pharmacol* **158**, S141-143, doi:10.1111/j.1476-5381.2009.00503_12.x (2009).
- 31 Bhattacharjee, A. & Kaczmarek, L. K. For K⁺ channels, Na⁺ is the new Ca²⁺. *Trends Neurosci* **28**, 422-428, doi:10.1016/j.tins.2005.06.003 (2005).
- 32 Kaczmarek, L. K. Slack, Slick and Sodium-Activated Potassium Channels. *ISRN Neurosci* **2013**, doi:10.1155/2013/354262 (2013).
- 33 Tamsett, T. J., Picchione, K. E. & Bhattacharjee, A. NAD⁺ activates KNa channels in dorsal root ganglion neurons. *J Neurosci* **29**, 5127-5134, doi:10.1523/JNEUROSCI.0859-09.2009 (2009).
- 34 Canto, C., Menzies, K. J. & Auwerx, J. NAD(+) Metabolism and the Control of Energy Homeostasis: A Balancing Act between Mitochondria and the Nucleus. *Cell Metab* **22**, 31-53, doi:10.1016/j.cmet.2015.05.023 (2015).
- 35 Tang, Q. Y. *et al.* Epilepsy-Related Slack Channel Mutants Lead to Channel Over-Activity by Two Different Mechanisms. *Cell Rep* **14**, 129-139, doi:10.1016/j.celrep.2015.12.019 (2016).
- 36 Yang, B., Desai, R. & Kaczmarek, L. K. Slack and Slick K(Na) channels regulate the accuracy of timing of auditory neurons. *J Neurosci* **27**, 2617-2627, doi:10.1523/JNEUROSCI.5308-06.2007 (2007).
- 37 Gertler, T. S., Thompson, C. H., Vanoye, C. G., Millichap, J. J. & George, A. L., Jr. Functional consequences of a KCNT1 variant associated with status dystonicus and early-onset infantile encephalopathy. *Ann Clin Transl Neurol* **6**, 1606-1615, doi:10.1002/acn3.50847 (2019).
- 38 Budelli, G. *et al.* Na⁺-activated K⁺ channels express a large delayed outward current in neurons during normal physiology. *Nat Neurosci* **12**, 745-750, doi:10.1038/nn.2313 (2009).
- 39 Yuan, A. *et al.* The sodium-activated potassium channel is encoded by a member of the Slo gene family. *Neuron* **37**, 765-773, doi:10.1016/s0896-6273(03)00096-5 (2003).
- 40 Bhattacharjee, A., Gan, L. & Kaczmarek, L. K. Localization of the Slack potassium channel in the rat central nervous system. *J Comp Neurol* **454**, 241-254, doi:10.1002/cne.10439 (2002).
- 41 Brown, M. R. *et al.* Amino-terminal isoforms of the Slack K⁺ channel, regulated by alternative promoters, differentially modulate rhythmic firing and adaptation. *J Physiol* **586**, 5161-5179, doi:10.1113/jphysiol.2008.160861 (2008).
- 42 <Joiner 1998 Intermediate Conductance channels Slack and Slo Interaction.pdf>
- 43 Joiner, W. J. *et al.* Formation of intermediate-conductance calcium-activated potassium channels by interaction of Slack and Slo subunits. *Nat Neurosci* **1**, 462-469, doi:10.1038/2176 (1998).
- 44 Santi, C. M. *et al.* Opposite regulation of Slick and Slack K⁺ channels by neuromodulators. *J Neurosci* **26**, 5059-5068, doi:10.1523/JNEUROSCI.3372-05.2006 (2006).
- 45 Bausch, A. E. *et al.* The sodium-activated potassium channel Slack is required for optimal cognitive flexibility in mice. *Learn Mem* **22**, 323-335, doi:10.1101/lm.037820.114 (2015).
- 46 Shore, A. N. *et al.* The paradoxical effects of K⁺ channel gain-of-function are mediated by GABAergic neuron hypoexcitability and hyperconnectivity. *bioRxiv*, 2020.2003.2005.978841, doi:10.1101/2020.03.05.978841 (2020).
- 47 Kim, G. E. *et al.* Human slack potassium channel mutations increase positive cooperativity between individual channels. *Cell Rep* **9**, 1661-1672, doi:10.1016/j.celrep.2014.11.015 (2014).
- 48 Martin, H. C. *et al.* Clinical whole-genome sequencing in severe early-onset epilepsy reveals new genes and improves molecular diagnosis. *Hum Mol Genet* **23**, 3200-3211, doi:10.1093/hmg/ddu030 (2014).
- 49 Quraishi, I. H. *et al.* An Epilepsy-Associated KCNT1 Mutation Enhances Excitability of Human iPSC-Derived Neurons by Increasing Slack KNa Currents. *J Neurosci* **39**, 7438-7449, doi:10.1523/JNEUROSCI.1628-18.2019 (2019).
- 50 Quraishi, I. H. *et al.* Impaired motor skill learning and altered seizure susceptibility in mice with loss or gain of function of the Kcnt1 gene encoding Slack (KNa1.1) Na(+)-activated K(+) channels. *Sci Rep* **10**, 3213, doi:10.1038/s41598-020-60028-z (2020).

- 51 Milligan, C. J. *et al.* KCNT1 gain of function in 2 epilepsy phenotypes is reversed by quinidine. *Ann Neurol* **75**, 581-590, doi:10.1002/ana.24128 (2014).
- 52 Du, W. *et al.* Calcium-sensitive potassium channelopathy in human epilepsy and paroxysmal movement disorder. *Nat Genet* **37**, 733-738, doi:10.1038/ng1585 (2005).
- 53 Derry, C. P. *et al.* Severe autosomal dominant nocturnal frontal lobe epilepsy associated with psychiatric disorders and intellectual disability. *Epilepsia* **49**, 2125-2129, doi:10.1111/j.1528-1167.2008.01652.x (2008).
- 54 McTague, A., Howell, K. B., Cross, J. H., Kurian, M. A. & Scheffer, I. E. The genetic landscape of the epileptic encephalopathies of infancy and childhood. *The Lancet Neurology* **15**, 304-316, doi:10.1016/s1474-4422(15)00250-1 (2016).
- 55 Brown, M. R. *et al.* Fragile X mental retardation protein controls gating of the sodium-activated potassium channel Slack. *Nat Neurosci* **13**, 819-821, doi:10.1038/nn.2563 (2010).
- 56 Zhang, Y. *et al.* Regulation of neuronal excitability by interaction of fragile X mental retardation protein with slack potassium channels. *J Neurosci* **32**, 15318-15327, doi:10.1523/jneurosci.2162-12.2012 (2012).
- 57 Guglielmi, L. *et al.* Update on the implication of potassium channels in autism: K(+) channelautism spectrum disorder. *Front Cell Neurosci* **9**, 34, doi:10.3389/fncel.2015.00034 (2015).
- 58 Perlman, R. L. Mouse models of human disease: An evolutionary perspective. *Evol Med Public Health* **2016**, 170-176, doi:10.1093/emph/eow014 (2016).
- 59 Waterston, R. H. *et al.* Initial sequencing and comparative analysis of the mouse genome. *Nature* **420**, 520-562, doi:10.1038/nature01262 (2002).
- 60 Lezak, K. R., Missig, G. & Carlezon, W. A., Jr. Behavioral methods to study anxiety in rodents. *Dialogues Clin Neurosci* **19**, 181-191 (2017).
- 61 Löscher, W. Critical review of current animal models of seizures and epilepsy used in the discovery and development of new antiepileptic drugs. *Seizure* **20**, 359-368, doi:10.1016/j.seizure.2011.01.003 (2011).
- 62 Gonzalez, D. *et al.* Audiogenic Seizures in the Fmr1 Knock-Out Mouse Are Induced by Fmr1 Deletion in Subcortical, VGlut2-Expressing Excitatory Neurons and Require Deletion in the Inferior Colliculus. *The Journal of Neuroscience* **39**, 9852-9863, doi:10.1523/jneurosci.0886-19.2019 (2019).
- 63 Lu, R. *et al.* Slack channels expressed in sensory neurons control neuropathic pain in mice. *J Neurosci* **35**, 1125-1135, doi:10.1523/JNEUROSCI.2423-14.2015 (2015).
- 64 Bausch, A. E. *et al.* Loss of Sodium-Activated Potassium Channel Slack and FMRP Differentially Affect Social Behavior in Mice. *Neuroscience* **384**, 361-374, doi:10.1016/j.neuroscience.2018.05.040 (2018).
- 65 Martinez-Espinosa, P. L. *et al.* Knockout of Slo2.2 enhances itch, abolishes KNa current, and increases action potential firing frequency in DRG neurons. *Elife* **4**, doi:10.7554/eLife.10013 (2015).
- 66 Moy, S. S. *et al.* Sociability and preference for social novelty in five inbred strains: an approach to assess autistic-like behavior in mice. *Genes Brain Behav* **3**, 287-302, doi:10.1111/j.1601-1848.2004.00076.x (2004).
- 67 Burbano, L. *et al.* in *Neurology*. P2.273.
- 68 Bearden, D. S., Alanna; Ehnot, Jessica; DiGiovine, Marissa; Dlugos, Dennis; Goldberg, Ethan M. Targeted Treatment of Migrating Partial Seizures of Infancy with Quinidine. *ANN NEUROL* **76**, 457-461, doi:10.1002/ana (2014).
- 69 de Los Angeles Tejada, M., Stolpe, K., Meinild, A. K. & Klaerke, D. A. Clofilium inhibits Slick and Slack potassium channels. *Biologics* **6**, 465-470, doi:10.2147/BTT.S33827 (2012).
- 70 Yang, B. *et al.* Pharmacological activation and inhibition of Slack (Slo2.2) channels. *Neuropharmacology* **51**, 896-906, doi:10.1016/j.neuropharm.2006.06.003 (2006).
- 71 Cole, B. A. *et al.* Structure-Based Identification and Characterization of Inhibitors of the Epilepsy-Associated KNa1.1 (KCNT1) Potassium Channel. *iScience* **23**, 101100, doi:10.1016/j.isci.2020.101100 (2020).
- 72 Milligan CJ, L. M., Gazina EV, Heron SE, Nair U, Trager C, Reid CA, Venkat A, Younkin DP, Dlugos DJ, Petrovski S, Goldstein DB, Dibbens LM, Scheffer IE, Berkovic SF, Petrou S. . KCNT1 gain-of-function mutations linked to human epilepsy are modulated by quinidine. *Molecular & Cellular Epilepsy* **75**, 581-590, doi:10.14800/mce.220 (2014).
- 73 Mullen, S. A. *et al.* Precision therapy for epilepsy due to KCNT1 mutations: A randomized trial of oral quinidine. *Neurology* **90**, e67-e72, doi:10.1212/WNL.0000000000004769 (2018).
- 74 Meador, K. J. & Shin, C. Pitfalls in developing precision medicine for genetic epilepsy. *Neurology* **90**, 16-17, doi:10.1212/WNL.0000000000004774 (2018).

- 75 Madaan, P., Jauhari, P., Gupta, A., Chakrabarty, B. & Gulati, S. A quinidine non responsive novel KCNT1 mutation in an Indian infant with epilepsy of infancy with migrating focal seizures. *Brain Dev* **40**, 229-232, doi:10.1016/j.braindev.2017.09.008 (2018).
- 76 Weaver, C. D., Harden, D., Dworetzky, S. I., Robertson, B. & Knox, R. J. A thallium-sensitive, fluorescence-based assay for detecting and characterizing potassium channel modulators in mammalian cells. *J Biomol Screen* **9**, 671-677, doi:10.1177/1087057104268749 (2004).
- 77 Niswender, C. M. *et al.* A novel assay of Gi/o-linked G protein-coupled receptor coupling to potassium channels provides new insights into the pharmacology of the group III metabotropic glutamate receptors. *Mol Pharmacol* **73**, 1213-1224, doi:10.1124/mol.107.041053 (2008).
- 78 Niswender, C. M. *et al.* Discovery, characterization, and antiparkinsonian effect of novel positive allosteric modulators of metabotropic glutamate receptor 4. *Mol Pharmacol* **74**, 1345-1358, doi:10.1124/mol.108.049551 (2008).
- 79 Williams, R. *et al.* Synthesis and SAR of a novel positive allosteric modulator (PAM) of the metabotropic glutamate receptor 4 (mGluR4). *Bioorg Med Chem Lett* **19**, 4967-4970, doi:10.1016/j.bmcl.2009.07.072 (2009).
- 80 Utle, T. *et al.* Synthesis and SAR of a novel metabotropic glutamate receptor 4 (mGlu4) antagonist: unexpected 'molecular switch' from a closely related mGlu4 positive allosteric modulator. *Bioorg Med Chem Lett* **21**, 6955-6959, doi:10.1016/j.bmcl.2011.09.131 (2011).
- 81 Ghamari-Langroudi, M. *et al.* G-protein-independent coupling of MC4R to Kir7.1 in hypothalamic neurons. *Nature* **520**, 94-98, doi:10.1038/nature14051 (2015).
- 82 Raphemot, R. *et al.* Eliciting renal failure in mosquitoes with a small-molecule inhibitor of inward-rectifying potassium channels. *PLoS One* **8**, e64905, doi:10.1371/journal.pone.0064905 (2013).
- 83 Raphemot, R. *et al.* Discovery, characterization, and structure-activity relationships of an inhibitor of inward rectifier potassium (Kir) channels with preference for Kir2.3, Kir3.x, and Kir7.1. *Front Pharmacol* **2**, 75, doi:10.3389/fphar.2011.00075 (2011).
- 84 Raphemot, R. *et al.* Discovery and characterization of a potent and selective inhibitor of *Aedes aegypti* inward rectifier potassium channels. *PLoS One* **9**, e110772, doi:10.1371/journal.pone.0110772 (2014).
- 85 Du, Y. *et al.* Development and validation of a thallium flux-based functional assay for the sodium channel NaV1.7 and its utility for lead discovery and compound profiling. *ACS Chem Neurosci* **6**, 871-878, doi:10.1021/acscchemneuro.5b00004 (2015).
- 86 Delpire, E. & Weaver, C. D. Challenges of Finding Novel Drugs Targeting the K-Cl Cotransporter. *ACS Chem Neurosci* **7**, 1624-1627, doi:10.1021/acscchemneuro.6b00366 (2016).
- 87 Shaw, G., Morse, S., Ararat, M. & Graham, F. L. Preferential transformation of human neuronal cells by human adenoviruses and the origin of HEK 293 cells. *Faseb j* **16**, 869-871, doi:10.1096/fj.01-0995fje (2002).
- 88 Biton, B. *et al.* The antipsychotic drug loxapine is an opener of the sodium-activated potassium channel slack (Slo2.2). *J Pharmacol Exp Ther* **340**, 706-715, doi:10.1124/jpet.111.184622 (2012).
- 89 Raphemot, R. *et al.* Development and validation of fluorescence-based and automated patch clamp-based functional assays for the inward rectifier potassium channel Kir4.1. *Assay Drug Dev Technol* **11**, 532-543, doi:10.1089/adt.2013.544 (2013).
- 90 Kharade, S. V. *et al.* Discovery, Characterization, and Effects on Renal Fluid and Electrolyte Excretion of the Kir4.1 Potassium Channel Pore Blocker, VU0134992. *Mol Pharmacol* **94**, 926-937, doi:10.1124/mol.118.112359 (2018).
- 91 Kozek, K. A. *et al.* Discovery and Characterization of VU0529331, a Synthetic Small-Molecule Activator of Homomeric G Protein-Gated, Inwardly Rectifying, Potassium (GIRK) Channels. *ACS Chem Neurosci* **10**, 358-370, doi:10.1021/acscchemneuro.8b00287 (2019).
- 92 Ko, A. *et al.* Targeted gene panel and genotype-phenotype correlation in children with developmental and epileptic encephalopathy. *Epilepsy Res* **141**, 48-55, doi:10.1016/j.epilepsyres.2018.02.003 (2018).
- 93 Johannesen, K. M. *et al.* Utility of genetic testing for therapeutic decision-making in adults with epilepsy. *Epilepsia* **61**, 1234-1239, doi:10.1111/epi.16533 (2020).
- 94 Borlot, F. *et al.* KCNT1-related epilepsy: An international multicenter cohort of 27 pediatric cases. *Epilepsia* **61**, 679-692, doi:10.1111/epi.16480 (2020).

- 95 Trump, N. *et al.* Improving diagnosis and broadening the phenotypes in early-onset seizure and severe developmental delay disorders through gene panel analysis. *J Med Genet* **53**, 310-317, doi:10.1136/jmedgenet-2015-103263 (2016).
- 96 Barcia, G. *et al.* Epilepsy with migrating focal seizures: KCNT1 mutation hotspots and phenotype variability. *Neurol Genet* **5**, e363, doi:10.1212/NXG.0000000000000363 (2019).
- 97 Mori, T. *et al.* Usefulness of ketogenic diet in a girl with migrating partial seizures in infancy. *Brain Dev* **38**, 601-604, doi:10.1016/j.braindev.2015.12.012 (2016).
- 98 Harvey, R. D. & Grant, A. O. in *Basic & Clinical Pharmacology, 14e* (ed Bertram G. Katzung) (McGraw-Hill Education, 2017).
- 99 Starmer, C. F., Grant, A. O. & Strauss, H. C. Mechanisms of use-dependent block of sodium channels in excitable membranes by local anesthetics. *Biophys J* **46**, 15-27, doi:10.1016/s0006-3495(84)83994-6 (1984).
- 100 Scholz, A. Mechanisms of (local) anaesthetics on voltage-gated sodium and other ion channels. *BJA: British Journal of Anaesthesia* **89**, 52-61, doi:10.1093/bja/aef163 (2002).
- 101 Abdelnour, E. *et al.* Does age affect response to quinidine in patients with KCNT1 mutations? Report of three new cases and review of the literature. *Seizure* **55**, 1-3, doi:10.1016/j.seizure.2017.11.017 (2018).
- 102 Lipkind, G. M. & Fozzard, H. A. Molecular model of anticonvulsant drug binding to the voltage-gated sodium channel inner pore. *Mol Pharmacol* **78**, 631-638, doi:10.1124/mol.110.064683 (2010).
- 103 Mulley, J. C. *et al.* Role of the sodium channel SCN9A in genetic epilepsy with febrile seizures plus and Dravet syndrome. *Epilepsia* **54**, e122-126, doi:10.1111/epi.12323 (2013).
- 104 Hwang, S. K. & Kwon, S. Early-onset epileptic encephalopathies and the diagnostic approach to underlying causes. *Korean J Pediatr* **58**, 407-414, doi:10.3345/kjp.2015.58.11.407 (2015).
- 105 Epilepsy Foundation. *Dravet Syndrome*, <<https://www.epilepsy.com/learn/types-epilepsy-syndromes/dravet-syndrome>> (2020).
- 106 Chen, Y. *et al.* Association between genetic variation of CACNA1H and childhood absence epilepsy. *Ann Neurol* **54**, 239-243, doi:10.1002/ana.10607 (2003).
- 107 Heron, S. E. *et al.* Extended spectrum of idiopathic generalized epilepsies associated with CACNA1H functional variants. *Ann Neurol* **62**, 560-568, doi:10.1002/ana.21169 (2007).
- 108 Uchino, T. *et al.* Voltage-dependent and frequency-independent inhibition of recombinant Cav3.2 T-type Ca²⁺ channel by bepridil. *Pharmacology* **74**, 174-181, doi:10.1159/000085329 (2005).
- 109 U.S. Department of Health and Human Services Food and Drug Administration: Center for Drug Evaluation and Research and Center for Biologics Evaluation and Research. (ed U.S. Department of Health and Human Services Food and Drug Administration Center for Drug Evaluation and Research (CDER) Center for Biologics Evaluation and Research (CBER)) 1-13 (Office of Training and Communication, Rockville, MD, 2005).
- 110 Sanguinetti, M. C. & Tristani-Firouzi, M. hERG potassium channels and cardiac arrhythmia. *Nature* **440**, 463-469, doi:10.1038/nature04710 (2006).
- 111 Witchel, H. J. Drug-induced hERG block and long QT syndrome. *Cardiovasc Ther* **29**, 251-259, doi:10.1111/j.1755-5922.2010.00154.x (2011).
- 112 Stork, D. *et al.* State dependent dissociation of HERG channel inhibitors. *Br J Pharmacol* **151**, 1368-1376, doi:10.1038/sj.bjp.0707356 (2007).
- 113 Tsujimae, K., Suzuki, S., Yamada, M. & Kurachi, Y. Comparison of kinetic properties of quinidine and dofetilide block of HERG channels. *Eur J Pharmacol* **493**, 29-40, doi:10.1016/j.ejphar.2004.04.015 (2004).
- 114 Pacico, N. & Mingorance-Le Meur, A. New in vitro phenotypic assay for epilepsy: fluorescent measurement of synchronized neuronal calcium oscillations. *PLoS One* **9**, e84755, doi:10.1371/journal.pone.0084755 (2014).
- 115 Bacci, A. V., Claudia; Pravettoni, Elena; Matteoli, Michela Synaptic and intrinsic mechanisms shape synchronous oscillations in hippocampal neurons in culture. *European Journal of Neuroscience* **11**, 389-397 (1999).
- 116 Heinemann, U. K., O.; Schuchmann, S. in *Models of Seizures and Epilepsy*. (ed Asla Pitkänen) Ch. 4, 35-44 (Elsevier, 2006).
- 117 Dravid, S. M. & Murray, T. F. Spontaneous synchronized calcium oscillations in neocortical neurons in the presence of physiological [Mg(2+)]: involvement of AMPA/kainate and metabotropic glutamate receptors. *Brain Res* **1006**, 8-17, doi:10.1016/j.brainres.2004.01.059 (2004).

- 118 Richards, G. R., Jack, A. D., Platts, A. & Simpson, P. B. in *Measuring Biological Responses with Automated Microscopy Methods in Enzymology* 335-347 (2006).
- 119 Kaufmann, K. *et al.* ML297 (VU0456810), the first potent and selective activator of the GIRK potassium channel, displays antiepileptic properties in mice. *ACS Chem Neurosci* **4**, 1278-1286, doi:10.1021/cn400062a (2013).
- 120 Dadi, P. K. *et al.* Selective Small Molecule Activators of TREK-2 Channels Stimulate Dorsal Root Ganglion c-Fiber Nociceptor Two-Pore-Domain Potassium Channel Currents and Limit Calcium Influx. *ACS Chem Neurosci* **8**, 558-568, doi:10.1021/acchemneuro.6b00301 (2017).
- 121 Xiang, Z. *et al.* The Discovery and Characterization of ML218: A Novel, Centrally Active T-Type Calcium Channel Inhibitor with Robust Effects in STN Neurons and in a Rodent Model of Parkinson's Disease. *ACS Chem Neurosci* **2**, 730-742, doi:10.1021/cn200090z (2011).
- 122 Chouabe, C. D., Milou-Daniel; Romey, Georges; Barhanin, Jacques; Lazdunski, Michel. HERG and KvLQT1/IsK, the Cardiac K⁺ Channels Involved in Long QT Syndromes, Are Targets for Calcium Channel Blockers. *Molecular Pharmacology* **54**, 695–703 (1998).
- 123 Dubin, A. E. *et al.* Identifying modulators of hERG channel activity using the PatchXpress planar patch clamp. *J Biomol Screen* **10**, 168-181, doi:10.1177/1087057104272295 (2005).
- 124 Zhao, Y. *et al.* Identification of a G-Protein-Independent Activator of GIRK Channels. *Cell Rep* **31**, 107770, doi:10.1016/j.celrep.2020.107770 (2020).
- 125 Montalbano, A., Corradetti, R. & Mlinar, B. Pharmacological Characterization of 5-HT_{1A} Autoreceptor-Coupled GIRK Channels in Rat Dorsal Raphe 5-HT Neurons. *PLoS One* **10**, e0140369, doi:10.1371/journal.pone.0140369 (2015).
- 126 Kuzhikandathil, E. O., Gerry S. . Classic D1 Dopamine Receptor Antagonist R-(\leq)-7-Chloro-8hydroxy-3-methyl-1-phenyl-2,3,4,5-tetrahydro-1H-3benzazepine hydrochloride (SCH23390) Directly Inhibits G Protein-Coupled Inwardly Rectifying Potassium Channels. *Molecular Pharmacology* **62**, 119–126 (2002).
- 127 Xie, X. *et al.* (National Center for Biotechnology Information (US), Bethesda (MD), 2010).
- 128 McCobb, D. P. *et al.* A human calcium-activated potassium channel gene expressed in vascular smooth muscle. *Am J Physiol* **269**, H767-777, doi:10.1152/ajpheart.1995.269.3.H767 (1995).
- 129 Uebele, V. N. *et al.* Cloning and functional expression of two families of beta-subunits of the large conductance calcium-activated K⁺ channel. *J Biol Chem* **275**, 23211-23218, doi:10.1074/jbc.M910187199 (2000).
- 130 Gribkoff, V. K., Starrett, J. E., Jr. & Dworetzky, S. I. Maxi-K potassium channels: form, function, and modulation of a class of endogenous regulators of intracellular calcium. *Neuroscientist* **7**, 166-177, doi:10.1177/107385840100700211 (2001).
- 131 Orio , P. & Latorre , R. Differential Effects of β 1 and β 2 Subunits on BK Channel Activity. *Journal of General Physiology* **125**, 395-411, doi:10.1085/jgp.200409236 (2005).
- 132 Xia, X. M., Ding, J. P., Zeng, X. H., Duan, K. L. & Lingle, C. J. Rectification and rapid activation at low Ca²⁺ of Ca²⁺-activated, voltage-dependent BK currents: consequences of rapid inactivation by a novel beta subunit. *J Neurosci* **20**, 4890-4903, doi:10.1523/jneurosci.20-13-04890.2000 (2000).
- 133 Brenner, R., Jegla, T. J., Wickenden, A., Liu, Y. & Aldrich, R. W. Cloning and functional characterization of novel large conductance calcium-activated potassium channel beta subunits, hKCNMB3 and hKCNMB4. *J Biol Chem* **275**, 6453-6461, doi:10.1074/jbc.275.9.6453 (2000).
- 134 Meera, P., Wallner, M. & Toro, L. A neuronal beta subunit (KCNMB4) makes the large conductance, voltage- and Ca²⁺-activated K⁺ channel resistant to charybdotoxin and iberiotoxin. *Proc Natl Acad Sci U S A* **97**, 5562-5567, doi:10.1073/pnas.100118597 (2000).
- 135 Liu, X. *et al.* Selective Blockade of Neuronal BK (α + β 4) Channels Preventing Epileptic Seizure. *J Med Chem* **63**, 216-230, doi:10.1021/acs.jmedchem.9b01241 (2020).
- 136 Rizzi, S., Knaus, H. G. & Schwarzer, C. Differential distribution of the sodium-activated potassium channels slick and slack in mouse brain. *J Comp Neurol* **524**, 2093-2116, doi:10.1002/cne.23934 (2016).
- 137 Tomasello, D. L., Hurley, E., Wrabetz, L. & Bhattacharjee, A. Slick (Kcnt2) Sodium-Activated Potassium Channels Limit Peptidergic Nociceptor Excitability and Hyperalgesia. *J Exp Neurosci* **11**, 1179069517726996, doi:10.1177/1179069517726996 (2017).
- 138 Salkoff, L., Butler, A., Ferreira, G., Santi, C. & Wei, A. High-conductance potassium channels of the SLO family. *Nat Rev Neurosci* **7**, 921-931, doi:10.1038/nrn1992 (2006).

- 139 Jamieson C, M. E., Rankovic Z, Wishart G. Medicinal Chemistry of hERG Optimizations: Highlights and Hang-Ups. *Journal of Medicinal Chemistry* **49**, 5029-5046 (2006).
- 140 Irwin, S. Comprehensive observational assessment: Ia. A systematic, quantitative procedure for assessing the behavioral and physiologic state of the mouse. *Psychopharmacologia* **13**, 222-257, doi:10.1007/bf00401402 (1968).
- 141 Redfern, W. S. *et al.* The functional observational battery and modified Irwin test as global neurobehavioral assessments in the rat: Pharmacological validation data and a comparison of methods. *J Pharmacol Toxicol Methods* **98**, 106591, doi:10.1016/j.vascn.2019.106591 (2019).
- 142 Silverman, J. L., Yang, M., Lord, C. & Crawley, J. N. Behavioural phenotyping assays for mouse models of autism. *Nat Rev Neurosci* **11**, 490-502, doi:10.1038/nrn2851 (2010).
- 143 Pasciuto, E. *et al.* Autism Spectrum Disorders: Translating human deficits into mouse behavior. *Neurobiol Learn Mem* **124**, 71-87, doi:10.1016/j.nlm.2015.07.013 (2015).
- 144 Kaidanovich-Beilin, O., Lipina, T., Vukobradovic, I., Roder, J. & Woodgett, J. R. Assessment of social interaction behaviors. *J Vis Exp*, doi:10.3791/2473 (2011).
- 145 Couture, S. M. *et al.* Comparison of social cognitive functioning in schizophrenia and high functioning autism: more convergence than divergence. *Psychol Med* **40**, 569-579, doi:10.1017/s003329170999078x (2010).
- 146 Powell, C. M. & Miyakawa, T. Schizophrenia-relevant behavioral testing in rodent models: a uniquely human disorder? *Biol Psychiatry* **59**, 1198-1207, doi:10.1016/j.biopsych.2006.05.008 (2006).
- 147 Geyer, M. A., McIlwain, K. L. & Paylor, R. Mouse genetic models for prepulse inhibition: an early review. *Molecular Psychiatry* **7**, 1039-1053, doi:10.1038/sj.mp.4001159 (2002).
- 148 Braff, D. L., Geyer, M. A. & Swerdlow, N. R. Human studies of prepulse inhibition of startle: normal subjects, patient groups, and pharmacological studies. *Psychopharmacology (Berl)* **156**, 234-258, doi:10.1007/s002130100810 (2001).
- 149 Kunugi, H. *et al.* Prepulse inhibition of acoustic startle in Japanese patients with chronic schizophrenia. *Neurosci Res* **59**, 23-28, doi:10.1016/j.neures.2007.05.006 (2007).
- 150 Braff, D. *et al.* Prestimulus effects on human startle reflex in normals and schizophrenics. *Psychophysiology* **15**, 339-343, doi:10.1111/j.1469-8986.1978.tb01390.x (1978).
- 151 Perry, W., Minassian, A., Lopez, B., Maron, L. & Lincoln, A. Sensorimotor gating deficits in adults with autism. *Biol Psychiatry* **61**, 482-486, doi:10.1016/j.biopsych.2005.09.025 (2007).
- 152 McAlonan, G. M. *et al.* Brain anatomy and sensorimotor gating in Asperger's syndrome. *Brain* **125**, 1594-1606, doi:10.1093/brain/awf150 (2002).
- 153 Cheng, C. H., Chan, P. S., Hsu, S. C. & Liu, C. Y. Meta-analysis of sensorimotor gating in patients with autism spectrum disorders. *Psychiatry Res* **262**, 413-419, doi:10.1016/j.psychres.2017.09.016 (2018).
- 154 Schneider, A. *et al.* Prepulse inhibition in patients with fragile X-associated tremor ataxia syndrome. *Neurobiol Aging* **33**, 1045-1053, doi:10.1016/j.neurobiolaging.2010.09.002 (2012).
- 155 Hessl, D. *et al.* Prepulse inhibition in fragile X syndrome: feasibility, reliability, and implications for treatment. *Am J Med Genet B Neuropsychiatr Genet* **150b**, 545-553, doi:10.1002/ajmg.b.30858 (2009).
- 156 Shiotsuki, H. *et al.* A rotarod test for evaluation of motor skill learning. *J Neurosci Methods* **189**, 180-185, doi:10.1016/j.jneumeth.2010.03.026 (2010).
- 157 Ennaceur, A. Tests of unconditioned anxiety - pitfalls and disappointments. *Physiol Behav* **135**, 55-71, doi:10.1016/j.physbeh.2014.05.032 (2014).
- 158 Walf, A. A. & Frye, C. A. The use of the elevated plus maze as an assay of anxiety-related behavior in rodents. *Nat Protoc* **2**, 322-328, doi:10.1038/nprot.2007.44 (2007).
- 159 Yin, H. H. *et al.* Dynamic reorganization of striatal circuits during the acquisition and consolidation of a skill. *Nat Neurosci* **12**, 333-341, doi:10.1038/nn.2261 (2009).
- 160 Bouwknecht, J. A. & Paylor, R. Pitfalls in the interpretation of genetic and pharmacological effects on anxiety-like behaviour in rodents. *Behav Pharmacol* **19**, 385-402, doi:10.1097/FBP.0b013e32830c3658 (2008).
- 161 Bouwknecht, J. A. & Paylor, R. Behavioral and physiological mouse assays for anxiety: a survey in nine mouse strains. *Behav Brain Res* **136**, 489-501, doi:10.1016/s0166-4328(02)00200-0 (2002).
- 162 Ray, W. J. *et al.* Startle response in generalized anxiety disorder. *Depress Anxiety* **26**, 147-154, doi:10.1002/da.20479 (2009).

- 163 Kohl, S. *et al.* Prepulse inhibition of the acoustic startle reflex in high functioning autism. *PLoS One* **9**, e92372, doi:10.1371/journal.pone.0092372 (2014).
- 164 Labbate, G. P., da Silva, A. V. & Barbosa-Silva, R. C. Effect of severe neonatal seizures on prepulse inhibition and hippocampal volume of rats tested in early adulthood. *Neurosci Lett* **568**, 62-66, doi:10.1016/j.neulet.2014.03.019 (2014).
- 165 Nygaard, H. B. *et al.* Brivaracetam, but not ethosuximide, reverses memory impairments in an Alzheimer's disease mouse model. *Alzheimers Res Ther* **7**, 25, doi:10.1186/s13195-015-0110-9 (2015).
- 166 Seneviratne, U., Boston, R. C., Cook, M. J. & D'Souza, W. J. Characteristics of Epileptiform Discharge Duration and Interdischarge Interval in Genetic Generalized Epilepsies. *Front Neurol* **9**, 36, doi:10.3389/fneur.2018.00036 (2018).
- 167 Ayala, G. F., Dichter, M., Gumnit, R. J., Matsumoto, H. & Spencer, W. A. Genesis of epileptic interictal spikes. New knowledge of cortical feedback systems suggests a neurophysiological explanation of brief paroxysms. *Brain Res* **52**, 1-17, doi:10.1016/0006-8993(73)90647-1 (1973).
- 168 McLin, J. P. & Steward, O. Comparison of seizure phenotype and neurodegeneration induced by systemic kainic acid in inbred, outbred, and hybrid mouse strains. *Eur J Neurosci* **24**, 2191-2202, doi:10.1111/j.1460-9568.2006.05111.x (2006).
- 169 Copping, N. A., Adhikari, A., Petkova, S. P. & Silverman, J. L. Genetic backgrounds have unique seizure response profiles and behavioral outcomes following convulsant administration. *Epilepsy Behav* **101**, 106547, doi:10.1016/j.yebeh.2019.106547 (2019).
- 170 Mehta, P. *et al.* Functional Access to Neuron Subclasses in Rodent and Primate Forebrain. *Cell Rep* **26**, 2818-2832.e2818, doi:10.1016/j.celrep.2019.02.011 (2019).